

Dissertation

# The Coupling of Discrete Electromagnetism and the Boundary Element Method for the Simulation of Accelerator Magnets

ausgeführt zum Zwecke der Erlangung des akademischen  
Grades eines Doktors der technischen Wissenschaften

unter der Leitung von

O.Univ.Prof. Dr.techn. Adalbert Prechtl

E351 - Institut für Grundlagen und  
Theorie der Elektrotechnik

durch

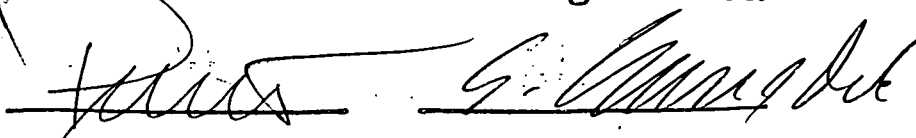
Dipl.-Ing. Bernhard Auchmann

Mat.-Nr. 9725965

A-1130 Wien, Bergheideng. 8/4/1/4

Wien, im Dezember 2004

Diese Dissertation haben begutachtet:



Two handwritten signatures are present below the text 'Diese Dissertation haben begutachtet:'. The first signature is on the left and the second is on the right. A large, stylized signature is also visible above the second reviewer's signature.

# Kurzfassung

Die Theorie des diskreten Elektromagnetismus (DEM) gewinnt in der numerischen Feldberechnung beständig an Boden. Der diskrete Elektromagnetismus spiegelt die fundamentalen topologischen und geometrischen Eigenschaften der elektromagnetischen Phänomene mit beispielloser Klarheit wider. In den vergangenen Jahren haben insbesondere die strukturellen Ähnlichkeiten der Methode der finiten Elemente (FEM) mit DEM-Formulierungen einige Aufmerksamkeit erregt.

In dieser Doktorarbeit wird gezeigt, dass FEM in der Tat eine weitere DEM-Formulierung darstellt. Zu diesem Zwecke wird ein Randterm sowie Transfermatrizen im diskreten Elektromagnetismus eingeführt. Beide Objekte besitzen Gegenstücke in der FE-Methode. Alternativ zum sogenannten Galerkin-Hodge Operator der FEM wird ein geometrisch definierter Hodge Operator auf simplizialen Zellkomplexen vorgeschlagen. Durch diesen Schritt kann eine strikt geometrisch und topologisch definierte Variante des diskreten Elektromagnetismus präsentiert werden.

Die Kopplung des diskreten Elektromagnetismus mit der Randelemente-Methode (BEM) vereint die Vorteile beider Methoden miteinander. Der resultierende DEM-BEM Algorithmus ist besonders gut für die Simulation von Beschleunigermagneten geeignet: Nichtlineares und leitfähiges Material wird für eine DEM-Formulierung diskretisiert, während die supraleitenden Spulen mit höchster Genauigkeit in einer BEM-Formulierung Berücksichtigung finden.

Das Ziel dieser Doktorarbeit ist die Implementierung einer DEM-BEM Kopplung unter Verwendung des Whitney-Form basierten Galerkin-Hodge Operators in der DEM-Formulierung.

# Abstract

The theory of discrete electromagnetism (DEM) is quickly gaining ground in the computational electromagnetism community. It reflects in an unprecedented clarity the topological and geometrical properties of the phenomena of electromagnetism. The structural analogies of the Finite Element Method (FEM) and DEM formulations has attracted many researchers' attention over the past years.

In this thesis we will show that FEM is indeed another DEM formulation. To this end we introduce a boundary term and transfer matrices in DEM, both of which find their analogue in a FEM equation system. As an alternative to the Galerkin-Hodge operator used in FEM we propose a geometrically defined Hodge operator on simplicial cells, thus presenting a solely geometrically and topologically defined variant of DEM formulations.

The coupling of DEM with a Boundary Element Method (BEM) has proven to combine the advantages of both methods. The resulting DEM-BEM algorithm is found to be suited for the simulation of accelerator magnets: non-linear and conductive material is discretized for a DEM formulation whereas the superconductive coils are considered at the highest accuracy in a BEM formulation.

The goal of this thesis is the implementation of a DEM-BEM coupling with the Whitney-form based Galerkin-Hodge operator being used in the DEM formulation.

# Acknowledgements

I want to thank colleagues, supervisors, friends and family who accompanied my efforts over the past 2 1/2 years. Thanks to Prof. Adalbert Prechtel who monitored the thesis from Vienna; to Stephan Russenschuck for sharing the passion for theoretical issues; to Stefan Kurz for introducing me to the subject; to Oliver Rain for being my companion in fortune and misfortune. Thanks to the Vienna and Graz Institutes of Fundamentals and Theory of Electrical Engineering.

Thanks to my friends in Geneva, Adrian, Ashwini, Christoph, Claus, Edda and Wener, Sophie and Martin. Special thanks to the bunch of maniacs, Herbert, Kurt (Thomas), Thomas and Peter who assured my physical and mental well-being. Life would have been *so* different without us doing such stupid things as La Poubelle, Matterhorn and their like. Thanks for teaching me the basics of alpinism and for being such nice fellows and friends. Equally very special thanks to Eva and Lene for keeping me from leading too monotonous a life.

To my dear friends in Vienna, Anna, Flo, Georg, Kathi, Kathrin, Lisa and Thomas, Lukas, Marie, Martina and Patrick, René, Roman, Stefan; knowing that I could go back and live near you gives me the stability I need to lead my life far from home.

Eventually, to my family: thanks for accepting my decision to live abroad; thanks for giving me your love. I do think of you all the time and I wish you all the strength and the luck you will need in the oncoming years.

Kisses to my nieces.

*Are you such a dreamer?  
To put the world to rights?  
I'll stay home forever  
Where 2+2 always makes up 5.*

*Thom Yorke, 2003*

# Contents

<b>1</b>	<b>Introduction</b>	<b>2</b>
<b>2</b>	<b>Discretization of Space</b>	<b>6</b>
2.1	Simplicial Complex . . . . .	6
2.1.1	Standard Simplex and Simplices . . . . .	6
2.1.2	Chains of Simplices . . . . .	8
2.1.3	Boundary Operator . . . . .	8
2.1.4	Homology Classes . . . . .	11
2.2	Cell Complex . . . . .	13
2.2.1	Cells . . . . .	13
2.2.2	Outer Orientation . . . . .	14
<b>3</b>	<b>Discretization of Fields</b>	<b>16</b>
3.1	Cochains and the Discretization of Maxwell Fields . . . . .	17
3.1.1	Cochains . . . . .	17
3.1.2	Integral Quantities and Related Maxwell Equations . . . . .	17
3.1.3	Discretization of the Faraday Complex . . . . .	19
3.1.4	Coboundary Operator . . . . .	20
3.1.5	Discretization of the Ampère-Maxwell Complex . . . . .	22
3.2	Discretization of deRham Currents . . . . .	23
3.3	Cohomology . . . . .	28
3.3.1	Converse of the Poincaré Lemma . . . . .	29
3.3.2	Cohomology Contributions to Cochains . . . . .	30
<b>4</b>	<b>Discrete Material Laws (1) - Discretization on Dual Complexes</b>	<b>35</b>
4.1	Topologically Dual Cell Complexes . . . . .	35
4.2	Topological Laws of DEM on Dual Complexes . . . . .	38
4.3	Interpolation of Simplices - Transfer Matrix . . . . .	39
4.4	The Boundary of the Dual Complex . . . . .	44
4.5	Topological Matrices on Dual Cell Complexes . . . . .	46
<b>5</b>	<b>Discrete Material Laws (2) - A Discrete Hodge Operator</b>	<b>50</b>
5.1	Discrete Hodge Operator on Brick-Shaped Cells . . . . .	50
5.2	Discrete Hodge Operator on Simplicial Cells . . . . .	52

5.3	DEM Equation Systems . . . . .	54
<b>6</b>	<b>Discrete Material Laws (3) - More Discrete Hodge Operators</b>	<b>59</b>
6.1	Whitney Hodge Operator . . . . .	59
6.2	Galerkin Hodge Operator . . . . .	61
6.3	Relationship between Hodge Operators . . . . .	63
<b>7</b>	<b>Boundary Element Method in DEM Notation</b>	<b>65</b>
7.1	Representation Formula . . . . .	65
7.2	Boundary Value Problem . . . . .	69
7.3	BEM Formulation . . . . .	70
<b>8</b>	<b>Coupling of DEM with BEM</b>	<b>73</b>
8.1	DEM-BEM Coupling . . . . .	73
8.2	The Kernel of the DEM-BEM System Matrix . . . . .	75
<b>9</b>	<b>Solver Strategies for the DEM-BEM Coupled System</b>	<b>77</b>
9.1	General Properties and Solver Strategies . . . . .	77
9.2	Regularization . . . . .	79
9.3	Adapted GMRES . . . . .	79
<b>10</b>	<b>Numerical Results</b>	<b>82</b>
10.1	The Existing FEM-BEM Code . . . . .	82
10.2	Whitney-Form Based FEM . . . . .	84
10.3	Whitney Form Based Coupling of FEM and BEM . . . . .	84
<b>11</b>	<b>Conclusions and Outlook</b>	<b>87</b>
<b>A</b>	<b>Selected Topics of Vector Analysis</b>	<b>89</b>
<b>B</b>	<b>Maxwell Equations in Differential Form Notation</b>	<b>93</b>
<b>C</b>	<b>Local Interpolation of Coefficient Vectors</b>	<b>96</b>
C.1	Whitney Forms . . . . .	96
C.2	Sobolev Spaces . . . . .	98
C.3	Special Sobolev Spaces . . . . .	99
<b>D</b>	<b>Discretization of the Poynting Theorem</b>	<b>101</b>
D.1	The Poynting Theorem . . . . .	101
D.2	Flux Linkage and Voltage Driven Coils . . . . .	103
<b>E</b>	<b>Discrete Material Laws (4) - Anisotropy, Eddy Currents, Non-linearity</b>	<b>105</b>
E.1	Anisotropy . . . . .	105
E.2	Eddy Currents . . . . .	106

E.3 Non-linearity . . . . .	106
<b>F BEM Potentials</b>	<b>108</b>
F.1 Double-Layer Potential of an Equivalence Class . . . . .	109
F.2 Equivalence of Current Loops and Magnetic Double Layers . . . . .	109



# Notation

$\mathbf{F}$	vector
$\bar{F}$	even differential form
$\tilde{F}$	odd differential form
$\underline{F}$	Whitney form
$\underline{\underline{F}}$	double form
$\{F\}$	coefficient vector
$\bar{F}$	cochain of cocells
$\tilde{\rho}^p$	$p$ -cocell
$\tilde{c}$	chain of cells
$\rho_p$	$p$ -cell
$\partial$	boundary operator
$d$	exterior derivative
$\delta$	coderivative
$\partial_p$	discrete boundary operator
$d_p$	discrete coboundary operator, discrete exterior derivative
$C$	cell complex
$\mathcal{F}^p(\Omega)$	linear space of differential forms of degree $p$ on $\Omega$
$\mathcal{W}^p(\Omega)$	linear space of Whitney forms of degree $p$ on $\Omega$
$\mathcal{C}^p(\Omega)$	linear space of $p$ -cochains on a complex that discretizes $\Omega$
$\mathcal{C}_p(\Omega)$	linear space of $p$ -chains on a complex that discretizes $\Omega$
$B_p(\Omega)$	$p$ -boundary space of a complex that discretizes $\Omega$
$Z_p(\Omega)$	$p$ -cycle space of a complex that discretizes $\Omega$
$H_p(\Omega)$	$p$ -homology space of a complex that discretizes $\Omega$
$B^p(\Omega)$	$p$ -coboundary space of a complex that discretizes $\Omega$
$Z^p(\Omega)$	$p$ -cocycle space of a complex that discretizes $\Omega$
$H^p(\Omega)$	$p$ -cohomology space of a complex that discretizes $\Omega$
${}^pH_d(\Omega)$	Sobolev spaces used to model the electromagnetic field differential forms
${}^pH_d(d, \Omega)$	Respective Sobolev spaces of closed differential forms

Note that all objects associated with the dual complex are denoted with an overbar, e.g.,  $\bar{F}$ ,  $\{\bar{F}\}$ ,  $\bar{F}$  or  $\bar{c}$ . Objects associated with an outer oriented primal complex are denoted with an overtilde, e.g.,  $\tilde{F}$ ,  $\{\tilde{F}\}$ ,  $\tilde{F}$  or  $\tilde{c}$ . Objects associated with an outer oriented dual complex are denoted with both signs, e.g.,  $\tilde{\bar{F}}$ ,  $\{\tilde{\bar{F}}\}$ ,  $\tilde{\bar{F}}$  or  $\tilde{\bar{c}}$ .

# 1

## Introduction

There are two main motivations for this thesis: The need for more accurate modelling of electromagnetic field problems in 3 dimensions on the one side and the urge for a full understanding of the Finite Element Method (FEM) as another variant of Discrete Electromagnetism (DEM) on the other side. Both interests converge in the implementation of a coupled Finite Element- Boundary Element Method with Whitney forms as shape functions.

The need for highest accuracy in the simulation of accelerator magnets has for a long time been a driving force for research and development in the domain of computational electromagnetism, [24], [35]. Over the past years the coupling of the Finite Element Method and the Boundary Element Method has proven to combine the advantages of both methods; the treatment of non-linear material with FEM and the accurate modelling of superconducting coils with BEM, [24].

Had the 2-dimensional FEM-BEM code delivered satisfying results, the 3-dimensional FEM-BEM coupling with node-based Lagrangian shape functions fell short of the 2-dimensional accuracy. Although the errors seemed to be negligible in most cases, under certain circumstances the code was known to yield unphysical results. Such behaviour is well-known and understood for node-based FEM codes and affects also the Boundary Element Method, [5]. The cure is also known to lie in the use of Whitney-forms as shape function instead of Lagrangian shape functions. The development of a Whitney-form based FEM-BEM coupling in three dimensions was desirable to improve the reliability of 3-dimensional computations with the CERN ROXIE program package (Routine for the Optimization of Magnet X-Sections, Inverse Field Calculation and Coil End Design).

Theoretical issues treated in this thesis can be summarized under the following three questions:

1. Is it possible to introduce a comprehensive and solely discrete theory of electromagnetism based on a simplicial cell complex (tetrahedral mesh)?

A discrete theory of electromagnetism must feature discrete fields, discrete derivative operators and discrete material laws, more generally called discrete Hodge

operators. Discrete fields and derivative operators are well-established and accepted in the computational electromagnetism community. The issue of discrete Hodge operators is still frequently discussed (e.g., [1], [6], [17]). Prevalent definitions of Hodge operators on simplicial cells have one common shortcoming; they are based on an interpolation of discrete fields by differential forms (or vector fields). It is seen by many that by the interpolation of fields the very paradigm of a discrete electromagnetism is violated. The continuous tools of vector analysis should not be a prerequisite to the establishment of a discrete theory. In any case it remains an interesting question whether we can find geometrically defined Hodge operators on simplicial cells that would complete a solely discrete theory of electromagnetism.

2. Can we interpret and rewrite the Finite Element Method (with Whitney-forms as shape functions) in terms of the operators of discrete electromagnetism?

The interesting and surprising issue of a reinterpretation of FEM in terms of DEM operators has been treated in various publications, (e.g., [7], [32]). The role of the discrete derivative operators and the Galerkin Hodge operator in FEM has been identified. Two open questions have prevailed to date. First, how can the boundary term in a FEM formulation be interpreted in terms of DEM operators and fields? And second, what is the correct interpretation of the second Galerkin-type matrix on the right-hand side of the FEM equation system? Are these two issues particular problems of FEM or will a deeper understanding of DEM lead us to recognize the necessity of those operators in any consistent discrete theory of electromagnetism?

3. Can a DEM formulation on a closed domain be coupled to a Boundary Element Method?

The coupling of DEM with a Boundary Element Method is directly related to the discussion of a boundary term appearing in a FEM formulation. If FEM can be shown to be another variant of DEM and FEM-BEM coupling with Whitney forms works, then any DEM method should be suited for the coupling with BEM.

This thesis is part of a collaborative effort of CERN with the Robert Bosch GmbH to implement a 3-dimensional FEM-BEM coupling with Whitney forms. The Boundary Element Method was implemented in the course of a doctoral thesis at the University of Saarbrücken, [28]. The implementation of a Finite Element Method was started as a diploma thesis at the University of Mittweida, [31]. This thesis is intended to finish the work on the FEM-part and to implement the coupling of both methods. Solver strategies were investigated and implemented. The new code was integrated in the ROXIE program package at CERN as well as the EDYSON program at the Robert Bosch GmbH. The thesis is structured as follows:

### **Discretization of Space (Chapter 2)**

We present the discretization of a bounded spatial domain by an oriented cell complex. Cell complexes are Finite Element Meshes, defined in the language of algebraic topology. Simplices, cells, cell complexes and chains of cells are defined,

and topological issues such as the boundary operator and homology classes on a cell complex are addressed.

### **Discretization of Fields (Chapter 3)**

Discrete fields are defined as mappings from cells (nodes, edges, faces or volumes) to physical quantities (magnetic flux, electric voltage, electric charge and electric current). These mappings are called cochains. The coboundary operator yields a discrete derivative operator for cochains. We introduce a notation that allows to take into account the contributions of concentrated fields (surface charges, surface currents, ...) and of jump discontinuities to the cochain coefficients. This allows for a novel notation for cohomology contributions in DEM.

### **Discrete Material Laws (1) -**

#### **Discretization on Dual Complexes (Chapter 4)**

To date, DEM formulations discretize the electromagnetic fields on topologically dual cell complexes; the Faraday fields<sup>1</sup> on the inner oriented primal cell complex and the Ampère-Maxwell fields<sup>2</sup> on the topologically dual outer oriented cell complex. As a consequence, the discrete Hodge operators are square. We introduce two novel aspects in the context of dual discretization. First, we introduce transfer matrices, matrices that transfer cochain coefficients on the primal complex into cochain coefficients on the dual complex. The otherwise redundant definition of simplices, simplicial complexes and chains of simplices preceding the definition of cells in Chapter 2 is aimed towards this section. Simplices allow for a mathematically correct introduction of the transfer matrices. The second novel aspect of this chapter concerns the boundary of the dual complex. We find that a comprehensive discrete theory of electromagnetism must feature boundary terms that appear if a discrete field on the dual complex is differentiated.

### **Discrete Material Laws (2) -**

#### **A Discrete Hodge Operator (Chapter 5)**

In this chapter we illustrate the basic "mechanism" of a discrete Hodge operator at the example of the material matrix of the Finite Integration Technique. Next, we introduce a geometrically defined discrete Hodge operator on simplicial cells. This new definition of a discrete Hodge operator completes the discrete theory of electromagnetism on a simplicial cell complex. Finally, we give examples for discrete equation systems for electrostatics, magnetostatics and magneto-quasistatics.

### **Discrete Material Laws (3) -**

#### **More Discrete Hodge Operators (Chapter 6)**

We compare the new, geometrical definition of discrete Hodge operators on simplicial cells to prevalent definitions that are based on the interpolation of fields by Whitney forms. It is found that, e.g., a vector potential formulation for magnetostatics yields identical equation systems whether we use the geometrical Hodge, a Whitney Hodge or a Galerkin Hodge operator. FEM is found to be another variant of DEM.

---

<sup>1</sup>Electric scalar potential, magnetic vector potential, electric field and magnetic induction.

<sup>2</sup>Magnetic field, electric flux density, electric charge density and electric current density.

### **Boundary Element Method in DEM Notation (Chapter 7)**

We derive a Boundary Element Method from the Kirchhoff representation formula with Whitney forms. We do so, using the notational conventions of DEM.

### **Coupling of DEM with BEM (Chapter 8)**

The introduction of a boundary term in the DEM formulation in Chapter 5 enables us to introduce a coupling of the DEM and BEM equation systems. An investigation of the kernels of the different matrix blocks reveals an interesting property of the DEM-BEM system matrix: its kernel is orthogonal to its image.

### **Solver Strategies for the DEM-BEM Coupled system(Chapter 9)**

Based on the findings of the previous chapter we can propose two approaches to solve the DEM-BEM coupled system. First, the standard regularization method used for FEM systems is applicable also for a DEM-BEM coupled system. And second, we introduce a new, adapted GMRES algorithm that is suited to deal with singular systems in the presence of a right-hand side that does not lie in the image of the matrix. The new algorithm will give an optimum solution to the system and detect convergence.

### **Numerical Results (Chapter 10)**

A coupling of a Finite Element Method and a Boundary Element Method with Whitney forms has been implemented and tested. We show that the new algorithm overcomes the problems of the previously implemented code based on Lagrangian shape functions. Furthermore, we calculate the field of an LHC short dipole model.

### **Appendices A-F**

Appendix A gives a short review of important aspects of modern vector analysis with differential forms. This paragraph cannot replace a textbook on the subject. Appendix B yields the Maxwell equations in differential form notation. Appendix C introduces Whitney forms on simplicial complexes. Appendix D yields aspects of the discrete electromagnetic theory related to the energy balance equation. The treatment of voltage driven coils in time-transient calculations is discussed. Appendix E introduces anisotropic discrete Hodge operators. The sections on time-transience and non-linearity are intended to document the implementation of the respective issues in the ROXIE/EDYSON codes. Finally, Appendix F yields interesting aspects of the Boundary Element Method with Whitney forms.

This thesis is not intended as an introduction to the topics of Discrete Electromagnetism, the Finite Element Method or the Boundary Element Method. Basic knowledge of linear algebra, algebraic topology and vector analysis on manifolds is required. We recommend [19], [20] and [21] as well as [2] and [3] as an introductory course.

# 2

## Discretization of Space

We present the topic of spatial discretization from the viewpoint of algebraic topology. In a first step we define the simplicial complex. We introduce a boundary operator on the simplicial complex and discuss the topological properties of a complex, encoded in its homology space. Later we extend the definition of the simplicial complex to the more general cell complex. Finite Element meshes (grids, tessellations) are cell complexes. They must fulfill certain intuitive criteria, e.g., the intersection of any two volumes is either a common face or the empty set.

Throughout this thesis we limit ourselves to dimensions  $n = 1, 2, 3$ . Time is considered as a parameter. The chapter is based on [30] and [20].

### 2.1 Simplicial Complex

#### 2.1.1 Standard Simplex and Simplices

Simplices of dimension  $p = 0, 1, 2, 3$  are the elementary building blocks of polyhedral objects. They are defined as the convex spans of  $(p + 1)$  vertices. A 0-simplex can be visualized by a point, a 1-simplex by a straight line segment, a 2-simplex by a triangle and a 3-simplex by a tetrahedron. We define the standard simplex as follows:

**Definition 2.1.1 (Standard Simplex)** A  $p$ -dimensional standard simplex  $\Delta_p$  is defined by

$$\Delta_p = \{(\lambda_1, \dots, \lambda_{p+1}) \in \mathbb{R}^{p+1} \text{ with } 0 \leq \lambda_k \leq 1 \text{ and } \lambda_1 + \dots + \lambda_{p+1} \leq 1\}. \quad (2.1)$$

Its vertices  $v^k$  are given by  $v^k = (\lambda_1 \dots \lambda_{p+1})$  with  $\lambda_j = \delta_j^k$ ,  $j, k = 1, \dots, p + 1$ .  $\delta_j^k$  is the Kronecker delta.  $\diamond$

We use the vertices of the standard simplex to assign an orientation to the simplex:

**Definition 2.1.2 (Inner Oriented Standard Simplex)** Let  $\Delta_p$  denote a standard simplex. Any fixed arbitrary ordering  $\langle v^1, \dots, v^{p+1} \rangle$  of its vertices is chosen. The equivalence class of even permutations of this ordering is called the positively oriented standard simplex. We write  $+\Delta_p$  for the positively oriented standard simplex, i.e., the pair of a standard simplex and an equivalence class of orderings, and  $-\Delta_p$  for the negatively oriented standard simplex. The orientation thus introduced is called an *inner orientation*.  $\diamond$

The inner orientation can be visualized by a '+'-sign for a node, a direction for a line (forward or backward), a sense of twist for a surface (clock-wise or counter-clock-wise) and a screw-rule for the volume (right-hand or left-hand rule), see Fig. 2.1.

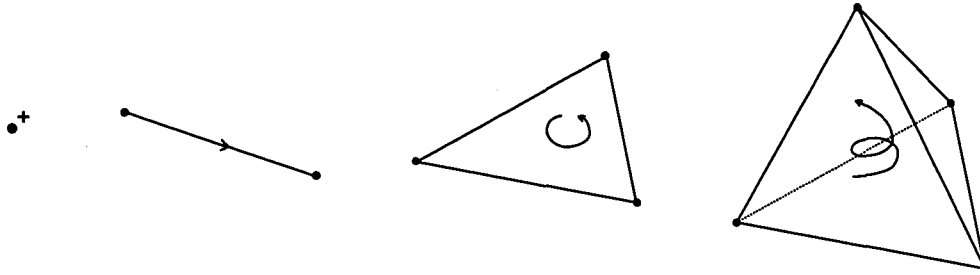


Figure 2.1: Visualization of inner oriented simplices of dimensions 0, 1, 2 and 3.

We can now proceed to construct a  $p$ -dimensional polyhedron (a simplicial complex) from standard simplices in two steps:

**Definition 2.1.3 (Simplices)** Let  $\Omega$  be an  $n$ -manifold. A  $p$ -dimensional simplex or  $p$ -simplex  $\sigma_p$  is a smooth mapping of the standard  $p$ -simplex to  $\Omega$ :

$$\sigma_p : \Delta_p \longrightarrow \Omega, \quad p = 0, \dots, n. \quad (2.2)$$

We denote with  $S_p$  a set of  $p$ -simplices and with  $n_p$  the number of  $p$ -simplices in the set. We shall sometimes omit the distinction between a simplex and its image in  $\Omega$ , as long as no ambiguities are to be expected.  $\diamond$

For a set of simplices to represent a meaningful spatial discretization, a number of conditions needs to be met regarding the way their sides touch.

The *sides* of a  $p$ -dimensional standard simplex  $\Delta_p$  are  $(p-1)$ -dimensional standard simplices  $\Delta_{p-1}^k$ . Their *canonical orientation* is given by  $\langle v^1 \dots \hat{v}^k \dots v^{p+1} \rangle$ , where the hat denotes that the orientation of the  $(p-1)$ -standard simplex is obtained from the  $p$ -standard simplex by omitting the  $k$ th vertex. Geometrically this means picking the side of  $\Delta_p$  opposite to the  $k$ th vertex.  $\sigma_{p-1}^k$  then means the restriction of the mapping  $\sigma_p$  to  $\Delta_{p-1}^k$ .

**Definition 2.1.4 (Simplicial Complex)** A simplicial complex, or polyhedron, is a set  $S$  of simplices that meets the following criteria:

1. With every simplex  $\sigma_p$ ,  $S$  also contains all sides  $\sigma_{p-1}^k$ ,  $k = 0, \dots, p$ , of the simplex.
2. The intersection of any two simplices in  $S$  is either empty or a common side.
3.  $S$  contains a finite number of simplices.

◇

We have now discretized a polyhedron by splitting it into a set of tetrahedra, triangles, straight lines and points. The polyhedron represented by the simplicial complex is more generally known as a (tetrahedral) mesh or grid.

## 2.1.2 Chains of Simplices

Before we treat important issues like the determination of a complex' boundary we need to introduce another formal instance:

**Definition 2.1.5 (Chains)** We endow a set of  $p$ -simplices with the structure of a linear space over a field  $\mathbb{K}$  ( $\mathbb{R}$  or  $\mathbb{C}$ ). Let  $\mathcal{C}_p(\Omega)$  denote this linear space called the  $p$ -chain space. Its elements are given by

$$\mathfrak{c} = c_1\sigma_p^1 + \dots + c_{n_p}\sigma_p^{n_p}, \quad c_i \in \mathbb{K}. \quad (2.3)$$

We denote chains with an under-check. The canonical basis isomorphism assigns an element of  $\mathbb{R}^{n_p}$  to every  $p$ -chain in a simplicial complex. We denote the coefficient vector with braces.

$$\cong: \mathcal{C}_p(\Omega) \longrightarrow \mathbb{R}^{n_p}, \quad \mathfrak{c} \longmapsto \{c\}. \quad (2.4)$$

◇

Chains are used to capture topological properties of a complex (determine boundaries, holes, cavities of the complex). But, as we will see, they are also used for the interpolation of simplices.

**Example:** Fig. 2.2 (left) shows a 2-dimensional oriented simplicial complex consisting of five faces, ten edges and six nodes. A 1-chain  $\mathfrak{e}$  with a coefficient vector  $\{e\} = (-1, 0, 0, 1, 1, 0, 0, 1, 1, 0)^T$  and a 2-chain  $\mathfrak{f}$  with coefficients  $\{f\} = (1, 0, 1, 1, 1)^T$  are displayed in the middle and on the right of Fig. 2.2. □

## 2.1.3 Boundary Operator

We shall discuss the issue of incidence matrices of  $p$ - and  $(p+1)$ -chains for simplicial complexes. Recall that a side of a  $p$ -simplex is found by eliminating the opposite vertex in the simplex, thus obtaining a  $(p-1)$ -simplex. The incidence number of



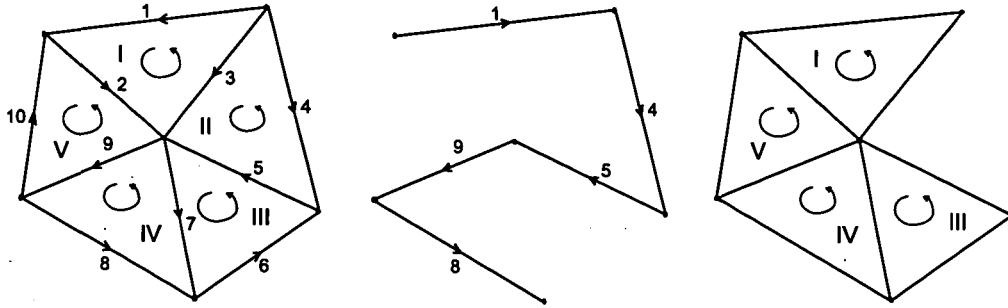


Figure 2.2: Left: 2-dimensional oriented simplicial complex. Middle: 1-chain. Right: 2-chain.

a  $p$ -simplex  $\sigma_p$  and its side  $\sigma_{p-1}^k$ , where  $k$  is the number of the opposite vertex,  $1 \leq k \leq p + 1$ , is given by

$$[\sigma_p, \sigma_{p-1}^k] = (-1)^{k+1}. \quad (2.5)$$

In a simplicial complex all  $p$ -simplices,  $p = 0, \dots, 3$ , must be given an orientation. 0-simplices can only have plus-orientation as there are no permutations of a single vertex. All other simplices need to be assigned a vertex-ordering and thus a positive orientation. The incidence number of a general  $(p - 1)$ -simplex in a complex with a  $p$ -simplex is given by

$$[A^p]^{ij} := [\sigma_p^i, \sigma_{p-1}^j] = \begin{cases} (-1)^{s+k+1}, & \text{if } \sigma_{p-1}^j \text{ is the } k\text{th side of } \sigma_p^i \\ 0, & \text{otherwise.} \end{cases} \quad (2.6)$$

For the first line on the right-hand side we assume  $\sigma_{p-1}^j$  to be the  $k$ th side of  $\sigma_p^i$ . The chosen ordering of vertices of  $\sigma_{p-1}^j$  will generally differ from the ordering of the  $k$ th side of  $\sigma_p^i$  obtained by eliminating the  $k$ th vertex.  $s$  is the multiplicity of permutations between these two orderings. Eq. (2.5) defines the incidence matrix  $[A^p]$  of  $p$ - and  $(p - 1)$ -chains in a complex.

**Example:** Figure 2.3 (left) shows two 2-simplices. Both faces are oriented by a vertex ordering  $\langle v^1, v^2, v^3 \rangle$ . The edges are oriented in the canonical way; edge 1 by  $\langle v^2, v^3 \rangle$ , edge 2 by  $\langle v^1, v^3 \rangle$  and edge 3 by  $\langle v^1, v^2 \rangle$ . The incidence numbers of the faces and their boundary edges are given by  $[\sigma_2, \sigma_1^k] = (-1)^{k+1}$ , compare Eq. (2.5).

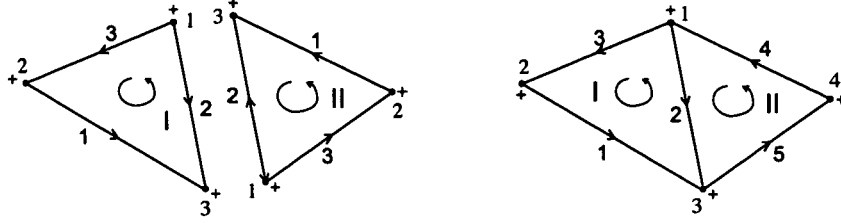


Figure 2.3: Left: Two oriented 2-simplices. Right: Simplicial 2-complex consisting of two 2-simplices.

Now we build a complex of the two faces. We choose face 1 to be oriented by  $\langle v^1, v^2, v^3 \rangle$  and face 2 by  $\langle v^3, v^4, v^1 \rangle$ , compare Fig. 2.3 (right). The canonical orientations of edge 2 in face 1 and in face 2 are in conflict. We have to make a choice and we choose  $\langle v^1, v^3 \rangle$  over  $\langle v^3, v^1 \rangle$ . The incidence number of edge 2 and face 1 is

$$[A^2]^{21} = [\varrho_2^1, \varrho_1^2] = (-1)^{0+2+1} = -1,$$

whereas the incidence of edge 2 with face 2 yields

$$[A^2]^{22} = [\varrho_2^2, \varrho_1^2] = (-1)^{1+2+1} = 1,$$

compare Eq. (2.6). □

**Definition 2.1.6 (Boundary Operator)** A boundary operator  $\partial_p$  on  $p$ -chains is defined by

$$\partial_p : \mathcal{C}_p(\Omega) \longrightarrow \mathcal{C}_{p-1}(\Omega), \quad \sum_i^{n_p} c_i \varrho_p^i \longmapsto \sum_i^{n_p} c_i \sum_j^{n_{p-1}} [\varrho_p^i, \varrho_{p-1}^j] \varrho_{p-1}^j. \quad (2.7)$$

◇

The following diagram commutes:

$$\begin{array}{ccc} c & \xrightarrow{\partial_p} & b \\ \cong \downarrow & & \downarrow \cong \\ \{c\} & \xrightarrow{[A^p]} & \{b\}. \end{array}$$

**Example:** The  $n_1 \times n_2$  incidence matrix  $[A^2]$  of the 2-complex in Fig. 2.2 (left) reads

$$[A^2] = \begin{pmatrix} 1 & 0 & 0 & 0 & 0 \\ 1 & 0 & 0 & 0 & -1 \\ -1 & 1 & 0 & 0 & 0 \\ 0 & 1 & 0 & 0 & 0 \\ 0 & -1 & 1 & 0 & 0 \\ 0 & 0 & 1 & 0 & 0 \\ 0 & 0 & 1 & -1 & 0 \\ 0 & 0 & 0 & 1 & 0 \\ 0 & 0 & 0 & 1 & -1 \\ 0 & 0 & 0 & 0 & -1 \end{pmatrix} \quad (2.8)$$

With  $\{f\} = (1, 0, 1, 1, 1)^T$  we obtain the boundary coefficients of the 2-chain  $f$  by

$$\{\partial f\} = [A^2]\{f\} = (1, 0, -1, 0, 1, 1, 0, 1, 0, -1)^T.$$

It can easily be verified in Fig. 2.2 (left) that this 1-chain is the boundary of the 2-chain in Fig. 2.2 (right).  $\square$

An important property of the boundary operator,

$$\partial_p \partial_{p+1} = 0, \quad (2.9)$$

i.e., the boundary of a boundary is empty. This property translates into

$$[A^p][A^{p+1}] = 0. \quad (2.10)$$

### 2.1.4 Homology Classes

The investigation of the topological properties of an  $n$ -dimensional simplicial complex essentially consists of the search for holes and cavities in the complex. If there is none, we call the complex (or manifold) *contractible*<sup>1</sup>. The topology of a complex is encoded in its boundary operators and thus by isomorphism, in its incidence matrices. More precisely it is the kernel and the image of the incidence matrices that yield information on the existence of holes and cavities in a topology.

We call the set of  $p$ -chains lying in the image of the boundary operator  $\partial_{p+1}$  the *boundary space*  $B_p(\Omega)$ . Those  $p$ -chains that are mapped to 0 by  $\partial_p$ , i.e., those that lie in the kernel of the boundary operator, form the *cycle space*  $Z_p(\Omega)$ . For 1-cycles this denomination is most intuitive. Because of  $\partial_p \partial_{p+1} = 0$ , the  $p$ -boundary space is a subset of the  $p$ -cycle space.

It has been shown, e.g. in [20], that a topology has a hole (or cavity) if there exist  $p$ -cycles which are not themselves boundaries of a  $(p+1)$ -chain,  $p = 1, 2$ .

<sup>1</sup>On a contractible  $n$ -manifold, any  $(n-1)$  submanifold can be smoothly contracted into a point.

These cycles belong to the *homology space*  $H_p(\Omega)$  which is defined as the quotient of the cycle space and the boundary space  $H_p(\Omega) = Z_p(\Omega)/B_p(\Omega)$ . The elements of the quotient space are equivalence classes of cycles  $[h^k] = z^k + B_p$  with  $z^k \in Z_p(\Omega)$ ; a homology class is the sum of a cycle and an arbitrary element of the boundary space.

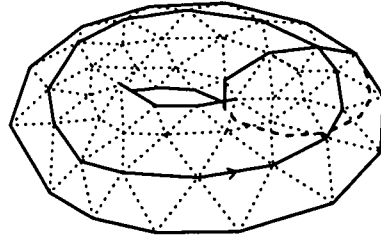


Figure 2.4: Discretization of the surface of a torus. Two members of the 1st homology space are displayed.

Fig. 2.4 shows a discretization of a torus surface, which is a 2-dimensional simplicial complex. It also displays two cycles  $h^1$  and  $h^2$  with  $\partial_1 h^i = 0$ .  $h^1$  and  $h^2$  cannot be expressed as boundaries  $\partial_2 f$  of any 2-chain  $f \in C_2(\Omega)$ . There are two holes in a torus surface, one being the middle of the ring and the other one being the inside of the torus. Topologically, this translates into the torus complex having a rank-2 homology space  $H_1(\Omega)$ , i.e., there are exactly two distinct equivalence classes of 1-cycles that are not boundaries of 2-chains. The two cycles in Fig. 2.4 are instances of these two homology classes. A "real-world" example for a cell complex with a non-empty homology space is given in Fig. 10.3. Fig. 2.5 illustrates how two cycles belonging to the same homology class differ from each other only by a boundary.

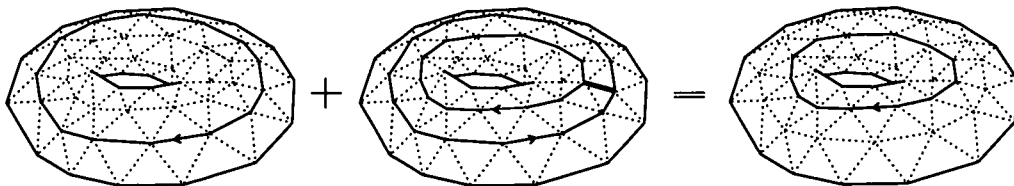


Figure 2.5: A member of a homology class plus a boundary gives another member of the same homology class.

Any cycle  $z \in Z_p(\Omega)$  can be decomposed into a linear combination of a boundary and one instance of each homology class,  $z = b + h^1 + \dots + h^{n_{H_p}}$ , with  $b \in B_p(\Omega)$ ,  $[h^1], \dots, [h^{n_{H_p}}] \in H_p(\Omega)$  and  $n_{H_p} = \dim H_p(\Omega)$ .

The determination of instances of homology classes from the incidence matrices of a complex is not within the scope of this thesis. Finding those instances of

homology classes, however, plays an important role in the discretization of the electromagnetic theory. We therefore state that efficient algorithms for their determination, relying on graph theory and algebraic topology exist, e.g., [16].

## 2.2 Cell Complex

For an efficient discretization of spatial domains, modern mesh-generators use a combination of different polyhedral elements such as hexahedra, prisms, tetrahedra and pyramids. Simplices account only for tetrahedron-shaped elements. We need to be equipped with more general tools to capture the properties of such "mixed complexes".

### 2.2.1 Cells

In analogy to the simplicial complex and chain above, we introduce the more general concept of a *cell complex* and of *chains of cells*. We denote by  $\Omega$  an  $n$ -dimensional bounded manifold.

**Definition 2.2.1 (Cell)** A  $p$ -cell  $\varrho_p$  is a  $p$ -dimensional, differentiable submanifold of  $\Omega$ . We denote  $C_p$  a set of  $p$ -cells and by  $n_p$  the number of  $p$ -cells in the set.  $\diamond$

**Definition 2.2.2 (Cell Complex)** A cell complex is a set  $C$  of cells of dimension  $p = 0, \dots, n$  that fulfills the following criteria:

1. Distinct cells are disjoint (regardless of dimension).
2. The intersection of the closures<sup>2</sup> of two cells (regardless of dimension) is either empty or it coincides with the closure of one and only one cell, be it one of the two above or a third cell.
3. The boundary of each  $p$ -cell,  $p \geq 1$ , is the union of a finite number of closures of  $(p - 1)$ -cells.
4. The union of the closures of all  $n$ -cells is equal to the closure of  $\Omega$ .

$\diamond$

Any simplicial complex defines a cell complex: Denote by  $\partial\sigma$  the union of the sides of a simplex<sup>3</sup>; we call  $\sigma \setminus \partial\sigma$  the *open simplex*. Open simplices are cells. The complex of open simplices is a cell complex. Cell complexes are far more flexible than simplicial ones. Their elements can have any polyhedral shape (hexahedra, prims, pyramids, triangles, rectangles). They may as well have non-polyhedral shapes if only the above conditions are met. In this thesis, however, we will assume cells to be polyhedral.

---

<sup>2</sup>The closure of a manifold  $m$  is  $m \cup \partial m$ , the manifold including its boundary. The interior of  $m$  is  $m \setminus \partial m$ , i.e., the manifold without its boundary.

<sup>3</sup>In slight notational abuse we identify the mapping  $\varrho$  and its image in  $\Omega$ .

**Redfinition 2.1.5 (Chains)** Let  $C_p(\Omega)$  denote the linear space of  $p$ -cells over some field  $\mathbb{K}$ . We call it the  $p$ -chain space. Its elements read

$$\mathfrak{c} = c_1 \mathfrak{c}_p^1 + \cdots + c_{n_p} \mathfrak{c}_p^{n_p}, \quad c_i \in \mathbb{K}, \mathfrak{c}_p^i \in C_p. \quad (2.11)$$

◇

A chain is oriented by orienting the tangent-spaces of its cells. Incidence numbers for cell complexes are defined as follows:

Let  $\mathfrak{c}_{p-1}^j$  be a side of  $\mathfrak{c}_p^i$ . Add an outward-pointing vector to the tangent-space basis of  $\mathfrak{c}_{p-1}^j$  as a  $p$ th basis vector. If the new basis yields a positive orientation of  $\mathfrak{c}_p^i$ , the incidence number  $[\mathfrak{c}_p^i, \mathfrak{c}_{p-1}^j]$  is  $+1$ , otherwise it is  $-1$ . It is zero if  $\mathfrak{c}_{p-1}^j$  does not belong to the boundary of  $\mathfrak{c}_p^i$ . More on the orientation of bounded manifolds can be found for example in [21].

Of course, the canonical basis isomorphism assigns a tuple in  $\mathbb{K}^{n_p}$  to any chain of cells and the commutative diagram of Section 2.1.3 still holds.

## 2.2.2 Outer Orientation

A manifold, e.g., a surface can be oriented in two ways: it can be assigned an inner orientation by choosing a sense of twist (given by the ordering of the vertices in case of a 2-simplex or by the ordering of its tangent vectors for a 2-cell), or it can be assigned a sense of passage.

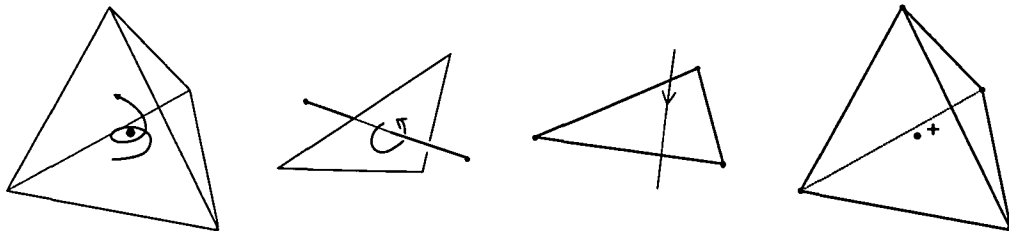


Figure 2.6:  $p$ -cells (simplices),  $p = 0, \dots, 3$ , endowed with outer orientation by "crossing"  $(n - p)$ -simplices.

Outer orientation cannot be assigned to a cell as such. As the name *outer* orientation suggests, additional information is needed.

**Definition 2.2.3 (Outer Orientation (1))** The outer orientation of a  $p$ -cell is given by the pair of an inner orientation of the  $p$ -cell and an inner orientation of the "ambient"  $n$ -manifold  $\Omega$ . Take an ordered set of  $p$  tangent-vectors of the  $p$ -cell and add to the ordering  $(n - p)$  tangent vectors of  $\Omega$  in positions  $p + 1, \dots, n$ . Choose and order the  $(n - p)$  tangent vectors such that the resulting set of  $n$  vectors forms a positively oriented basis of the tangent space of the ambient manifold  $\Omega$ . The

ordered orthogonal complement of a  $p$ -cell's tangent vectors, i.e., the last  $(n - p)$  ordered tangent vectors of the tangent space of  $\Omega$ , is called the *positive outer orientation* of the  $p$ -cell.  $\diamond$

The following definition is equally valid:

**Definition 2.2.4 (Outer Orientation (2))** The outer orientation of a  $p$ -cell is given by the inner orientation of a crossing  $(n - p)$ -cell. By "crossing" we understand, that the  $p$ -cell  $\varrho_p$  and the inner oriented  $(n - p)$ -cell  $\bar{\varrho}_{n-p}$  intersect in a point.  $\diamond$

Fig. 2.6 yields a visualization of outer orientation of different simplicial cells. A point is assigned a screw-rule, a line a sense of twist, a surface a sense of passage and a volume is oriented by a sign.

# 3

## Discretization of Fields

We know that the physical quantities of electromagnetism, e.g., electric voltage and magnetic flux, are obtained from the electromagnetic fields by integration over manifolds (points, lines, surfaces or volumes). Electric voltage is obtained from a point evaluation of the scalar potential or from the integral of the electric field along a line. Magnetic flux is the result of an integration of the magnetic vector potential along a closed line or of the magnetic induction over a surface. Accordingly, in modern vector-analysis the electric scalar potential is modelled by a 0-form, the electric field and the magnetic vector potential by a 1-form and the magnetic induction by a 2-form. The degree of the form corresponds to the dimension of the integration domain, compare Annex B.

This chapter presents a discretization scheme for electromagnetic fields in terms of integral quantities: a discrete scalar potential is found to be a set of point evaluations in the nodes of the cell complex; a discrete electric field is given by the line integrals of the electric field along the edges of the cell complex; the magnetic induction is integrated over the faces in the complex, and so forth. Mathematically speaking, we define the cospaces of the  $p$ -chain spaces, that were introduced in the previous chapter. Discrete fields are cochains. The coboundary operator represents a derivative operator and the cohomology spaces yield information on the reversibility of the Poincaré lemma.

Section 3.2 introduces a novel notation that allows to include contributions of concentrated fields, e.g., surface currents or surface charges, to cochain coefficients. We first use this notation in Section 3.3 when we discretize cohomology contributions to discrete fields.

For a maximum of symmetry between the discrete and continuous settings, we use the differential form notation on manifolds to describe the continuous electromagnetic theory. From the vast amount of literature on the topic we recommend [2] as an introduction. A short collection of theorems and definitions can be found in Annex A.



## 3.1 Cochains and the Discretization of Maxwell Fields

### 3.1.1 Cochains

**Definition 3.1.1 (Cocell)** A  $p$ -cocell  $\underline{\varrho}^p$  is a mapping

$$\underline{\varrho}_i^p : C_p(\Omega) \longrightarrow \mathbb{K}, \underline{\varrho}_p^j \longmapsto \delta_i^j, \quad (3.1)$$

that assigns to the  $i$ th  $p$ -cell in a complex the unit element of a field  $\mathbb{K}$ , mostly  $\mathbb{R}$  or  $\mathbb{C}$  and zero to all others.  $\delta_i^j$  is the Kronecker delta. The set of cocells is denoted by  $C^p$  with a superscript dimension-index to distinguish it from the set of cells (subscript dimension-index).  $\diamond$

**Definition 3.1.2 (Cochains)** The  $p$ -cochain space  $C^p(\Omega)$  is the linear space of cocells over a field  $\mathbb{K}$ , usually  $\mathbb{R}$  or  $\mathbb{C}$ . Its elements read

$$\underline{F} = F^1 \underline{\varrho}_1^p + \cdots + F^{n_p} \underline{\varrho}_{n_p}^p, \quad F^i \in \mathbb{K}, \underline{\varrho}_i^p \in C^p(\Omega). \quad (3.2)$$

$\diamond$

Following the convention we use superscripts to indicate the dimension of the cochain space, whereas we used subscripts for the chain-space dimension. Cochains are denoted by an under-hat. The  $n_p$ -tuples of coefficients of  $p$ -cochains are written in braces,  $\{F\}$ , as we did for chains. Cochains will be used to assign integral values of Maxwell fields to the corresponding  $p$ -cells in a complex.

### 3.1.2 Integral Quantities and Related Maxwell Equations

The Maxwell fields in a 3-dimensional representation are localizations of four integral quantities: voltage  $U$ , magnetic flux  $\Phi$ , electric charge  $Q$  and electric current  $I$ . The integral quantities are obtained from the respective  $p$ -forms by integration over inner or outer oriented  $p$ -manifolds, compare Annex B. We use the duality-product notation for an integral of a differential form  $\underline{F} \in \mathcal{F}^p(m)$  over a  $p$ -manifold  $m$ :

$$\int_m \underline{F} = \langle \underline{F} | m \rangle.$$

We use  $e$ ,  $f$  and  $v$  for 1, 2 and 3-dimensional manifolds (edges, faces and volumes). The electromagnetic fields are integrated as follows:

$$\begin{aligned} U &= -\langle \underline{\varphi} | \partial e \rangle - \langle \partial_t \underline{A} | e \rangle = \underline{\varphi}^1 - \underline{\varphi}^2 - \langle \partial_t \underline{A} | e \rangle, \\ &= \langle \underline{E} | e \rangle, \\ \Phi &= \langle \underline{A} | \partial f \rangle = \langle \underline{B} | f \rangle, \\ Q &= \langle \underline{\tilde{D}} | \partial \tilde{v} \rangle = \langle \underline{\tilde{\rho}} | \tilde{v} \rangle, \\ I &= \langle \underline{\tilde{H}} | \partial \tilde{f} \rangle - \langle \partial_t \underline{\tilde{D}} | \tilde{f} \rangle = \langle \underline{\tilde{j}} | \tilde{f} \rangle. \end{aligned} \quad (3.3)$$

The tilde-sign indicates outer orientation. The under-bar denotes differential forms, compare the reference of notations used in the thesis on page 1.

Chains and cochains are used to model physical quantities in a discrete setting. Mathematical objects that represent physical quantities have to be equipped with a structure that represents their physical dimension. We will give a short introduction to physical dimensions in a mathematical context. A more detailed survey can be found in [27].

**Definition 3.1.3 (Dimension System)** A dimension system  $\mathcal{D}$  has the structure of a multiplicative module over a ring  $R$  which is  $\mathbb{Z}$  or  $\mathbb{Q}$ .  $1_{\mathcal{D}}$  is the unit element. A basis of  $\mathcal{D}$  is a set  $\{D_1, D_2, \dots, D_r\} \subset \mathcal{D}$  with the properties

$$D_1^{q_1} D_2^{q_2} \dots D_r^{q_r} = 1_{\mathcal{D}} \implies q_1 = q_2 = \dots = q_r = 0, \quad \forall q_i \in R,$$

and

$$\{D_1^{q_1} D_2^{q_2} \dots D_r^{q_r} \mid q_i \in R\} = \mathcal{D},$$

where  $r$  is the rank of the module. ◇

For the purposes of this thesis we use

$$\{\mathbb{L}, \mathbb{T}, \mathbb{U}, \mathbb{I}\}$$

as a basis for the dimension system, that is length, time, voltage and electrical current. All other relevant physical dimensions can be derived from these basis dimensions. A dimension mapping is introduced that assigns a physical dimension to a set  $\mathcal{S}$  of mathematical objects:

$$pd : \mathcal{S} \longrightarrow \mathcal{D}, \quad x \longmapsto pd(x).$$

**Example:**

$$pd(\underline{B}) = \mathbb{U}\mathbb{T}, \quad pd(\underline{\tilde{D}}) = \mathbb{I}\mathbb{T}, \quad pd(\underline{\tilde{H}}) = \mathbb{I}, \quad pd(\mu_0) = \mathbb{U}\mathbb{T}\mathbb{I}^{-1}.$$

□

The mathematical objects used for numerical field computation are tuples of real or complex numbers with physical dimension  $1_{\mathcal{D}}$ . In order to derive a dimensionless discrete formulation it is useful to relate the mathematical objects involved to some typical quantities, e.g.,  $L_0, T_0, U_0, I_0$ , of which further quantities may be derived. We introduce related differential forms for electromagnetic quantities. The following examples illustrate the procedure:

$$\underline{B}' = \underline{B} \Phi_0^{-1}, \quad \underline{A}' = \underline{A} \Phi_0^{-1}, \quad \underline{j}' = \underline{j} I_0^{-1}. \quad (3.4)$$

The physical dimension of the primed quantities is  $1_D$ , e.g.,

$$pd(\underline{A}') = pd(\underline{A}) pd(\Phi_0^{-1}) = \mathbf{U} \mathbf{T} \mathbf{U}^{-1} \mathbf{T}^{-1} = 1_D.$$

The set of typical quantities needs to be chosen in accordance with the problem type. Some choices might be more useful than others. In this thesis we will mostly deal with field problems that can be formulated in the magneto(quasi)static approximation of the Maxwell equations. Accordingly, we suggest the following set of typical quantities built of problem specific quantities: the typical magnetic flux  $\Phi_0$ , the typical electric conductivity  $\kappa_0$  and the magnetic reluctivity of free space  $\nu_0 = \frac{1}{\mu_0}$ . We derive further typical quantities:

$$T_d = \frac{\kappa_0}{\nu_0}, \quad U_0 = \frac{\Phi_0}{T_d}, \quad I_0 = \kappa_0 U_0 = \nu_0 \Phi_0. \quad (3.5)$$

$T_d$  is called the diffusion time. In magneto(quasi)statics the charge-related forms  $\underline{\tilde{D}}$  and  $\underline{\tilde{\rho}}$  do not figure in the Maxwell equations. They could, however be related to a typical charge  $Q_0 = T_d I_0$ .

The so-called curl-curl equation,

$$d*\nu d\underline{A} + *\kappa \partial_t \underline{A} = \underline{\tilde{j}}_s, \quad (3.6)$$

reads in a related form

$$d*\nu_r d\underline{A}' + *\kappa' \partial_t \underline{A}' = \underline{\tilde{j}}_s', \quad (3.7)$$

where  $\nu_r = \nu/\nu_0$  is called the relative magnetic reluctivity. According to proposition (3.5), the above curl-curl equations (3.6) and (3.7) are related via a division by  $\nu_0 \Phi_0$ . Generally,  $\Phi_0$  is chosen to be 1 Vs. In the following we will assume all quantities to be related to typical quantities in the way that is suggested in Eq. (3.4). Unless otherwise stated, we will use the SI-units as typical quantities:  $L_0 = 1 \text{ m}$ ,  $T_0 = 1 \text{ s}$ ,  $U_0 = 1 \text{ V}$  and  $I_0 = 1 \text{ A}$ . The derived quantities read  $\Phi_0 = 1 \text{ Vs}$  and  $Q_0 = 1 \text{ As}$ . This choice of little sophistication will allow us to deal with tuples and matrices of real numbers instead of physical quantities. The primes will generally be omitted in the notation.

### 3.1.3 Discretization of the Faraday Complex

We use cochains to discretize the electromagnetic fields. The  $i$ th coefficient of a  $p$ -cochain  $\underline{F}$  is determined by integrating the  $p$ -form over the  $i$ th  $p$ -cell in the complex,

$$\{F\}^i = \langle \underline{F} | \underline{g}_p^i \rangle.$$

The discretization of the Faraday complex is straight forward. The fields  $\varphi$ ,  $\underline{A}$ ,  $\underline{E}$ ,  $\underline{B}$  and possibly the 2-form of a magnetic current and the 3-form of a magnetic

charge density, denoted  $\underline{j}_M$  and  $\underline{\rho}_M$ , are integrated over the respective inner oriented  $p$ -cells: the 0-form  $\underline{\varphi}$  is evaluated in nodes  $\underline{g}_0^i$ ,  $i = 1, \dots, n_0$ , the 1-forms  $\underline{A}$  and  $\underline{E}$  are integrated along edges  $\underline{g}_1^j$ ,  $j = 1, \dots, n_1$ , the 2-forms  $\underline{B}$  and  $\underline{j}_M$  are integrated over faces  $\underline{g}_2^k$ ,  $k = 1, \dots, n_2$  and the 3-form  $\underline{\rho}_M$  is integrated over volumes  $\underline{g}_3^l$ ,  $l = 1, \dots, n_3$ .

We have thus obtained the coefficient vectors  $\{\varphi\}$ ,  $\{A\}$ ,  $\{E\}$  and  $\{B\}$  of the cochains  $\underline{\varphi}$ ,  $\underline{A}$ ,  $\underline{E}$  and  $\underline{B}$ . The integral value of a cochain over a chain is given by a duality product<sup>1</sup>, e.g.:

$$U(\underline{c}) = \langle \underline{E} | \underline{c} \rangle = \{c\}^T \{E\}. \quad (3.8)$$

### 3.1.4 Coboundary Operator

The coboundary operator is a mapping  $d_p : \mathcal{C}^p(\Omega) \longrightarrow \mathcal{C}^{p+1}(\Omega)$ . By isomorphism between a cochain and its coefficient vector the coboundary operator can be represented in matrix-form. It is given by the transpose of the incidence matrix:

$$[D^p] := [A^{p+1}]^T. \quad (3.9)$$

The following diagram commutes:

$$\begin{array}{ccc} \underline{G} & \xrightarrow{d_p} & \underline{F} \\ \cong \downarrow & & \downarrow \cong \\ \{G\} & \xrightarrow{[D^p]} & \{F\}, \end{array}$$

where  $\underline{G} \in \mathcal{C}^p(\Omega)$ ,  $\underline{F} \in \mathcal{C}^{p+1}(\Omega)$ ,  $\{G\} \in \mathbb{R}^{n_p}$ , and  $\{F\} \in \mathbb{R}^{n_{p+1}}$ . We will see that coboundary operator is a discrete derivative operator. The definition of the coboundary operator assures that the Stokes Theorem, which reads

$$\langle \underline{F} | \partial c \rangle = \langle d\underline{F} | c \rangle,$$

for differential forms on bounded manifolds, holds also for chains and cochains and their coefficient vectors:

$$\begin{aligned} \langle \underline{F} | \partial_{p+1} c \rangle &= \langle d_p \underline{F} | c \rangle, \\ ([A^{p+1}]\{c\})^T \{F\} &= \{c\}^T [A^{p+1}]^T \{F\} = \{c\}^T [D^p] \{F\}. \end{aligned}$$

The discrete coboundary operator acting on cochains is a valid discretization of the continuous coboundary operator, i.e., of the exterior derivative operator

<sup>1</sup>Note that the right equality in Eq. (3.8) holds only if we use a related quantity  $\underline{E}$ , compare Section 3.1.2. Otherwise the product of coefficient vectors (tuples of real numbers) would yield a real number, whereas the duality product of a chain and a cochain would yield a physical quantity, represented by a real number with a physical unit.

$d : \mathcal{F}^p(\Omega) \rightarrow \mathcal{F}^{p+1}(\Omega)$  that maps  $p$ -forms into  $(p+1)$ -forms. The exterior derivative yields a gradient operator when it acts on 0-forms, a curl operator on 1-forms and a divergence operator on 2-forms. By analogy  $[D^0]$  represents a discrete gradient,  $[D^1]$  a discrete curl and  $[D^2]$  a discrete divergence operator.

The following examples demonstrate in which way the coboundary operator is indeed a discretization of the exterior derivative:

**Examples:**

1.  $\underline{E} = -d\underline{\varphi} - \partial_t \underline{A}$  translates into  $\{E\} = -[D^0]\{\varphi\} - \{\partial_t A\}$ :

$$\begin{aligned} \{E\}^j &= \langle \underline{E} | \underline{g}_1^j \rangle = -\langle d\underline{\varphi} + \partial_t \underline{A} | \underline{g}_1^j \rangle \\ &= -\langle \underline{\varphi} | \partial_1 \underline{g}_1^j \rangle - \langle \partial_t \underline{A} | \underline{g}_1^j \rangle \\ &= -(\langle \underline{\varphi} | \underline{g}_0^2 \rangle - \langle \underline{\varphi} | \underline{g}_0^1 \rangle) - \langle \partial_t \underline{A} | \underline{g}_1^j \rangle \\ &= -[D^0]^{j*}\{\varphi\} - \{\partial_t A\}^j, \end{aligned}$$

where  $\underline{g}_0^1$  and  $\underline{g}_0^2$  denote the bounding nodes of edge  $j$  and  $[D^0]^{j*}$  denotes the  $j$ th row of  $[D^0]$ .

2.  $\underline{B} = d\underline{A}$  translates into  $\{B\} = [D^1]\{A\}$ :

$$\{B\}^k = \langle \underline{B} | \underline{g}_2^k \rangle = \langle d\underline{A} | \underline{g}_2^k \rangle = \langle \underline{A} | \partial_2 \underline{g}_2^k \rangle = [D^1]^{k*}\{A\}.$$

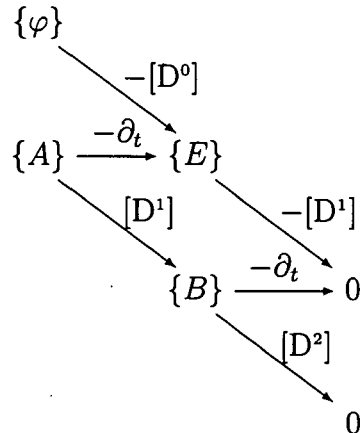
3. Similarly, the Faraday law,  $d\underline{E} = -\partial_t \underline{B}$ , reads in its discrete representation  $[D^1]\{E\} = -\{\partial_t B\}$  and the Gauss law  $d\underline{B} = 0$  translates to  $[D^2]\{B\} = 0$ .  $\square$

A discretization of the 1<sup>st</sup> Poincaré lemma follows directly from Eq. (2.10):

$$([A^p][A^{p+1}])^T = [A^{p+1}]^T[A^p]^T = [D^p][D^{p-1}] = 0. \quad (3.10)$$

This is a discretization of  $dd = 0$  which generalizes the  $\text{rot grad} = 0$  and  $\text{div rot} = 0$  identities in classical vector analysis.

At this point we can summarize the topological laws of what we shall call the *Faraday complex* in a topological diagram (also denoted Maxwell's house, [5], or Tonti-diagram, [33]):



Every position in the diagram is to be read as the sum over incoming arrows.

### 3.1.5 Discretization of the Ampère-Maxwell Complex

The integrals of the Ampère-Maxwell fields  $\tilde{H}$ ,  $\tilde{D}$ ,  $\tilde{j}$  and  $\tilde{\rho}$  (and possibly an electric vector potential  $\tilde{V}$  and a magnetic scalar potential  $\tilde{\varphi}_M$ ) over a manifold are, by definition, independent of the inner orientation of the manifold. The sign of the integrated Ampère-Maxwell fields is decided by an outer orientation, e.g., by assigning a sense of passage to a surface that allows to count charges per unit of time as a positive or negative current.

Recall that an outer orientation of a  $p$ -dimensional submanifold  $K$  of an  $n$ -dimensional manifold  $M$ ,  $K \subseteq M$ , is given by the orientation of an  $(n-p)$ -dimensional submanifold  $L$ ,  $L \subset M$ . The orientation of  $L$  is chosen such that the ordered tangent vectors of  $K$  plus the ordered tangent vectors of  $L$  yield a positively oriented basis of the tangent space of  $M$ , compare Definition 2.2.3. Now we see that a change in inner orientation of  $K$  and  $M$  leaves the induced orientation of  $L$  unchanged. An integral of an Ampère-Maxwell field over an outer oriented manifold thus does not change sign under a change of inner orientation. This property distinguishes Ampère-Maxwell fields from Faraday fields.

Differential forms on outer oriented manifolds are called odd forms, those on inner oriented manifolds are called even forms. Mathematically, odd forms differ from even forms in that they "sense" a change of inner orientation of the manifold by changing their sign. The integral value of an odd form thus remains unchanged under a change of inner orientation, whereas the integral of an even form changes its sign. We denote odd forms by a tilde sign, indicating that they are meant to be integrated over outer oriented manifolds. We also denote outer oriented manifolds with tilde signs.

We use  $p$ -cochains  $\tilde{F} \in \tilde{C}^p(\Omega)$  acting on outer oriented chains  $\tilde{c} \in \tilde{C}_p(\Omega)$  to discretize odd  $p$ -forms. The following examples illustrate the discretization of Ampère-Maxwell fields on an outer oriented cell complex. We denote also the matrix operators acting on cochain coefficients of odd differential forms with the tilde sign.

#### Examples:

1. The discrete Ampère-Maxwell Law  $\tilde{j} = d\tilde{H} - \partial_t \tilde{D}$  reads  $\{\tilde{j}\} = [\tilde{D}^1]\{\tilde{H}\} - \{\partial_t \tilde{D}\}$ :

$$\begin{aligned} \{\tilde{j}\}^i &= \langle \tilde{j} | \tilde{c}_2^i \rangle = \langle d\tilde{H} - \partial_t \tilde{D} | \tilde{c}_2^i \rangle = \langle \tilde{H} | \partial_2 \tilde{c}_2^i \rangle - \langle \partial_t \tilde{D} | \tilde{c}_2^i \rangle \\ &= [\tilde{D}_0^1]^{i*} \{\tilde{H}\} - \{\partial_t \tilde{D}\}^i. \end{aligned}$$

2.  $\tilde{\rho} = d\tilde{D}$  translates to  $\{\tilde{\rho}\} = [\tilde{D}^2]\{\tilde{D}\}$ :

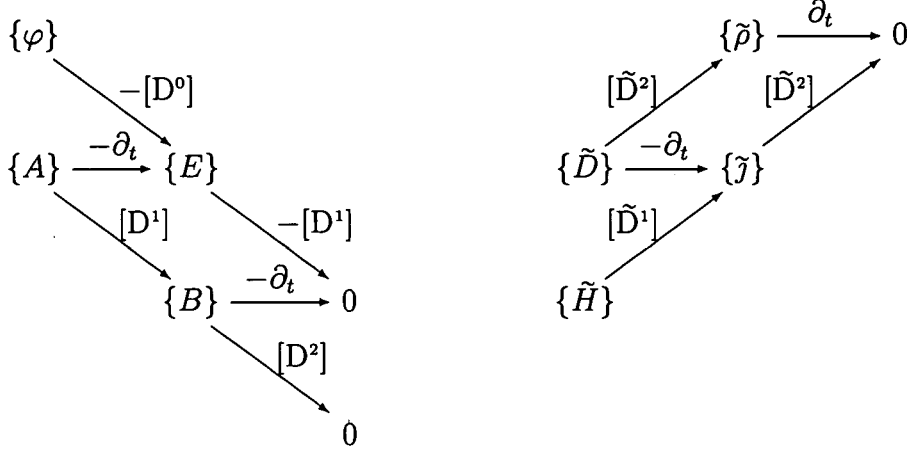
$$\{\tilde{\rho}\}^j = \langle \tilde{\rho} | \tilde{c}_3^j \rangle = \langle d\tilde{D} | \tilde{c}_3^j \rangle = \langle \tilde{D} | \partial_3 \tilde{c}_3^j \rangle = [\tilde{D}^2]^{j*} \{\tilde{D}\}.$$

3. Charge conservation  $d\tilde{j} = -\partial_t \tilde{\rho}$  is represented by  $[\tilde{D}^2]\{\tilde{j}\} = -\{\partial_t \tilde{\rho}\}$ :

$$\{d\tilde{j}\}^k = \langle d\tilde{j} | \tilde{c}_3^k \rangle = \langle \tilde{j} | \partial_3 \tilde{c}_3^k \rangle = [\tilde{D}^2]^{k*} \{\tilde{j}\} = -\{\partial_t \tilde{\rho}\}^k.$$

□

The *Ampère-Maxwell complex* can now be added to the topological diagram:



We note that this diagram comprises all the topological equations of the discrete electromagnetic theory. The equations hold on any cell complex, regardless of measures or shapes. Metric considerations enter the theory in the material equations, relating the Faraday with the Ampère-Maxwell complex. The metric laws will be treated to some extent at a later stage.

### 3.2 Discretization of deRham Currents

Electromagnetic fields are often concentrated on surfaces, lines or points.<sup>2</sup> Common examples are surface-, line- or point-charges and surface- or line-currents. These concentrated fields are mathematically described by so-called *deRham Currents*<sup>3</sup> DeRham Currents are an extension to differential forms in the way distributions extend mathematical functions to describe singularities such as jump discontinuities and their derivatives. The above mentioned concentrated fields are described by deRham Currents which are zero everywhere on a  $p$ -dimensional manifold except on an  $r$ -dimensional submanifold, where they are infinite. The integral over the manifold, equals the integral of an  $r$ -form over the submanifold and is finite. We denote concentrated fields with under-bars and two indices:  $\underline{F}^p$ . For a standard differential form we have  $\underline{F} = \underline{F}^p$ . Throughout this section we may want to express by  $\underline{F} = \underline{F}^p + \underline{F}^{p-1} + \dots + \underline{F}^0$  the total distribution of a field on a manifold including its singular concentrations.

**Examples:**

1. The *delta-distribution* (or Dirac-impulse)

$$\delta(x) := \begin{cases} \infty & \text{for } x = 0 \\ 0 & \text{for } x \neq 0 \end{cases}, \quad \int_{-\infty}^{\infty} \delta(x) dx = \int_{0^-}^{0^+} \delta(x) dx = 1,$$

<sup>2</sup>In this section we assume the boundary  $\partial_q \mathfrak{s}_q$  of the support  $\mathfrak{s}_q$  of concentrated fields to be identical with the intersection of  $\mathfrak{s}_q$  with the domain boundary  $\partial\Omega$ .

<sup>3</sup>Georges deRham introduced currents initially with surface currents and line currents in mind - hence the name 'current'.

may be interpreted as a 1-deRham Current  $\underline{\delta} = \underline{\delta}_0^1$  on the 1-manifold of real numbers  $\mathbb{R}$ . The integral of  $\underline{\delta}$  over  $\mathbb{R}$  is defined as

$$\langle \underline{\delta}_0^1 | \mathbb{R} \rangle = \langle \underline{e} | 0 \rangle = 1, \quad (3.11)$$

where  $\underline{e} = 1$  is the unit 0-form.

2. We determine the electric current through an outer oriented face  $\tilde{f}$ . The electric current is concentrated in a 2-dimensional manifold  $\tilde{s}$  which cuts the face  $\tilde{f}$  in a 1-dimensional submanifold  $\tilde{f} \cap \tilde{s}$ . The concentrated current is described as a deRham Current  $\tilde{j}_1^2$  that is zero everywhere in  $\tilde{f}$  except on  $\tilde{f} \cap \tilde{s}$ , where it is infinite. The integral of  $\tilde{j}_1^2$  over  $\tilde{f}$  equals the integral of a surface-current 1-form  $\tilde{K}$  living on  $\tilde{s}$  over  $\tilde{f} \cap \tilde{s}$ . Fig. 3.1 illustrates the example. The total current through the face is given by:

$$I(\tilde{f}) = \langle \tilde{j}_1^2 | \tilde{f} \rangle = \langle \tilde{K} | \tilde{f} \cap \tilde{s} \rangle. \quad (3.12)$$

□

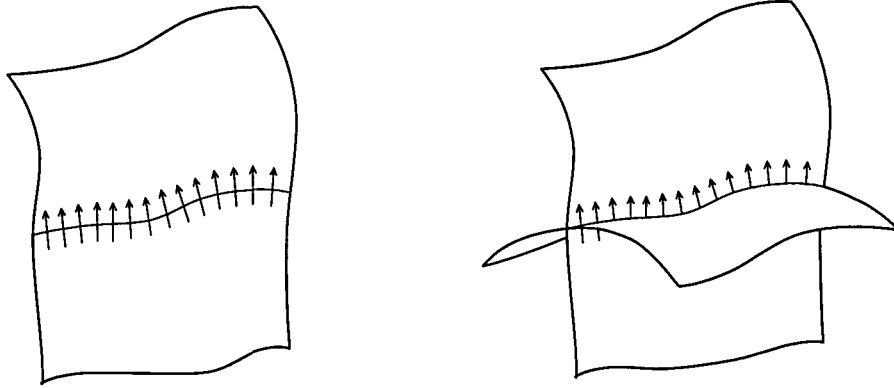


Figure 3.1: Left: A surface current in a 2-dimensional manifold. Surface currents are odd 1-forms to be integrated over outer oriented 1-submanifolds. Note that outer orientation of a line in a 2-dimensional manifold is given by a sense of passage through the line. Right: Surface currents cutting through a face, contributing to the total current through that face.

To cope with the following tasks, we introduce an integration of  $p$ -forms  $\underline{F} \in \mathcal{F}^p(\Omega)$  over  $p$ -chains  $\underline{c}_p \in \mathcal{C}_p(\Omega)$  by:

$$\langle \underline{F} | \underline{c}_p \rangle := c_1 \langle \underline{F} | \underline{c}_p^1 \rangle + \cdots + c_{n_p} \langle \underline{F} | \underline{c}_p^{n_p} \rangle. \quad (3.13)$$

Furthermore we define the intersection of a submanifold  $m \subset \Omega$  and a chain  $\underline{c}_p \in \mathcal{C}_p(\Omega)$  such that the result is a new chain:

$$m \cap \underline{c}_p := c_1 m \cap \underline{c}_p^1 + \cdots + c_{n_p} m \cap \underline{c}_p^{n_p}. \quad (3.14)$$

In particular the intersection of two chains is another chain.



Assume that the  $p$ -chain  $\mathfrak{m}_p$  of all  $p$ -dimensional cells of an  $n$ -dimensional complex is intersected by a  $q$ -manifold (possibly a  $q$ -chain)  $\mathfrak{s}_q$ . The set of intersections is an  $r$ -chain of submanifolds,  $\mathfrak{c}_r = \mathfrak{m}_p \cap \mathfrak{s}_q \in \mathcal{C}_r(\Omega)$ ,  $r = q - (n - p) \geq 0$ ,  $n \geq p$ ,  $n > q$ . A  $p$ -form  $\underline{F}$  is concentrated on the  $q$ -submanifold, modeled by a deRham Current  $\underline{F}^p$ : For a surface current the dimension indices yield  $n = 3$ ,  $p = 2$ ,  $q = 2$  and  $r = 1$ ; for a surface charge  $n = 3$ ,  $p = 3$ ,  $q = 2$  and  $r = 2$  and for a line current  $n = 3$ ,  $p = 2$ ,  $q = 1$  and  $r = 0$ . Table 3.1 gives an overview of admissible combinations of  $p$ ,  $q$  and  $r$  in dimensions 1, 2 and 3:

The following expression gives the integral value of a combination of deRham

	$p$	$q$	$r$	$p$	$q$	$r$	$p$	$q$	$r$
$n=3$	3	2	2	2	2	1	1	2	0
	3	1	1	2	1	0			
	3	0	0						
$n=2$	2	1	1	1	1	0			
	2	0	0						
$n=1$	1	0	0						

Table 3.1: Admissible combinations of  $p$ ,  $q$ , and  $r$  on an  $n = 3$ -, 2- and 1-dimensional cell complex.  $p$  is the dimension of the form (deRham current) to be integrated over  $p$ -cells.  $q$  is the dimension of the manifold that intersects the  $p$ -cells and on which the  $p$ -form is concentrated.  $r$  is the dimension of the intersection submanifold.

Currents:

$$\langle \underline{F} | \mathfrak{m}_p \rangle = \langle \underline{F}_p^p + \underline{F}_{p-1}^p + \cdots + \underline{F}_0^p | \mathfrak{m}_p \rangle. \quad (3.15)$$

**Example:** The total electrical charge in a volume is given by:

$$\begin{aligned} Q(\tilde{\nu}) &= \langle \tilde{\rho}_3^3 + \tilde{\rho}_2^3 + \tilde{\rho}_1^3 + \tilde{\rho}_0^3 | \tilde{\nu} \rangle \\ &= \langle \tilde{\rho} | \tilde{\nu} \rangle + \langle \tilde{\sigma} | \tilde{\nu} \cap \tilde{\mathfrak{s}}_2 \rangle + \langle \tilde{\tau} | \tilde{\nu} \cap \tilde{\mathfrak{s}}_1 \rangle + \langle \tilde{q} | \tilde{\nu} \cap \tilde{\mathfrak{s}}_0 \rangle, \end{aligned} \quad (3.16)$$

with  $\tilde{\rho}$  the odd charge density 3-form,  $\tilde{\sigma}$  the surface charge 2-form,  $\tilde{\tau}$  the line charge 1-form and  $\tilde{q}$  the point charge. A similar relation can be given for the total electrical current through a face:

$$\begin{aligned} I(\tilde{f}) &= \langle \tilde{j}_2^2 + \tilde{j}_1^2 + \tilde{j}_0^2 | \tilde{f} \rangle \\ &= \langle \tilde{j}^2 | \tilde{f} \rangle + \langle \tilde{K} | \tilde{f} \cap \tilde{\mathfrak{s}}_2 \rangle + \langle \tilde{I} | \tilde{f} \cap \tilde{\mathfrak{s}}_1 \rangle, \end{aligned} \quad (3.17)$$

with  $\tilde{j}$  the odd current density 2-form,  $\tilde{K}$  the surface current 1-form and  $\tilde{I}$  the line current 0-form.  $\square$

Equation (3.15) paves the way for a discretization of deRham Current contributions to cochain coefficients:

$$\begin{aligned} \langle \underline{F} | \mathfrak{m}_p \rangle &= \{ \mathfrak{m}_p \}^T \{ F \} \\ &= \{ \mathfrak{m}_p \}^T ( \{ F_p^p \} + [dR_{p-1}^p] \{ F_{p-1}^p \} + \cdots + [dR_0^p] \{ F_0^p \} ) \end{aligned} \quad (3.18)$$

The  $[dR_r^p]$  matrices (deRham Current matrices) are rectangular matrices of  $n_p$  rows. The number of columns equals the number of  $p$ -cells that are intersected by the manifold (or chain)  $\mathfrak{s}_q$ , the intersections being  $r = q - (n - p)$ -dimensional submanifolds. The row and column entries are given by

$$[dR_r^p]^{ij} = \begin{cases} 1 & \text{if } \mathfrak{g}_p^i \text{ is the } j\text{th cell in } \mathfrak{m}_p \text{ to be intersected by } \mathfrak{s}_q, \\ 0 & \text{if } \mathfrak{g}_p^i \cap \mathfrak{s}_q = \emptyset, \text{ or if } \mathfrak{g}_p^i \text{ is the } k\text{th cell} \\ & \text{to be intersected by } \mathfrak{s}_q \text{ with } k \neq j. \end{cases} \quad (3.19)$$

**Example:** In the discrete (cochain) setting the coefficient vector of a current cochain in the presence of concentrated currents reads in accordance with Eq. (3.17):

$$\{\tilde{j}\} = \{\tilde{j}^2\} + [d\tilde{R}_1^2]\{\tilde{K}\} + [d\tilde{R}_0^2]\{\tilde{I}\}. \quad (3.20)$$

□

### Discretization of Jump Discontinuities

Jump discontinuities are another essential feature of the electromagnetic theory. There is a direct connection between the above introduced concentrated fields and jump discontinuities. Both are modeled by deRham Currents. The connection lies in the potential formulation of a concentrated field:

Let  $\underline{F} \in \mathcal{F}^p(\mathfrak{m}_p)$  be an odd  $p$ -form on an outer oriented  $p$ -manifold  $\mathfrak{m}_p$ . We call  $\underline{G} \in \mathcal{F}^{p-1}(\mathfrak{m}_p)$  a potential of  $\underline{F}$  if  $\underline{F} = d\underline{G}$ . Assume that  $\mathfrak{m}_p$  is intersected by a  $q = (n - 1)$ -dimensional manifold  $\mathfrak{s}_q$ . The intersection  $\mathfrak{m}_p \cap \mathfrak{s}_q$  is a  $(p - 1)$ -submanifold  $\mathfrak{c}_{p-1} \subset \mathfrak{s}_q$ . The intersecting manifold  $\mathfrak{s}_q$  divides the manifold  $\mathfrak{m}_p$  into two domains  $\mathfrak{m}_p^-$  and  $\mathfrak{m}_p^+$  with  $\mathfrak{m}_p^- \cup \mathfrak{m}_p^+ = \mathfrak{m}_p \setminus \mathfrak{c}_{p-1}$ . The inner orientation of  $\mathfrak{c}_{p-1}$  is chosen to be consistent with the inner orientation of  $\mathfrak{m}_p^-$ . An outer orientation of  $\tilde{\mathfrak{m}}_p$  induces an outer orientation of  $\tilde{\mathfrak{c}}_{p-1}$  in  $\tilde{\mathfrak{s}}_q$ .

Let now the  $p$ -form  $\underline{F}$  be in part concentrated on  $\mathfrak{s}_q$ ,  $\underline{F} = \underline{F}_p^p + \underline{F}_{p-1}^p$ . The integral of  $\underline{F}_{p-1}^p$  over  $\mathfrak{m}_p$  is given by the integral of a  $(p - 1)$ -form  $\underline{L}$  over  $\mathfrak{c}_{p-1}$ ,

$$\langle \underline{F} | \mathfrak{m}_p \rangle = \langle \underline{F}_p^p + \underline{F}_{p-1}^p | \mathfrak{m}_p \rangle = \langle \underline{F}_p^p | \mathfrak{m}_p \rangle + \langle \underline{L} | \mathfrak{c}_{p-1} \rangle. \quad (3.21)$$

The potential  $\underline{G}$  is defined on both domains  $\mathfrak{m}_p^-$  and  $\mathfrak{m}_p^+$  such that

$$\langle \underline{F}_p^p | \mathfrak{m}_p \rangle = \langle d\underline{G} | \mathfrak{m}_p^- \rangle + \langle d\underline{G} | \mathfrak{m}_p^+ \rangle = \langle d\underline{G} | \mathfrak{m}_p \setminus \mathfrak{c}_{p-1} \rangle. \quad (3.22)$$

$\underline{G}$  is not defined on  $\mathfrak{c}_{p-1}$  and so neither is  $d\underline{G}$ . The traces  $\mathfrak{t} \underline{G}$  on both sides of the singularity, however, exist and are finite. The difference of the traces on both sides is called the jump of the potential:

$$\mathfrak{j} \underline{G} := \mathfrak{t}^+ \underline{G} - \mathfrak{t}^- \underline{G}.$$

Forms with  $\mathbf{j}\mathcal{G} \neq 0$  are described by deRham Currents. Here again deRham currents extend the classical definition of forms to include singularities. It can be shown that the jump of the potential,  $\mathbf{j}\mathcal{G}$ , yields the  $(p-1)$ -form  $\underline{L}$  which defines the integral value of  $\underline{F}_{p-1}^p$  over  $\mathfrak{m}_p$ ,

$$\langle \underline{F}_{p-1}^p | \mathfrak{m}_p \rangle = \langle \mathbf{j}\mathcal{G} | \mathcal{C}_{p-1} \rangle. \quad (3.23)$$

Inserting Eqs. (3.22) and (3.23) in (3.21) finally yields

$$\langle \underline{F} | \mathfrak{m}_p \rangle = \langle d\mathcal{G} | \mathfrak{m}_p \setminus \mathcal{C}_{p-1} \rangle + \langle \mathbf{j}\mathcal{G} | \mathcal{C}_{p-1} \rangle. \quad (3.24)$$

The integral value of a form  $\underline{F}$  over a manifold is given by the integral of the exterior derivative of the potential  $\mathcal{G}$  plus the jump of the potential due to a  $(p-1)$ -singularity of  $\underline{F}$ . We find that Eq. (3.24) is related to the Stokes' theorem in presence of jump discontinuities by setting  $\langle \underline{F} | \mathfrak{m}_p \rangle = \langle \mathcal{G} | \partial\mathfrak{m}_p \rangle$ :

$$\langle \mathcal{G} | \partial\mathfrak{m}_p \rangle = \langle d\mathcal{G} | \mathfrak{m}_p \setminus \mathcal{C}_{p-1} \rangle + \langle \mathbf{j}\mathcal{G} | \mathcal{C}_{p-1} \rangle. \quad (3.25)$$

Below we give some familiar examples for the above findings.

### Examples:

1. The 0-deRham Current  $\underline{h}(x)$  is defined by

$$\underline{h}(x) := \begin{cases} 0 & \text{if } x < 0, \\ 1 & \text{if } x > 0. \end{cases}$$

$\underline{h}$  is called the *Heaviside jump*; it is not defined in  $x = 0$ . The exterior derivative of  $\underline{h}$  yields

$$d\underline{h} = \underline{\delta},$$

the Dirac impulse, with

$$\langle d\underline{h} | \mathbb{R} \rangle = \langle \underline{\delta} | \mathbb{R} \rangle = \langle \mathbf{j}\underline{h} | 0 \rangle,$$

compare Eq. (3.11) with  $\langle \mathbf{j}\underline{h} | 0 \rangle = \langle \underline{e} | 0 \rangle$ .

2. A charge 3-form  $\underline{\tilde{\rho}}$ , defined on a volume  $\tilde{\mathfrak{v}}$ , is concentrated on a surface  $\tilde{\mathfrak{s}}$  (a  $(p-1)$ -singularity):  $\underline{\tilde{\rho}} = \underline{\tilde{\rho}}_3^3 + \underline{\tilde{\rho}}_2^3$ . The surface divides  $\tilde{\mathfrak{v}}$  into two volumes  $\tilde{\mathfrak{v}}^-$  and  $\tilde{\mathfrak{v}}^+$ ,  $\tilde{\mathfrak{v}}^- \cup \tilde{\mathfrak{v}}^+ = \tilde{\mathfrak{v}} \setminus \tilde{\mathfrak{s}}$ . Mathematically, the potential of the charge is the electrical flux density  $\underline{\tilde{D}}$ . The following evaluations of a total charge in the volume are identical:

$$\begin{aligned} Q(\tilde{\mathfrak{v}}) &= \langle \underline{\tilde{\rho}}_3^3 + \underline{\tilde{\rho}}_2^3 | \tilde{\mathfrak{v}} \rangle, \\ &= \langle \underline{\tilde{\rho}}_3^3 | \tilde{\mathfrak{v}} \rangle + \langle \underline{\tilde{\sigma}} | \tilde{\mathfrak{v}} \cap \tilde{\mathfrak{s}} \rangle, \\ &= \langle d\underline{\tilde{D}} | \tilde{\mathfrak{v}}^- \rangle + \langle d\underline{\tilde{D}} | \tilde{\mathfrak{v}}^+ \rangle + \langle \mathbf{j}\underline{\tilde{D}} | \tilde{\mathfrak{v}} \cap \tilde{\mathfrak{s}} \rangle, \\ &= \langle \underline{\tilde{D}} | \partial\tilde{\mathfrak{v}} \rangle. \end{aligned}$$

We see that  $\mathbf{j}\underline{\tilde{D}} = \underline{\tilde{\sigma}}$ .

3. The current through a face  $\tilde{f}$  is to be evaluated. The current is in part concentrated on a surface  $\tilde{\xi}$ . The following evaluations are identical:

$$\begin{aligned}
I(\tilde{f}) &= \langle \tilde{j}_2^2 + \tilde{j}_1^2 | \tilde{f} \rangle, \\
&= \langle \tilde{j}_2^2 | \tilde{f} \rangle + \langle \tilde{K} | \tilde{f} \cap \tilde{\xi} \rangle, \\
&= \langle d\tilde{H} | \tilde{f}^- \rangle + \langle d\tilde{H} | \tilde{f}^+ \rangle + \langle \mathbf{j} \tilde{H} | \tilde{f} \cap \tilde{\xi} \rangle, \\
&= \langle \tilde{H} | \partial\tilde{f} \rangle.
\end{aligned}$$

Again we note that  $\mathbf{j} \tilde{H} = \tilde{K}$ . □

The discretization of Eq. (3.25) unveils a lack of symmetry between the discrete and the continuous setting:  $[D^{p-1}]\{G\}$  is actually a representation of  $\langle G | \partial m \rangle$  rather than of  $\langle dG | m \rangle$ . In the absence of jumps this difference can be neglected because of Stokes' theorem. In the presence of jumps, however, the jump-term in Eq. (3.25) breaks that balance. We therefore have

$$\{F\} = [D^{p-1}]\{G\}$$

even in the presence of jump discontinuities and

$$\{F_p^j\} = [D^{p-1}]\{G\} - [dR_{p-1}^p]\{\mathbf{j} G\}, \quad (3.26)$$

for the discretization of the non-singular part of  $\underline{F}$ . Note that in the continuous setting we had

$$\langle \underline{F} | m_p \rangle = \langle dG | m_p \setminus \mathcal{C}_{p-1} \rangle + \langle \mathbf{j} G | \mathcal{C}_{p-1} \rangle,$$

and

$$\langle \underline{F}_p^j | m_p \rangle = \langle dG | m_p \setminus \mathcal{C}_{p-1} \rangle.$$

We introduce an optional notation for the  $(p-1)$ -deRham matrix:

$$[J^{p-1}] := [dR_{p-1}^p]. \quad (3.27)$$

We call  $[J^{p-1}]$  the jump matrix. Applications of jump matrices can be found in the following section as well as in Section 4.4.

### 3.3 Cohomology

This section will give an answer to the following question: If  $d_p \underline{F} = 0$ , is there a potential  $\underline{G}$  such that  $\underline{F} = d_{p-1} \underline{G}$ ? The Poincaré lemma states that the coboundary of a coboundary is empty, i.e., if  $\underline{F} = d_{p-1} \underline{G}$  then  $d_p \underline{F} = 0$ . The above question comes to ask whether the Poincaré lemma is reversible?

The issue of principal reversibility of the Poincaré lemma is discussed in Section 3.3.1. Section 3.3.2 presents an adjustment of the potential formulation in cases when the Poincaré lemma is not reversible - the so-called cohomology contributions.

### 3.3.1 Converse of the Poincaré Lemma

The following example illustrates that the Poincaré lemma is not always reversible:

**Example:** The magnetic field of a line current  $\tilde{j}_0^2$  concentrated in a point  $\tilde{p}$  on a 2-manifold  $\tilde{m}$  reads in cylindrical coordinates  $\tilde{H} = (\tilde{I}/2\pi r)rd\phi$ , with  $\tilde{I}$  the line-current 0-form and  $\phi$  and  $r$  the cylindrical coordinates. This field is a closed 1-form,  $d\tilde{H} = 0$  on  $\tilde{m} \setminus \tilde{p}$ . It can, however, not be written as the gradient of a magnetic scalar potential,  $\tilde{H} \neq -d\tilde{\varphi}_M$ . If it could be, then  $\tilde{H}$  would be exact, but at the same time all line integrals along closed lines would have to vanish. We know, however, that  $\langle \tilde{H} | \tilde{z} \rangle = NI$  with  $\tilde{z}$  a 1-cycle and  $N$  the number of times the path encloses the line current. The Poincaré lemma cannot be reversed.

The same reasoning as above applies to the discrete setting shown in Fig. 3.3 (right), where from  $[\tilde{D}^1]\{\tilde{H}\} = 0$  it does not follow that  $\{\tilde{H}\} = -[\tilde{D}^0]\{\tilde{\varphi}_M\}$ .  $\square$

Henceforth we call a *period* the integral of a closed differential form on a cyclic manifold or the duality product of a closed cochain and a cycle. In the above example, the periods of  $\tilde{H}$  yield  $NI$ .

Having introduced a coboundary operator in Section 3.1.4, we can investigate its image and its kernel in analogy to the investigation of the image and the kernel of the boundary operator in Section 2.1.4 that yielded the introduction of homology classes. The following definitions will be used to give a formal answer to the introductory question:

Cochains lying in the image of the  $d_{p-1}$  coboundary operator belong to the *coboundary space*  $B^p(\Omega)$ . CochAINS that can be expressed as coboundaries (in a potential formulation  $\tilde{F} = d_{p-1}\tilde{G}$ ) are called *exact* cochains. The terms coboundary and exact cochain are synonymous.

Cochains lying in the kernel of the  $d_p$  operator are members of the *cocycle space*  $Z^p(\Omega)$ . Cocycles are also called *closed* cochains, both terms being synonymous.

Finally, the quotient space of cocycles over coboundaries is called the *cohomology space*  $H^p(\Omega) = Z^p(\Omega)/B^p(\Omega)$ . Its members are equivalence classes  $[\tilde{h}] = \tilde{z}^p + B^p$  with  $\tilde{z}^p \in Z^p(\Omega)$ . We have placed the dimension-indices for the cospaces in superscripts to distinguish them from the respective spaces of chains (with subscript dimension-indices). Figure 3.2 illustrates the relationship of the coboundary operator, and the coboundary, cocycle and cohomology spaces. Any cocycle can be expressed as the sum of an instance of each cohomology class and a coboundary. We state the following important theorem without proof:

The dimension of the  $p$ th cohomology space is always equal to the dimension of the  $p$ th homology space.

The above definitions yield a clear answer to the introductory question: a closed  $p$ -cochain is exact if the  $p$ th cohomology space is the empty space. This statement is obvious as the very definition of an empty cohomology space is that all cocycles

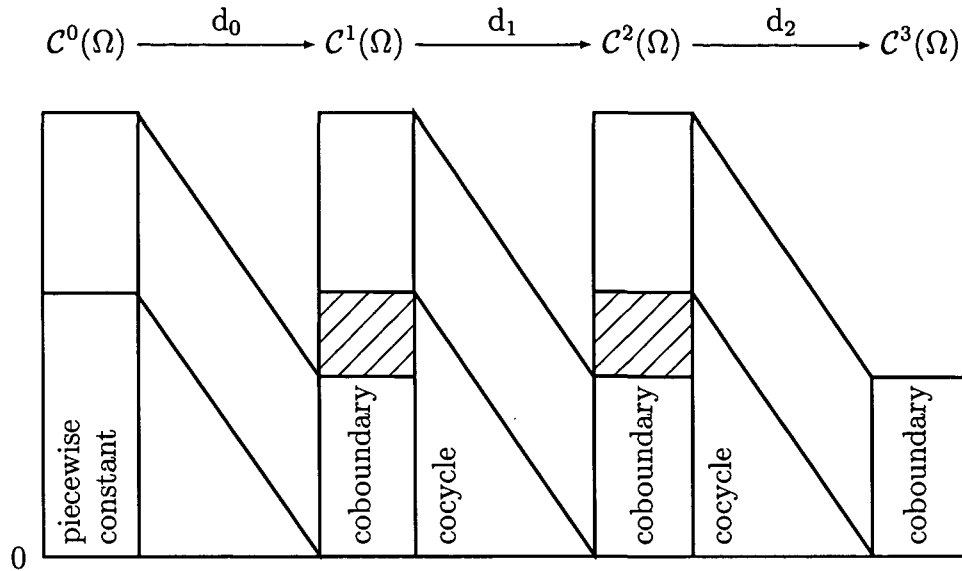


Figure 3.2: The DeRham complex of cochains. Any cocycle can be expressed as the sum of an instance of each cohomology class (dashed area) and a coboundary.

are coboundaries. The equality of dimensions of the homology and cohomology space, however, implies a useful information: a closed cochain is exact if the  $p$ th homology space of the cell complex is empty, i.e., if the cell complex does not have holes or cavities. In this case we say that the complex is contractible.

The Poincaré lemma is reversible on contractible complexes,

$$d_p \underline{F} = 0 \iff \underline{F} = d_{p-1} \underline{G} \quad \text{if} \quad \dim H_p(\Omega) = 0.$$

The requirement of contractibility is too strong. It can be released; we state the *Converse of the Poincaré lemma* without proof:

A (closed) cochain  $\underline{F}$  is exact if and only if all of its periods vanish.

At this point we see that the above attempts to describe the (closed) magnetic field in presence of the line current by a potential had to fail. Now our focus will be put on the determination of an adjusted potential formulation that will account for the non-zero periods of closed forms and cochains.

### 3.3.2 Cohomology Contributions to Cochains

#### Continuous Setting

For the configuration given in Fig. 3.4 (left), the curl of  $\tilde{H}$  is zero everywhere except on the current singularity  $\tilde{p}$  where it is not defined. By  $d\underline{B} = d*\mu_0\tilde{H} = 0$ , compare Annex B, the magnetic field of a line current is a harmonic field (divergence and

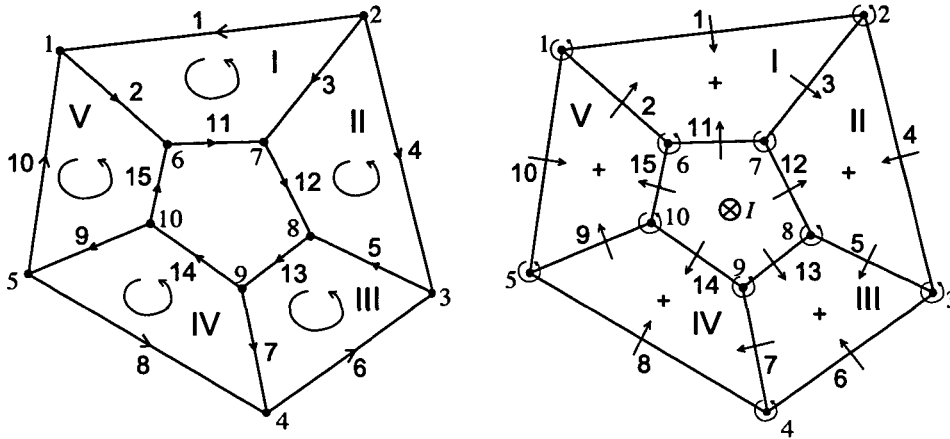


Figure 3.3: 2-dimensional oriented cell complex with a hole. Left: Inner oriented complex. Right: Outer oriented complex

curl-free 1-form). We know that  $\tilde{H}$  cannot be expressed by a gradient  $-d\tilde{\varphi}_M$  due to the presence of the line current. The closed form  $\tilde{H}$  can, however, be decomposed into a coboundary of a scalar potential and a harmonic field,  $\tilde{H} = -d\tilde{\varphi}_M + \tilde{h}$ , e.g.,  $\tilde{\varphi}_M = \text{const.}$ ,  $\tilde{h} = (\tilde{I}/2\pi r) r d\phi$ . The harmonic field represents the cohomology contribution to the potential formulation. The cohomology contribution is a closed form that is not exact. The periods of  $\tilde{H}$  are fixed by the cohomology contribution. Their values depend only on how many times the current is enclosed in the respective cycle.

For an alternative approach we exploit the equivalence of current loops and double-layers of magnetic charges, compare Fig. 3.4 (right). We introduce a magnetic double-layer  $\underline{\sigma}_{M,DL}$  with  $\|\underline{\sigma}_{M,DL}\| = I/\mu_0$  on a manifold that is bounded by the line-current loop. The shape of the support manifold  $\tilde{d}$  is arbitrary, provided that its boundary coincides with the line current loop. The magnetic scalar potential due to the double-layer jumps on  $\tilde{d}$ ,  $j\tilde{\varphi}_M = -*\mu_0\underline{\sigma}_{M,DL}$ . On  $\tilde{m}' = \tilde{m} \setminus \tilde{d}$  the magnetic field can now be described as  $\tilde{H} = -d\tilde{\varphi}_M$ . The jump of the potential ensures that the periods of  $\tilde{H}$  yield a multiple of  $I$ . It causes a concentration  $\tilde{H}^1$  of the magnetic field on  $\tilde{d}$  with  $\langle \tilde{H}^1 | \tilde{z} \rangle = \langle -j\tilde{\varphi}_M | \tilde{z} \cap \tilde{d} \rangle$ .

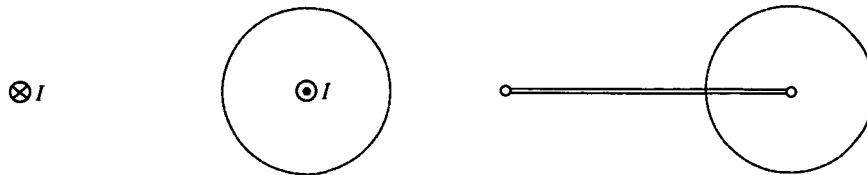


Figure 3.4: Equivalence of a current loop (left) and a double-layer of magnetic surface charges (right). Both source-configurations yield the same magnetic field outside the support of the source fields.

The two proposed methods to calculate  $\tilde{H}$  are identical everywhere except on the submanifolds  $\tilde{d}$  and  $\tilde{p}$ . The magnetic double-layer causing a concentrated magnetic field is a valid instrument to introduce the cohomology contribution to the potential formulation of  $\tilde{H}$ .

The same procedure can be applied for a single line current that is assumed to return on a cylinder centered at  $\tilde{p}$  at some arbitrarily large reference radius, see Fig. 3.5.



Figure 3.5: Equivalence of a line current (left) and a double-layer of magnetic surface charges (right). Both source configurations yield the same magnetic field outside the support of the source fields.

### Discrete Setting

The latter approach to account for the cohomology contribution is especially suited for a discretization, recall Section 3.2. Fig. 3.6 illustrates the process. The cohomology contribution is discretized as a concentrated field  $\{\tilde{H}_0^1\}$ . The field is concentrated on a submanifold that has to intersect exactly once every cycle that encloses the complex' hole. The absolute value of the concentrated field cochain coefficients is  $I$ . This accounts for the resulting field cochain's periods. Note that an equal number of positive and negative currents in the hole of the cavern yields a zero-cohomology contribution. The decomposition of the magnetic field cochain into coboundary and cohomology contribution reads

$$\{\tilde{H}\} = -[\tilde{D}^0]\{\tilde{\varphi}_M\} + [d\tilde{R}_0^1]\{\tilde{H}_0^1\}. \quad (3.28)$$

The entries of  $\{\tilde{H}_0^1\}$  are either  $I$  or  $-I$ , depending on the orientation of the intersected 1-cell. Considering the sign in the deRham current matrix, the cohomology cochain vector transforms into scalar  $I$  for which we write  $\{\tilde{H}_{Ch}\}$ ;  $[d\tilde{R}_0^1]$  transforms into a single column  $[\tilde{Ch}^0]$ . For Fig. 3.6 we find

$$[\tilde{Ch}^0]^{i1} = \begin{cases} 1 & \text{if } i = 1, \\ -1 & \text{if } i = 11, \\ 0 & \text{otherwise.} \end{cases}$$

Equation (3.28) now reads

$$\{\tilde{H}\} = -[\tilde{D}^0]\{\tilde{\varphi}_M\} + [\tilde{Ch}^0]\{\tilde{H}_{Ch}\}.$$

Apart from the denomination of the cohomology matrix and vector, this equation



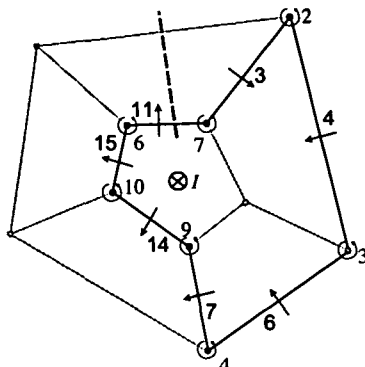


Figure 3.6: Cohomology cut on a 2-complex. The submanifold cuts every cycle that encloses the hole in the complex exactly once. One instance of the 1-dimensional homology space is indicated.

is identical to Eq. (3.28).

In what follows we give a general description of the formalism to include cohomology contributions in a potential formulation:

Cohomology contributions to a potential formulation are effectively discretized as concentrated fields, compare Section 3.2. A closed field  $\{F\}$  can be decomposed into a coboundary  $[D^{p-1}]\{G\}$  and a concentrated field  $[dR_0^p]\{F_0^p\}$ . The field is concentrated on a suitable  $(n-p)$ -submanifold  $\mathfrak{g}$ . Suitable means that  $\mathfrak{g}$  cuts all instances of a homology class exactly once, compare Figs. 3.6 and 3.7. If the homology space has a dimension  $n_{Hp} > 1$ , several concentrated fields need to be taken into account:

$$\{F\} = [D^{p-1}]\{G\} + [dR_0^{p,1}]\{F_0^{p,1}\} + \dots + [dR_0^{p,n_{Hp}}]\{F_0^{p,n_{Hp}}\}. \quad (3.29)$$

Each concentrated field has a uniform integral value that is given by the period of the field along an instance of the respective homology class. The cohomology coefficient-vectors have identical entries up to a factor  $(-1)$  due to different orientation. Considering the sign-change in the respective entries of the  $[dR_0^{p,i}]$  matrices, the coefficient vectors can be reduced to scalar coefficients and the  $[dR_0^{p,i}]$  matrices reduce to columns. The  $n_{Hp}$  columns of  $[dR_0^{p,i}]$  form the cohomology matrix  $[\text{Ch}^0]$ . The vector of scalar coefficients writes  $\{F_{\text{ch}}\}$ . Eq. (3.29) now reads

$$\{F\} = [D^{p-1}]\{G\} + [\text{Ch}^0]\{F_{\text{ch}}\}. \quad (3.30)$$

For  $p = 1$ , e.g., for the magnetic field  $\tilde{H}$  in the above example, the concentrated field that represents the cohomology contribution can be interpreted as a jump in the (scalar) potential, compare Section 3.2. For 1-cochains Eq. (3.30) can be rewritten

$$\{F\} = [D^0]\{G\} + [J_{\text{ch}}^0]\{G_{\text{ch}}\},$$

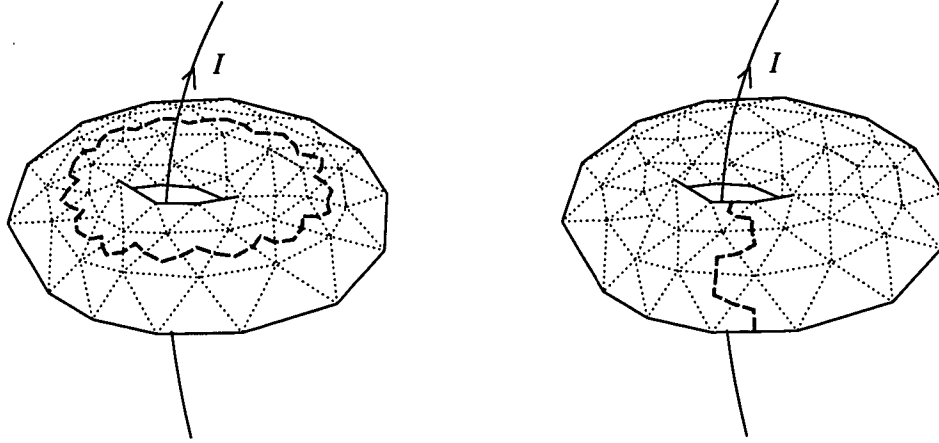


Figure 3.7: Instances of homology classes on a torus surface. The instances act as mutually cutting submanifolds bearing the concentrated cohomology fields. The chosen submanifolds follow straight paths from barycenters of faces to barycenters of edges thus avoiding to cut the complex in one of its nodes.

where  $\{G_{\text{Ch}}\}$  yields the cohomology coefficients in terms of a jump of the potential. In this perspective, Eq. (3.28) can be written

$$\{\tilde{H}\} = -[\tilde{D}^0]\{\tilde{\varphi}_M\} - [\tilde{J}_{\text{Ch}}^0]\{\tilde{\varphi}_{M,\text{Ch}}\}.$$

Note that the magnetic scalar potential  $\tilde{\varphi}_M$  is not unique; any constant field may be added, since the gradient of a constant field is zero and the jump is invariant under the addition of a constant on both sides of the jump-discontinuity.

# 4

## Discrete Material Laws (1) - Discretization on Dual Complexes

The concept of dual discretization underlies most DEM theories. Two cell complexes, denoted 'primal' and 'dual', discretize the same spatial domain. The inner orientation of one complex induces an outer orientation on the other complex. In three dimensions, each primal edge intersects a dual face and each primal face intersects a dual edge.

The dual discretization aims at the discretization of the Faraday and the Ampère-Maxwell complex on topologically dual cell complexes. As a consequence, we will find in Chapter 5 that the material equations relating, e.g.,  $\underline{B}$  and  $\underline{\tilde{H}}$  or  $\underline{E}$  and  $\underline{\tilde{D}}$  are represented by square matrices. This motivates the chapter title.

We present the concept of dual discretization, followed by the discretization of the electromagnetic fields on dual complexes. We then introduce a novel operator to DEM: the transfer matrix. The transfer matrix maps coefficient vectors on the primal complex into coefficient vectors on the dual complex. Next, we investigate the boundary of the dual complex. We propose to assume that all electromagnetic fields jump to zero on the boundary of the primal complex. Consequently, a jump term on the domain boundary is introduced to the DEM theory. We will use this jump term to specify the Neumann data of a boundary value problem and to couple a DEM formulation to a Boundary Element Method, see Chapter 8.

### 4.1 Topologically Dual Cell Complexes

The simplest example of a dual cell complex is given by a complex of regular hexahedral cells or bricks. Figure 4.1 illustrates the concept of topological duality:

**Definition 4.1.1 (Topologically Dual Cell Complexes)** Let  $C$  and  $\bar{C}$  be two cell complexes. By convention  $C$  is called the primal complex and  $\bar{C}$  the dual

complex. Let further one of the complexes be endowed with an inner orientation. The two complexes are said to be *topologically dual* if each primal  $p$ -cell  $\mathcal{C}_p^i$  is related to one dual  $(n - p)$ -cell  $\bar{\mathcal{C}}_p^j$ :

$$\mathcal{C}_p^i \cap \bar{\mathcal{C}}_p^j = \begin{cases} p & \text{if } i = j \\ \emptyset & \text{if } i \neq j, \end{cases}$$

where  $p$  is a point.

If  $C$  is endowed with an inner orientation, it induces an outer orientation on  $\bar{C}$  and vice versa (compare Definition 2.2.3). All mathematical objects that are related to the dual complex are written with an overbar. The pair of a primal and a (topologically) dual complex then writes  $(C, \bar{C})$  or  $(\bar{C}, C)$ , depending on what complex is initially oriented.  $\diamond$

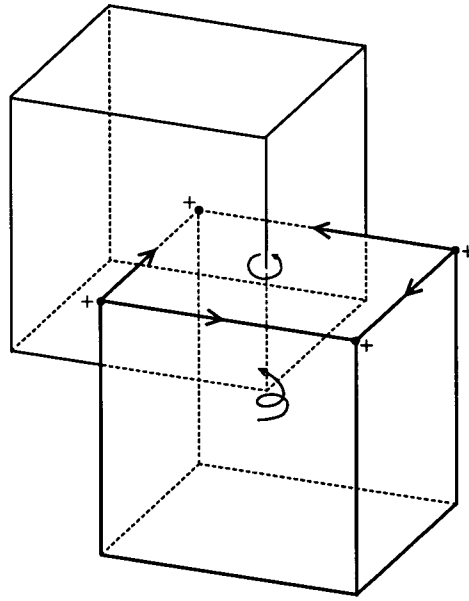


Figure 4.1: Inner oriented primal cell and topologically dual outer oriented cell. The inner orientation of the primal  $p$ -cells induces an outer orientation in the dual  $(3 - p)$ -cells.

The incidence matrices on the topologically dual complexes are related by

$$[\bar{A}^p] = (-1)^p [A^{n-p+1}]^T. \quad (4.1)$$

Also on the dual complex the boundary of a boundary is empty,

$$[\bar{A}^{p-1}][\bar{A}^p] = 0.$$

It follows from Eq. (3.9) that

$$[\bar{D}^p] = (-1)^{p+1} [D^{n-p-1}]^T, \quad (4.2)$$

and the Poincaré lemma holds on the dual complex,

$$[\bar{D}^{p+1}][\bar{D}^p] = 0.$$

The pair of an inner oriented complex and its outer oriented dual provides the geometrical framework for a discretization of the Faraday- and the Ampère-Maxwell complex.

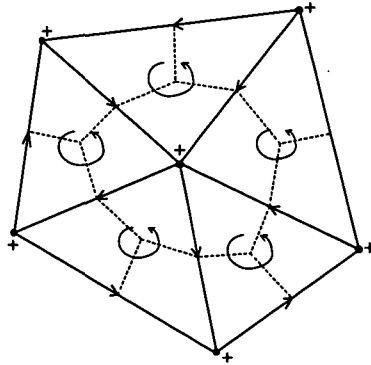


Figure 4.2: Inner oriented 2-dimensional simplicial complex and its outer oriented barycentric dual (dashed line). Note that the outer orientation of an edge in 2 dimensions is given by a sense of passage, of a node by a sense of twist and of a face by a sign.

Finding a dual spatial discretization is usually not as easy as with brick-cells, where it can be found from mere translation of the primal complex by one half of a cell, compare Fig. 4.1. Generally, we will use the *barycentric* dual of the primal complex as a dual complex. Figs. 4.2 and 4.3 illustrate the following description:

We observe that, for  $q > 0$ , dual  $q$ -cells intersect more than one primal  $n$ -cell. Especially for  $n = 3$  we find that

- the dual nodes are given by the barycenters of the primal volumes.
- the dual edges are composed of 2 subcells lying in 2 primal volumes that intersect in a common face. Each subcell is a straight line from the barycenter of the respective volume to the barycenter of their common face.
- the dual faces are partitioned into as many subcells as there are volumes that share a common edge. They are bounded by the dual edges and they intersect in the barycenter of their common primal edge.
- the dual volume is bounded by the dual faces and, therefore, lies in as many primal volumes as there are primal volumes that share a common node.

We can verify that the dual of the brick-complex is a barycentric dual. More importantly, the above description yields dual complexes for tetrahedra-, Fig. 4.3, and prism-complexes, Fig. 4.4, and of mixed cell complexes.

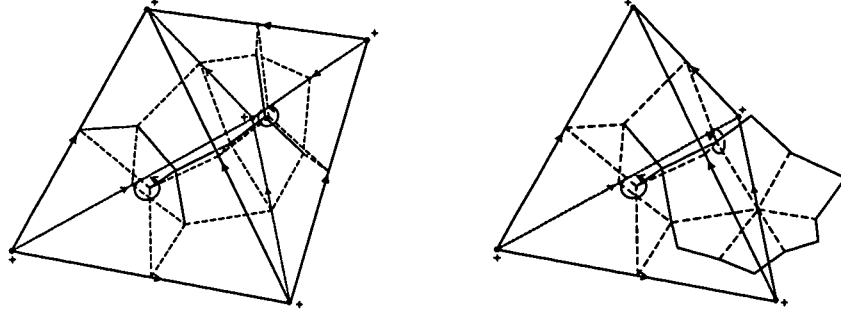
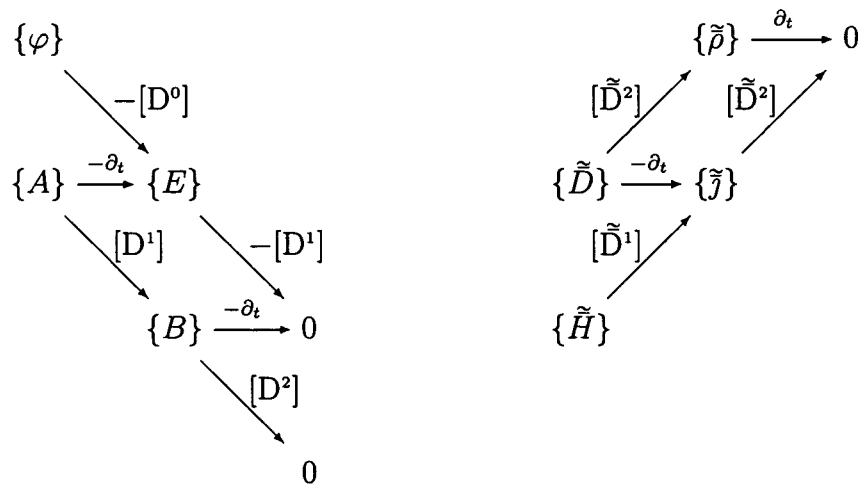


Figure 4.3: Left: 2 primal tetrahedra cells with the respective subcells of a barycentric dual complex. Right: Outer oriented dual face composed of the subcells lying in those primal volumes that share a common edge.

## 4.2 Topological Laws of DEM on Dual Complexes

As indicated above, the whole exercise of finding a topologically dual complex is aimed towards a discretization of the Faraday complex and the Ampère-Maxwell complex on the pair of inner- and an outer oriented complexes. One might argue that this could be achieved by merely copying the primal complex and endowing the copy with an outer orientation. Such a discretization scheme would, however, not yields square material matrices. If  $\tilde{j}$ ,  $\tilde{D}$  and  $\tilde{H}$  are cochains on the outer oriented dual complex and  $\underline{E}$  and  $\underline{B}$  are  $\hat{c}$ ochains on the primal complex, then all pairs of quantities that are connected by a material law in the electromagnetic theory are discretized on cells that are dual to each other.

The discretization of the topological laws of the electromagnetic theory on topologically dual cell complexes follows the same principles as the discretization on the primal complex. The continuous field is integrated over the respective dual cells to fill the coefficient vectors. In the following diagram, the Faraday complex is assumed to be discretized on an inner oriented primal complex.



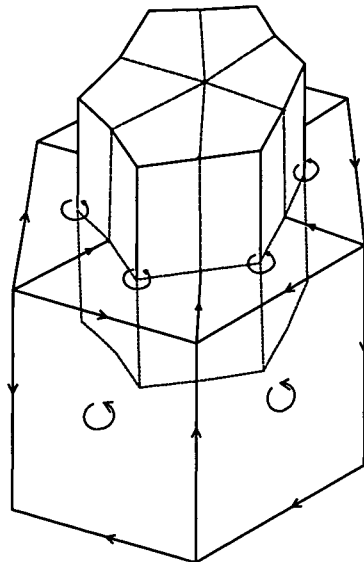


Figure 4.4: Six primal cells of a prism complex and one dual cell of the barycentric dual complex. The dual 3-cell consists of 12 subcells.

### 4.3 Interpolation of Simplices - Transfer Matrix

We might be required to interpolate a cochain, e.g., to determine the value of the magnetic field  $\tilde{H}$  in an arbitrary point inside an  $n$ -cell from the cochain coefficients  $\{\tilde{H}\}$ . Shape-functions are used for the interpolation, compare Annex C. Accurate shape-functions, so-called Whitney forms, exist for certain cell-types (tetrahedra, hexahedra, prisms, pyramids). However, no Whitney forms have been derived for the generally very irregular geometrical objects in the barycentric dual cell complex. Consequently, a discrete field that is defined on the barycentric dual complex cannot be interpolated. The problem can be avoided if we can define the cochain coefficients of the Ampère-Maxwell complex on an outer oriented copy  $\tilde{C}$  of the primal complex and then map them into coefficient vectors of cochains on the barycentric dual complex  $\tilde{C}$ . This transfer from  $\tilde{C}$  to  $\tilde{C}$  is done by the *transfer matrix*  $[\tilde{K}^p]$ .

In this section we denote by  $n_p$  the number of  $p$ -simplices in the boundary of an  $n$ -simplex, e.g., for  $n = 3$ ,  $n_0 = 4$ ,  $n_1 = 6$ ,  $n_2 = 4$  and  $n_3 = 1$ .<sup>1</sup> Note that a  $p$ -simplex, e.g., a 2-simplex  $\sigma_2$  will be indicated in two ways:  $\sigma_2^i$ ,  $1 \leq i \leq n_2$  or  $\sigma_2^{jkl}$ ,  $0 \leq j, k, l \leq n_0$  to indicate that the 2-simplex is bounded by the nodes  $i$ ,  $j$  and  $k$ . Furthermore, we denote with a prime,  $[K'^p]$ , the  $n$ -cell (element-) matrix and with  $[K^p]$  the global transfer matrix. We assume the simplex and its sides to be oriented in the canonical way, see page 7.

A standard  $p$ -simplex was introduced in Definition 2.1.1 as a set of  $(p+1)$ -tuples

<sup>1</sup>We will, throughout this section, deliberately confuse a  $p$ -simplex that is a mapping of a standard simplex to a manifold and its image that is the simplicial  $p$ -cell, compare Definition 2.1.3.

of reals. An isomorphism between a  $p$ -simplex and a set of 0-chains is given by

$$\mathcal{C}_p \cong \{p = \lambda_1 \mathcal{C}_0^1 + \dots + \lambda_{p+1} \mathcal{C}_0^{p+1} \mid 0 \leq \lambda_i \leq 1 \text{ and } \lambda_1 + \dots + \lambda_{p+1} = 1\}, \quad (4.3)$$

where the 0-simplices  $\mathcal{C}_0^i$  represent the nodes in the boundary of the  $p$ -simplex.

We can draw two conclusions from this isomorphism:

- A  $p$ -simplex is isomorphic to a set of 0-chains. Each 0-chain is interpreted as a point in the simplicial  $p$ -cell. The  $\lambda_i$ 's are called the *barycentric coordinates*.
- Any point inside a simplicial  $p$ -cell can be represented as a weighted sum of the nodes in the boundary of the  $p$ -cell. The name "barycentric coordinates" comes from the consideration that for a point to become the barycenter of the simplex, we need to put the weights  $\lambda_1, \dots, \lambda_{p+1}$  on the cell's nodes.

### 0-Transfer Matrix

We can represent any point  $\mathfrak{s}_0$  inside a simplicial  $n$ -cell as a weighted sum of nodes:

$$\mathfrak{s}_0 = \lambda_1 \mathcal{C}_0^1 + \dots + \lambda_{n_0} \mathcal{C}_0^{n_0}, \quad (4.4)$$

with  $\lambda_1 + \dots + \lambda_{n_0} = 1$  and  $0 \leq \lambda_i \leq 1$ . The dual node is the barycenter of the primal  $n$ -cell, thus for  $n = 3$  we find

$$\bar{\mathcal{C}}_0^1 = \frac{1}{4} \mathcal{C}_0^1 + \frac{1}{4} \mathcal{C}_0^2 + \frac{1}{4} \mathcal{C}_0^3 + \frac{1}{4} \mathcal{C}_0^4. \quad (4.5)$$

We require the dual cochain  $\bar{F}$  to fulfill

$$\langle \bar{F} \mid \bar{\mathcal{C}}_0^1 \rangle = \langle F \mid \lambda_1 \mathcal{C}_0^1 + \dots + \lambda_{n_0} \mathcal{C}_0^{n_0} \rangle.$$

It follows with

$$[K'^0] = \left( \frac{1}{4}, \frac{1}{4}, \frac{1}{4}, \frac{1}{4} \right)$$

that

$$\{\bar{F}\} = [K^0] \{F\}.$$

$[K^0]$  is the 0-transfer matrix. The matrix of the entire complex is given by the sum of the respective cell-matrices in a global numbering scheme, taking into account orientation. The transfer matrix maps coefficient vectors of 0-cochains on the primal complex into coefficient vectors of 0-cochains on the barycentric dual complex.

**Example:** A magnetic scalar potential cochain can be mapped from  $\tilde{C}$  to  $\tilde{C}$  by

$$\{\tilde{\varphi}_M\} = [\tilde{K}^0] \{\tilde{\varphi}_M\}.$$

□

The transfer matrix is invariant under affine transformations (mappings that conserve barycenters). Therefore, transfer matrices belong to the class of *topological matrices* like  $[D^p]$  or  $[dR_p^p]$ . Topological matrices only depend on the topology of the complex and not on its actual size or shape, as opposed to the so-called metric matrices that we will encounter in the form of material operators in the subsequent chapters.



### 1-Transfer Matrix

To find transfer matrices for  $p > 0$ , we generalize the above approach: we derive a representation of a dual  $p$ -cell as a weighted sum of primal simplicial  $p$ -cells, compare Eq. (4.5). For  $p = 1$ , we derive a representation of a general line segment  $\xi_1$ :

$$\xi_1 = \mu_1 \sigma_1^1 + \cdots + \mu_{n_1} \sigma_1^{n_1}, \quad (4.6)$$

with  $0 \leq \mu_i \leq 1$  and  $\mu_1 + \cdots + \mu_{n_1} = 1$ . Figure 4.5 illustrates the problem for  $\xi_1 = \bar{\sigma}_1^i$ , the dual edges.

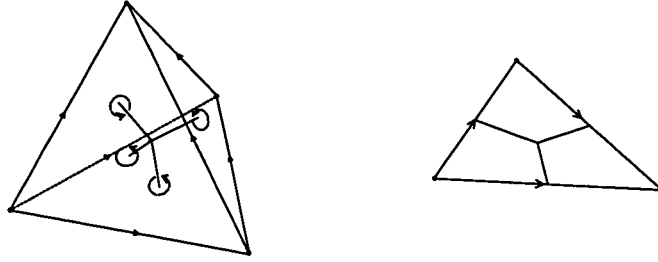


Figure 4.5: Parts of outer oriented dual edges in a simplicial  $n$ -cells for  $n=3$  (left) and  $n=2$  (right).

As a consequence of Eq. (4.3) we write for  $\xi_1$

$$\xi_1 \cong \{ \nu_1 x^1 + \nu_2 x^2, \}$$

where  $x^1$  and  $x^2$  are the bounding points of the line segment,  $0 \leq \nu_1, \nu_2 \leq 1$  and  $\nu_1 = 1 - \nu_2$ . For the sake of simplicity, in what follows we omit the curly braces. Interpolating the points according to Eq. (4.4) yields

$$\xi_1 \cong \sum_i \nu_1 \lambda_i(x^1) \sigma_0^i + \sum_i \nu_2 \lambda_i(x^2) \sigma_0^i. \quad (4.7)$$

Since  $\sum_j \lambda_j(x^1) = \sum_j \lambda_j(x^2) = 1$  we can rewrite Eq. (4.7) as

$$\xi_1 \cong \sum_{i,j} (\nu_1 \lambda_i(x^1) \lambda_j(x^2) \sigma_0^i + \nu_2 \lambda_i(x^2) \lambda_j(x^1) \sigma_0^j).$$

Furthermore, from

$$\sum_{i,j} \nu_2 \lambda_i(x^2) \lambda_j(x^1) \sigma_0^i = \sum_{i,j} \nu_2 \lambda_j(x^2) \lambda_i(x^1) \sigma_0^j$$

it follows that

$$\xi_1 \cong \sum_{i,j} \lambda_i(x^1) \lambda_j(x^2) (\nu_1 \sigma_0^i + \nu_2 \sigma_0^j).$$

Finally, the expression in the brackets is isomorphic to the primal edges  $\sigma_1^{ij}$ . After choosing an orientation for  $\sigma_1^{ij}$  from node  $i$  to node  $j$ , we obtain

$$\underline{s}_1 = \sum_{i < j} (\lambda_i(\underline{x}^1)\lambda_j(\underline{x}^2) - \lambda_i(\underline{x}^2)\lambda_j(\underline{x}^1)) \sigma_1^{ij}. \quad (4.8)$$

Here we neglect the degenerate edges  $\sigma_1^{ii}$ . Equation (4.8) defines the coefficients  $\mu_1, \dots, \mu_{n_1}$  in Eq. (4.6).

As the  $[K^1]$ -matrix is a topological matrix, we can calculate its coefficients for  $n = 3$  on a reference tetrahedron, compare Fig. 4.6. The coordinates of the vertices of the simplicial reference 3-cell read  $\varphi(\sigma_0^1) = (0, 0, 0)$ ,  $\varphi(\sigma_0^2) = (1, 0, 0)$ ,  $\varphi(\sigma_0^3) = (0, 1, 0)$ ,  $\varphi(\sigma_0^4) = (0, 0, 1)$ , where  $\varphi : \sigma_3 \rightarrow \mathbb{R}^3$ ,  $\underline{x} \mapsto (\xi, \eta, \zeta)$  is a coordinate chart. A point  $\underline{x}$  with coordinates  $(\xi, \eta, \zeta)$  has the barycentric coordinates

$$\begin{aligned} \lambda_1(\underline{x}) &= 1 - \xi - \eta - \zeta, \\ \lambda_2(\underline{x}) &= \xi, \\ \lambda_3(\underline{x}) &= \eta, \\ \lambda_4(\underline{x}) &= \zeta. \end{aligned}$$

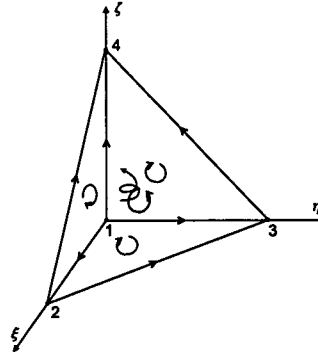


Figure 4.6: Oriented reference tetrahedron.

Now we can determine from Eq. (4.8) the coefficients of any line segment, e.g., of a dual edge, that is expressed as a linear combination of primal edges. Plugging into Eq. (4.8) the bounding points of the dual edges, i.e., the barycenters of the volume and of the respective faces, yields the coefficients of the 1-transfer matrix:

$$[K^{11}] = \begin{pmatrix} 0 & 0 & \frac{1}{12} & 0 & \frac{1}{12} & \frac{1}{12} \\ 0 & -\frac{1}{12} & 0 & -\frac{1}{12} & 0 & \frac{1}{12} \\ -\frac{1}{12} & 0 & 0 & \frac{1}{12} & \frac{1}{12} & 0 \\ \frac{1}{12} & \frac{1}{12} & \frac{1}{12} & 0 & 0 & 0 \end{pmatrix}.$$

## 2-Transfer Matrix

We will not give a full derivation of a representation

$$\mathfrak{s}_2 = \nu_1 \mathcal{C}_2^1 + \cdots + \nu_1 \mathcal{C}_2^{n_2}$$

of an arbitrary 2-simplex  $f$  inside a 3-simplex and simply state that

$$\mathfrak{s}_2 = \sum_{i,j,k} \lambda_i(\mathfrak{x}^1) \lambda_j(\mathfrak{x}^2) \lambda_k(\mathfrak{x}^3) \mathcal{C}_2^{ijk},$$

or, equivalently,

$$\mathfrak{s}_2 = \sum_{i < j < k} \left( \sum_{\pi \in \text{Perm}\{i,j,k\}} \text{sgn}(\pi) \lambda_i(\mathfrak{x}^1) \lambda_j(\mathfrak{x}^2) \lambda_k(\mathfrak{x}^3) \mathcal{C}_2^{ijk} \right), \quad (4.9)$$

compare [14].

From Eq. (4.9) we can derive the 2-transfer matrix  $[K^2]$ . To do so, we need to split the quadrangles that form the parts of the dual faces inside a primal volume into two triangles. The coefficients of  $[K^2]$  are the sum of the coefficients of both triangles:

$$[K^2] = \begin{pmatrix} 0 & 0 & -\frac{1}{12} & \frac{1}{12} \\ 0 & -\frac{1}{12} & 0 & \frac{1}{12} \\ \frac{1}{12} & 0 & 0 & \frac{1}{12} \\ 0 & -\frac{1}{12} & \frac{1}{12} & 0 \\ \frac{1}{12} & 0 & \frac{1}{12} & 0 \\ \frac{1}{12} & \frac{1}{12} & 0 & 0 \end{pmatrix}.$$

We observe that  $[K^2] = [K^1]^T$ . More generally, we will find in Chapter 6 that

$$[K^p] = (-1)^{p(n-p)} [K^{n-p}]^T. \quad (4.10)$$

## 3-Transfer Matrix

Finally, the interpolation formula for  $p = 3$  reads

$$\mathfrak{s}_3 = \sum_{\pi \in \text{Perm}\{i,j,k,l\}} \text{sgn}(\pi) \lambda_i(\mathfrak{x}^1) \lambda_j(\mathfrak{x}^2) \lambda_k(\mathfrak{x}^3) \lambda_l(\mathfrak{x}^4) \mathcal{C}_3.$$

We would be required to split the dual volumes into tetrahedra and evaluate the above formula. From Eq. (4.10), however, and from geometrical considerations we easily derive that

$$[K^3] = \begin{pmatrix} \frac{1}{4} \\ \frac{1}{4} \\ \frac{1}{4} \\ \frac{1}{4} \end{pmatrix}.$$

We can now define cochains of, e.g., Ampère-Maxwell fields on an outer oriented copy of the primal simplicial complex and only lateron transfer them to the dual complex by the multiplication of the coefficient vectors with  $[K^p]$ . Transfer matrices can also be geometrically defined for prism cells and their barycentric duals. This process, however, is rather tedious. A more general definition of the transfer matrices on various complexes will be given in Chapter 6.

## 4.4 The Boundary of the Dual Complex

We start this section with an observation: Let  $\tilde{v}$  denote the chain of all dual 3-cells. Then  $\{\tilde{v}\}^1 = \dots = \{\tilde{v}\}^{\bar{n}_3} = 1$  and, hence,

$$[\tilde{A}^3]\{\tilde{v}\} = 0,$$

since  $[\tilde{A}^3] = -[\tilde{A}^1]^T$  and  $[\tilde{A}^1]^T = [\tilde{D}^0]$ , compare Eqs. (4.1) and (3.9), and constant coefficient vectors lie in the kernel of the discrete gradient matrix. The boundary of the dual complex is empty!

Somehow this finding should come as a relief since the description of the barycentric dual complex in Section 4.1 does not give any indication as to how to define a barycentric dual *outside* the primal cells. Figure 4.7 suggests that no dual  $p$ -cell,  $p = 1, \dots, 3$  can be defined outside the primal complex. We propose the following interpretation of the situation:

In the mathematical model problem, all electromagnetic fields jump to zero on the boundary of the primal complex.

This implies that all contributions to dual cochains on the outside of the primal complex are zero and that we need not care about the actual shape of the dual complex outside the primal one. This interpretation is in agreement with the fact that  $\{\bar{F}\} = [K^p]\{F\}$  yields contributions to the dual cochain only from fields in the primal complex into those fractions of the dual complex that lie inside the primal complex.

In Section 3.2 we have introduced the impact of jump discontinuities on the discrete formulation. Equation (3.26) with Eq. (3.27) yields a potential formulation

$$\{\bar{F}_p^p\} = [\bar{D}^{p-1}]\{\bar{G}\} - [d\bar{R}_{p-1}^p]\{j\bar{G}\}. \quad (4.11)$$

Recall the definition of the jump:  $j\bar{G} = \mathbf{t}^+ \bar{G} - \mathbf{t}^- \bar{G}$ . With, in the case of the boundary jump,  $\mathbf{t}^+ \bar{G} = 0$ , we can set

$$j\bar{G} = -\mathbf{t}^- \bar{G} = -\bar{G}_{\partial\Omega}$$

and rewrite Eq. (4.11)

$$\{\bar{F}_p^p\} = [\bar{D}^{p-1}][K^{p-1}]\{G\} + [j_{\partial\Omega}^{p-1}]\{\bar{G}_{\partial\Omega}\}. \quad (4.12)$$

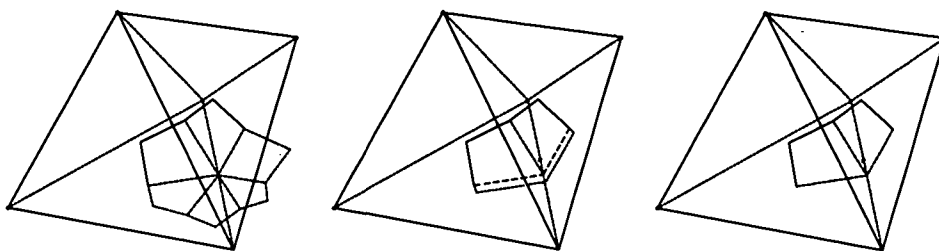


Figure 4.7: Dual cell at the boundary of the primal complex. The barycentric partitioning suggested in the left image is not defined outside the primal complex; it lacks the barycenters of further primal cells. The image in the middle illustrates that the boundary might, therefore, take any arbitrary shape outside the primal cells. The right image suggests that there is no dual complex outside the primal one.

**Example:** Take Ampère's law on the boundary of the dual face  $\tilde{q}_2$  displayed in Fig. 4.7:

$$\langle \tilde{j} | \tilde{q}_2 \rangle = \langle \tilde{H} | \partial \tilde{q}_2 \rangle - \langle \mathbf{j} \tilde{H} | \tilde{q}_2 \cap \partial \tilde{\Omega} \rangle,$$

or, with  $\mathbf{t}^+ \tilde{H} = 0$ ,

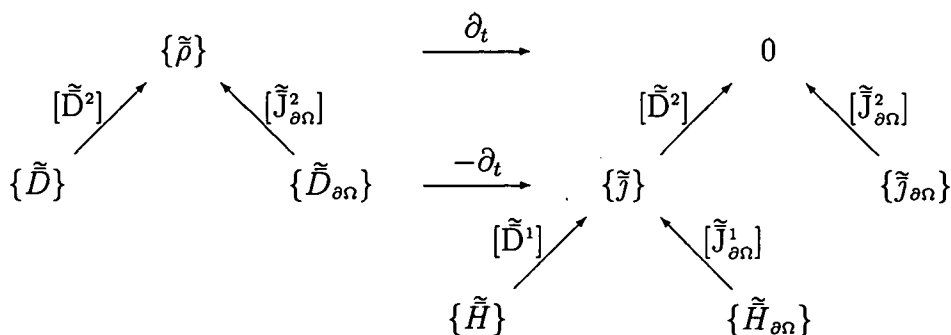
$$\langle \tilde{j} | \tilde{q}_2 \rangle = \langle \tilde{H} | \partial \tilde{q}_2 \rangle + \langle \tilde{H}_{\partial\Omega} | \tilde{q}_2 \cap \partial \tilde{\Omega} \rangle,$$

where  $\mathbf{t}^- \tilde{H} = \tilde{H}_{\partial\Omega}$ . The latter equation yields an alternative interpretation of the boundary term: The boundary term simply closes the cycle along which  $\tilde{H}$  is to be integrated to yield the total current through those fractions of the dual faces that lie inside the primal complex. We will, however, stick to the interpretation of fields jumping to zero outside  $\tilde{C}$ , as this view will lead to a very intuitive understanding of the coupling of a Boundary Element Method with the DEM formulation. The resulting matrix equation reads

$$\{\tilde{j}\} = [\tilde{D}^1] \{\tilde{H}\} + [\tilde{J}_{\partial\Omega}^1] \{\tilde{H}_{\partial\Omega}\}.$$

□

The Ampère-Maxwell side of the diagram on page 38 needs to be adjusted to the new findings:



Unless otherwise stated, we read the coefficient vectors in the diagram as the cochain coefficients of non-singular fields,  $\{\tilde{F}\} = \{\tilde{F}_\sharp^p\}$ . We find

$$\begin{aligned} \{\tilde{\rho}\} &= [\tilde{D}^2]\{\tilde{D}\} + [\tilde{J}_{\partial\Omega}^2]\{\tilde{D}_{\partial\Omega}\}, \\ -\{\partial_t\tilde{\rho}\} &= [\tilde{D}^2]\{\tilde{J}\} + [\tilde{J}_{\partial\Omega}^2]\{\tilde{J}_{\partial\Omega}\}, \\ \{\tilde{J}\} &= -\{\partial_t\tilde{D}\} + [\tilde{D}^1]\{\tilde{H}\} + [\tilde{J}_{\partial\Omega}^1]\{\tilde{H}_{\partial\Omega}\}. \end{aligned}$$

Furthermore we observe that

$$\{\tilde{J}_{\partial\Omega}\} = -\partial_t\{\tilde{D}_{\partial\Omega}\} + [\tilde{D}_{\partial\Omega}^1]\{\tilde{H}_{\partial\Omega}\}.$$

$[\tilde{D}_{\partial\Omega}^p]$  is a coboundary matrix on the 2-dimensional outer oriented dual of the primal boundary complex. Figs. 4.4 and 4.8 illustrate the definition of the outer oriented dual boundary 2-complex.

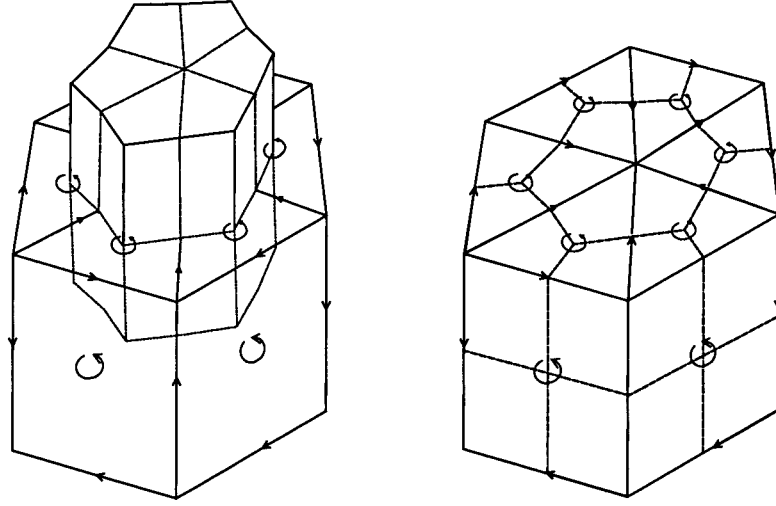


Figure 4.8: Left: Six Primal 3-cells (prisms) and one barycentric dual cell. Right: Cell complex of six primal 3-cells. The 2-dimensional barycentric boundary complex is displayed. Comparison with the left picture shows that the dual boundary complex is equivalent to the intersection of the barycentric dual 3-cells with the primal complex' boundary: the dual boundary faces are equivalent to the intersections of the primal boundary with the dual volumes; the dual boundary edges are the intersections of the primal boundary with the dual faces; the dual boundary nodes are equivalent to the intersections of the primal boundary with the dual edges.

## 4.5 Topological Matrices on Dual Cell Complexes

In this section we give a summary of the most important topological matrices  $[D^p]$ ,  $[K^p]$ ,  $[J^p]$  and the trace matrix  $[T^p]$ . We will specify rules, e.g., for permutations of the matrices, and give an example for the application of the rules.

We have established in Eq. (4.2) that

$$[\bar{D}^p] = (-1)^{p+1} [D^{n-p-1}]^T.$$

We now introduce the  $n_{p,\partial\Omega} \times n_p$  trace matrix

$$[T^p]^{ij} := \begin{cases} 1 & \text{if } p\text{-cell } j \text{ is the } i\text{th } p\text{-cell that belongs} \\ & \text{to the } n\text{-complex' boundary,} \\ 0 & \text{otherwise.} \end{cases}$$

The trace matrix extracts the boundary-coefficients of  $p$ -cochains into a vector with  $n_{p,\partial\Omega}$  entries.

**Example:** The boundary-coefficients of a magnetic field cochain are extracted by

$$\{\tilde{H}_{\partial\Omega}\} = [\tilde{T}^1] \{\tilde{H}\}.$$

The trace matrix for the 2-complex in Fig. 4.9 reads

$$[T^1] = \begin{pmatrix} 1 & 0 & 0 & 0 & 0 \\ 0 & 0 & 1 & 0 & 0 \\ 0 & 0 & 0 & 1 & 0 \\ 0 & 0 & 0 & 0 & 1 \end{pmatrix}.$$

□

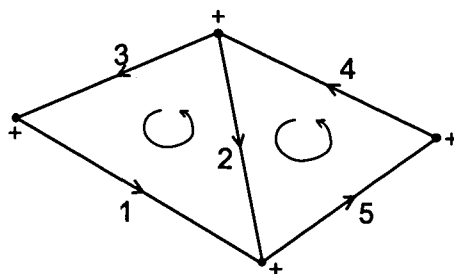


Figure 4.9: Inner oriented simplicial 2-complex.

As in the continuous differential form setting, the trace operator commutes with the coboundary operator

$$[T^{p+1}][D^p] = [D_{\partial\Omega}^p][T^p]. \quad (4.13)$$

We observe with Eq. (3.27) that

$$[\bar{J}^p] = [T^{n-p-1}]^T. \quad (4.14)$$

The jump matrix permutes with the dual coboundary matrix according to

$$[\bar{D}^p][\bar{J}^{p-1}] = -[\bar{J}^p][\bar{D}_{\partial\Omega}^{p-1}]. \quad (4.15)$$

Furthermore, the following equality will be of great importance

$$[K^{p+1}][D^p] = [\bar{D}^p][K^p] + [\bar{J}^p][K_{\partial\Omega}^p][T^p]. \quad (4.16)$$

This rule is a direct consequence of Eq. (4.12). On a closed  $n$ -chain, e.g., a boundary, Eq. (4.16) reads

$$[K_{\partial\Omega}^{p+1}][D_{\partial\Omega}^p] = [\bar{D}_{\partial\Omega}^p][K_{\partial\Omega}^p] \quad (4.17)$$

The following example illustrates the application of the above rules.

**Example:** In the magnetostatic regime, the divergence of the electric current vanishes ( $d\tilde{j} = -\partial_t\tilde{\rho} = 0$ ). We want to determine what constraint we have to put on  $\{\tilde{H}\}$  to ensure that  $[\tilde{D}^2]\{\tilde{j}\} = 0$ . Note that, on the primal complex, representing  $\{\tilde{j}\}$  by a coboundary,

$$\{\tilde{j}\} = [\tilde{D}^1]\{\tilde{H}\},$$

is sufficient to have

$$[\tilde{D}^2]\{\tilde{j}\} = [\tilde{D}^2][\tilde{D}^1]\{\tilde{H}\} = 0.$$

We start with

$$\{\tilde{j}\} = [\tilde{D}^1]\{\tilde{H}\} + [\tilde{J}^1]\{\tilde{H}_{\partial\Omega}\}.$$

Now we apply the coboundary operator and find

$$[\tilde{D}^2]\{\tilde{j}\} = [\tilde{D}^2][\tilde{D}^1]\{\tilde{H}\} + [\tilde{D}^2][\tilde{J}^1]\{\tilde{H}_{\partial\Omega}\}, \quad (4.18)$$

where the first term vanishes due to the Poincaré lemma. The equation then is equivalent to

$$\begin{aligned} [\tilde{D}^2][\tilde{K}^2]\{\tilde{j}\} &= [\tilde{D}^2][\tilde{J}^1][\tilde{K}_{\partial\Omega}^1]\{\tilde{H}_{\partial\Omega}\}, \\ &= -[\tilde{J}^2][\tilde{D}_{\partial\Omega}^1][\tilde{K}_{\partial\Omega}^1]\{\tilde{H}_{\partial\Omega}\}, \\ &= -[\tilde{J}^2][\tilde{K}_{\partial\Omega}^1][\tilde{D}_{\partial\Omega}^1]\{\tilde{H}_{\partial\Omega}\}, \end{aligned} \quad (4.19)$$

by successively using Eqs. (4.15) and (4.17). At the same time we can apply Eq. (4.16) to the left-hand side of Eq. (4.18) and we obtain

$$\begin{aligned} [\tilde{D}^2][\tilde{K}^2]\{\tilde{j}\} &= [\tilde{K}^3][\tilde{D}^2]\{\tilde{j}\} - [\tilde{J}^2]\{\tilde{j}_{\partial\Omega}\}, \\ &= [\tilde{K}^3][\tilde{D}^2][\tilde{D}^1]\{\tilde{H}\} - [\tilde{J}^2][\tilde{K}_{\partial\Omega}^2][\tilde{D}_{\partial\Omega}^1]\{\tilde{H}_{\partial\Omega}\}. \end{aligned}$$

Both calculations lead to the same result. We see that for  $[\tilde{D}^2]\{\tilde{j}\}$  to vanish, not only does the primal current cochain have to be a coboundary of a magnetic field



cochain; the current density on the primal domain boundary must not jump and thus the magnetic field on the boundary must be a closed cochain!

Closed cochains can be decomposed into a coboundary and a cohomology contribution:

$$\{\tilde{H}_{\partial\Omega}\} = -[\tilde{D}_{\partial\Omega}^0]\{\varphi_{M,\partial\Omega}\} + [\tilde{C}h_{\partial\Omega}^0]\{\tilde{H}_{\partial\Omega,Ch}\},$$

or, equivalently,

$$\{\tilde{H}_{\partial\Omega}\} = -[\tilde{D}_{\partial\Omega}^0]\{\tilde{\varphi}_{M,\partial\Omega}\} - [\tilde{J}_{\partial\Omega,Ch}^0]\{\tilde{\varphi}_{M,\partial\Omega,Ch}\}.$$

This is the condition that we need to impose for the dual current cochain to be divergence free. In addition to  $\{\tilde{j}\} = [\tilde{D}^1]\{\tilde{H}\}$  we have to require that the electric current density on the boundary does not jump, i.e., the electric current density on the boundary is zero.  $\square$

# 5

## Discrete Material Laws (2) - A Discrete Hodge Operator

The continuous theory of electromagnetism expresses material laws by Hodge operators and material parameters, as shown in Annex B:

$$\begin{aligned}\tilde{H} &= *\nu B, \\ \tilde{j} &= *\kappa E, \\ \tilde{D} &= *\varepsilon E.\end{aligned}$$

The continuous Hodge-operator is metric- and orientation dependent.

This chapter first presents the intuitive concept of a geometrically defined Hodge operator on brick-shaped cells that is used in the Finite Integration Technique (FIT), [34]. Section 5.2 then introduces a novel definition of discrete Hodge operators on simplicial cells. The new definition is solely based on topological and geometric properties of the cell complex. It represents the last building block of a discrete theory of electromagnetism on a simplicial cell complex. We conclude the chapter with a list of discrete equation systems for quasistatic electromagnetic field problems.

We write  $[M_{\text{type},\alpha}^{n,p}]$  for a discrete Hodge operator.  $n$  is the spatial dimension of the field problem,  $p$  is the degree of the cochain that is being mapped into an  $(n-p)$ -cochain on the dual complex, 'type' refers to the different definitions of Hodge operators and  $\alpha$  is the material parameter. We generally omit the dimension index for  $n = 3$ . Furthermore, we denote with a prime the  $n$ -cell's (element-) matrix as well as those parts of dual cells that lie inside the primal  $n$ -cell.

### 5.1 Discrete Hodge Operator on Brick-Shaped Cells

Recall that the entries of the field coefficient vectors are given by the integral values of the field over the respective  $p$ -cell. For topologically dual brick complexes

( $n = 3$ ), geometrical discrete Hodge operators  $[M_{\text{FIT},\alpha}^1]$  and  $[M_{\text{FIT},\alpha}^2]$  are given by<sup>1</sup>

$$[M_{\text{FIT},\alpha}^1]^{ii} := \alpha \frac{\|\bar{f}^i\|}{\|e^i\|},$$

$$[M_{\text{FIT},\alpha}^2]^{ii} := \alpha \frac{\|\bar{e}^i\|}{\|f^i\|},$$

where  $e$  and  $f$  denote edges and faces. The cell method that uses brick elements with the above discrete Hodge operators is called the Finite Integration Technique (FIT), [34]. The FIT Hodge operators defined above are square, diagonal and positive definite matrices. Their being square is due to the dual discretization of the field domain and thus the equal number of primal edges and dual faces as well as primal faces and dual edges. The diagonality of the matrices can be ascribed to the orthogonality of the primal and the dual complex, compare Fig. 5.1. Every pair of a primal cell  $i$  and its dual is assigned a material parameter  $\alpha$ .

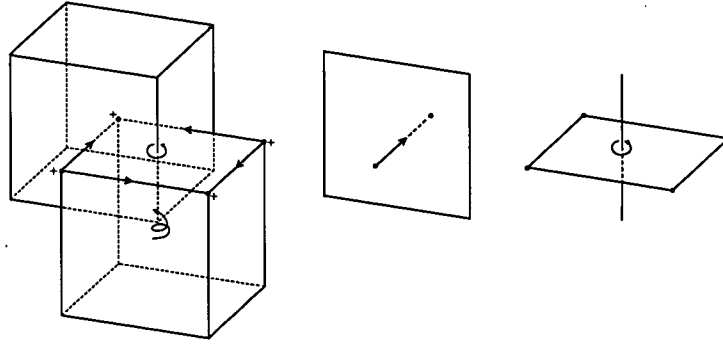


Figure 5.1: Left: Topologically dual cells (bricks). Middle: primal edge and dual face. Right: primal face and dual edge.

### Examples:

1.  $\tilde{D} = * \epsilon E$  translates into

$$\{\tilde{D}\}^i = \epsilon \frac{\|\bar{f}^i\|}{\|e^i\|} \{E\}^i,$$

$$\{\tilde{D}\} = [M_{\text{FIT},\epsilon}^1] \{E\}.$$

2.  $\tilde{H} = * \nu B$  translates into

$$\{\tilde{H}\}^i = \nu \frac{\|\bar{e}^i\|}{\|f^i\|} \{B\}^i,$$

$$\{\tilde{H}\} = [M_{\text{FIT},\nu}^2] \{B\}.$$

□

<sup>1</sup>By the norm of a face or edge we understand the area or length of the respective cell related to the respective SI unit, so that  $pd(\|f\|) = pd(\|e\|) = 1_{\text{D}}$ , compare Section 3.1.2.

Of course, similar discrete Hodge operators can be given for orthogonal, rectangular dual cell complexes in  $n = 2$  dimensions:

$$[M_{\text{FIT},\alpha}^{2,1}]^{ii} := \alpha \frac{\|\bar{e}^i\|}{\|e^i\|} \quad \text{and} \quad [M_{\text{FIT},\alpha}^{2,0}]^{ii} := \alpha^i \|\bar{f}^i\|.$$

## 5.2 Discrete Hodge Operator on Simplicial Cells

In this section we introduce a Hodge operator on simplicial cells. Note that, in the definitions to follow, we assume the simplex and its sides to be oriented according to Eq. (2.6) in Section 2.1.3.

In [6] we find a number of criteria that a discrete Hodge operator has to fulfill in order to give a valid approximation of its continuous counterpart:

1. The discrete Hodge operator should be *regular* (the dimension of its kernel is zero).
2. The continuous Hodge operators introduce material laws that are of a local character. The corresponding discrete operators should therefore be represented by *sparse* matrices.
3. From the continuous Hodge operator we know that  $\underline{F} \wedge * \alpha \underline{G} = \underline{G} \wedge * \alpha \underline{F}$  for  $\underline{F}, \underline{G} \in \mathcal{F}^p(\Omega)$ . This equation translates into  $\{F\}^T [M_\alpha^p] \{G\} = \{G\}^T [M_\alpha^p] \{F\}$ , i.e., a discrete Hodge operator should be a *symmetric* matrix.
4. Since  $\underline{F} \wedge * \alpha \underline{F} > 0$  for  $\alpha > 0$  we require the matrix to be *positive definite*.
5. Knowing that the discrete material law will only give an approximation of the continuous law, we require that at least for spatially constant fields the discrete material law yields exact results:

$$\begin{array}{ccc} \underline{F} & \xrightarrow{* \alpha} & \underline{G} \\ \downarrow d_\Omega & & \downarrow \\ \{F\} & \xrightarrow{[M_\alpha^p]} & \{G\} \end{array}$$

where  $d_\Omega$  denotes discretization, commutes only if  $\underline{F} = \text{const.}$  and  $\alpha = \text{const.}$

It can be easily verified that the FIT-discrete Hodge operator defined in the previous section fulfills the above criteria. In this section we will introduce a similar class of operators on simplicial cell complexes that we shall call the *geometric* discrete Hodge operators. We can generally not expect them to be diagonal matrices, as the primal faces and the barycentric dual edges in a simplicial complex are not orthogonal to each other. Geometric properties of the elements such as angles or aspect ratios will figure in the definition.

**Example:** As an example we choose Ohm's law in 2 dimensions:

For  $\underline{E} = E_x dx + E_y dy$ ,  $\underline{j} = \tilde{j}_x dx + \tilde{j}_y dy$  and  $E_z = \tilde{j}_z = 0$  it reads  $\underline{j} = *^2 \kappa \underline{E}$  where

$*^2\kappa$  is the continuous Hodge operator in 2 dimensions and the electric conductivity. In this 2-dimensional model,  $\underline{E}$  and  $\tilde{j}$  are even and odd 1-forms, respectively. The discrete equation will read  $\{\tilde{j}\} = [M_{\text{ge},\kappa}^{2,1}]\{E\}$  with  $\{\tilde{j}\} \in \mathbb{R}^{\bar{n}_1}$  and  $\{E\} \in \mathbb{R}^{n_1}$ ,  $n_1 = \bar{n}_1$ .

From a given electric field coefficient vector  $\{E\}$  we have to find a coefficient vector  $\{\tilde{j}\}$  on the barycentric dual complex. We claim that a discrete Hodge operator is given by

$$[M_{\text{ge},\kappa}^{2,1}]^{ij} := \frac{\|\bar{e}^i \wedge * \kappa \tilde{e}^j\|}{\|f\|},$$

which can be rewritten

$$[M_{\text{ge},\kappa}^{2,1}]^{ij} = \kappa \frac{1}{\|f\|} \|\bar{e}^i\| \|\bar{e}^j\| \cos \gamma^{ij}.$$

The primed dual edges denote the parts of the dual edges that lie in the respective face. By virtue of

$$\|f\| = \frac{3}{2} \|e^j\| \|\bar{e}^j\| \cos \delta^j$$

we obtain

$$[M_{\text{ge},\kappa}^{2,1}]^{ij} = \kappa \frac{2}{3} \frac{\|\bar{e}^j\| \cos \gamma^{ij}}{\|e^i\| \cos \delta^j}$$

and

$$\{\tilde{j}'\}^i = \kappa \frac{2}{3} \frac{\|\bar{e}^j\| \cos \gamma^{ij}}{\|e^i\| \cos \delta^j} \{E\}^j.$$

The angles  $\gamma^{ij}$  and  $\delta^j$  are explained in Fig. 5.2 for  $i = 3, j = 1$ . The global matrix is obtained by adding the element matrices in a global numbering scheme. The geometric Hodge operator is sparse, symmetric and regular.

□

Generalizing the above reasoning for  $p$ -Hodge operators in  $n$  dimensions we define the geometrical Hodge operator by

$$[M_{\text{ge},\alpha}^{n,p}]^{ij} := \frac{\|\bar{\varrho}_{n-p}^i \wedge * \alpha \tilde{\varrho}_{n-p}^j\|}{\|\varrho_n\|}. \quad (5.1)$$

This is a symmetric, sparse and regular operator. With

$$\|\varrho_n\| = \frac{n_p}{q} \|\varrho_p^j \wedge \bar{\varrho}_{n-p}^j\| = \frac{n_p}{q} \|\varrho_p^j\| \|\bar{\varrho}_{n-p}^j\| \cos \delta^j = \|\varrho_n\|,$$

where  $q = p(n-p) + 1$  and  $n_p$  denotes the number of primal  $p$ -cells in the primal  $n$ -cell, we can rewrite the definition as

$$[M_{\text{ge},\alpha}^{n,p}]^{ij} = \alpha \frac{q}{n_p} \frac{\|\bar{\varrho}_{n-p}^i\| \cos \gamma^{ij}}{\|\varrho_p^j\| \cos \delta^j}. \quad (5.2)$$

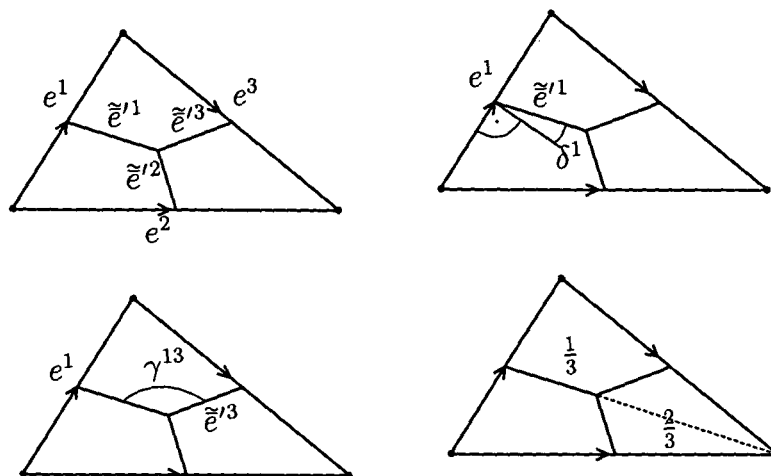


Figure 5.2: Factors in the definition of the 2-dimensional geometrical 1-Hodge. We display the mapping of an integral quantity on primal edge 1 into an integral quantity on the dual edge 3.

The coefficients  $q/n_p$  and the angles  $\gamma^{ij}$  and  $\delta^j$  are displayed in Figs. 5.3 and 5.4 for  $n = 3, p = 1$  and  $n = 3, p = 2$ . With  $\|g_0\| = 1$  and by setting the angles to zero for  $p = 0$  and  $p = n$ , we can give the comprehensive list of geometrical discrete Hodge operators:

$n = 1, p = 0, 1$ :

$$[M'_{ge,\alpha}]^{ij} = \alpha \frac{1}{2} \|\bar{e}^i\|, \quad [M'^{1,1}] = \alpha \frac{1}{\|e^j\|},$$

$n = 2, p = 0, 1, 2$ :

$$[M'^{2,0}]^{ij} = \alpha \frac{1}{3} \|\bar{f}^i\|, \quad [M'^{2,1}]^{ij} = \alpha \frac{2}{3} \frac{\|\bar{e}^i\| \cos \gamma^{ij}}{\|e^j\| \cos \delta^j}, \quad [M'^{2,2}]^{ij} = \alpha \frac{1}{\|f^j\|},$$

$n = 3, p = 0, 1, 2, 3$ :

$$[M'^{3,0}]^{ij} = \alpha \frac{1}{4} \|\bar{v}^i\|, \quad [M'^{3,1}]^{ij} = \alpha \frac{1}{2} \frac{\|\bar{f}^i\| \cos \gamma^{ij}}{\|e^j\| \cos \delta^j},$$

$$[M'^{3,2}]^{ij} = \alpha \frac{3}{4} \frac{\|\bar{e}^i\| \cos \gamma^{ij}}{\|f^j\| \cos \delta^j}, \quad [M'^{3,3}]^{ij} = \alpha \frac{1}{\|v^j\|}.$$

### 5.3 DEM Equation Systems

The following linear equation systems can be derived directly from the topological diagram and the metric laws on page 58:

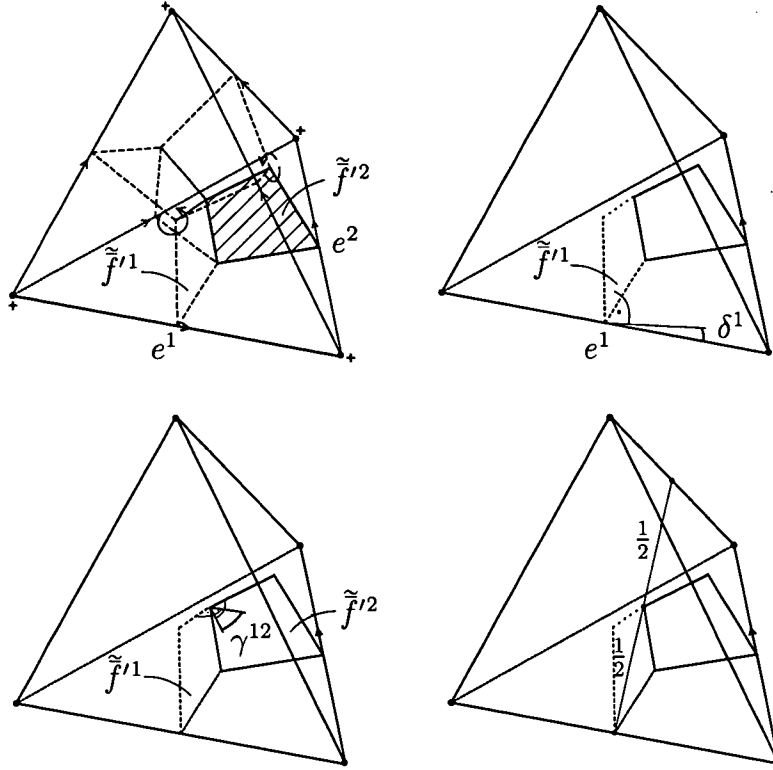


Figure 5.3: Factors in the definition of the geometrical 1-Hodge, mapping integral quantities on primal edges into integral quantities on dual faces.  $\delta^j$  is measured between the primal edge and the normal vector to the corresponding dual face.  $\gamma^{ij}$  in the middle is found to lie between the normal vectors to the respective dual faces. The factor  $1/2$  may be interpreted as the linear decrease of the field from the primal edge to the barycentre of the tetrahedron towards the opposite edge.

1. Magnetic vector-potential formulation of a magneto-quasistatic field problem:

$$[\tilde{D}^1][M_v^2][D^1]\{A\} + [\tilde{J}^1](\{\tilde{H}_{\partial\Omega}\} - \{\tilde{M}_{o,\partial\Omega}\}) + [M_\kappa^1]\{\partial_t A\} = \{\tilde{J}\} + [\tilde{D}^1]\{\tilde{M}_o\},$$

where  $\{\tilde{M}_o\}$  denotes a permanent magnetization. The magnetostatic equation without permanent magnets reads

$$[\tilde{D}^1][M_v^2][D^1]\{A\} + [\tilde{J}^1]\{\tilde{H}_{\partial\Omega}\} = \{\tilde{J}\}. \quad (5.3)$$

Owing to Eq. (4.19),  $[\tilde{D}_{\partial\Omega}^1]\{\tilde{H}_{\partial\Omega}\} = 0$ . As shown in Section 3.3, it follows that

$$\{\tilde{H}_{\partial\Omega}\} = -[\tilde{D}_{\partial\Omega}^0]\{\tilde{\varphi}_M\} - [\tilde{J}_{\partial\Omega,Ch}^0]\{\tilde{\varphi}_{M,Ch}\}.$$

2. Electric scalar-potential formulation for an electrostatic field problem:

$$-[\tilde{D}^2][M_\epsilon^1][D^0]\{\varphi\} + [\tilde{J}^2]\{\tilde{D}_{\partial\Omega}\} = \{\tilde{\rho}\}. \quad (5.4)$$

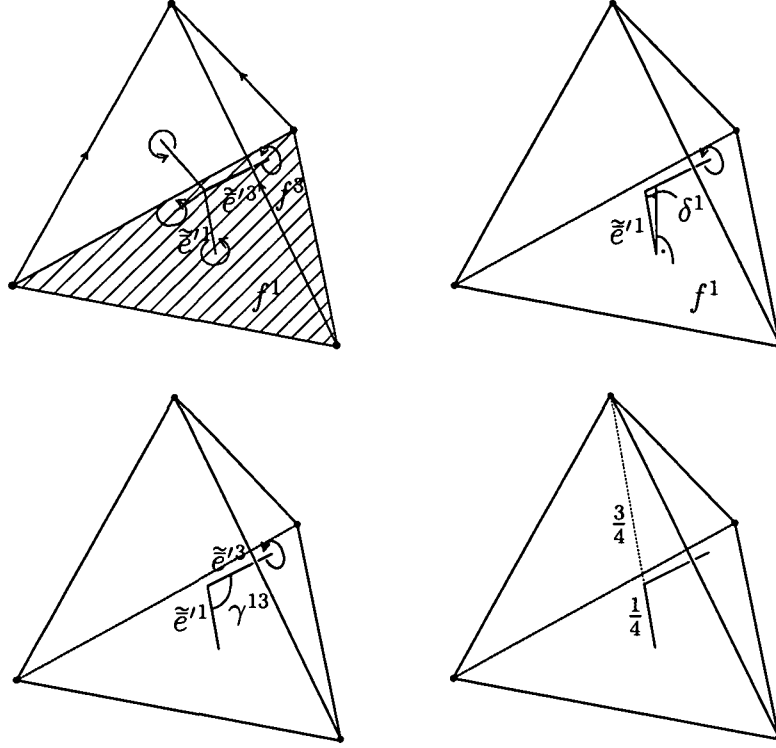


Figure 5.4: Factors in the definition of the geometrical 2-Hodge, mapping integral quantities on primal faces into integral quantities on dual edges.  $\delta^j$  is the angle between the normal vector to the primal face and the dual edge intersecting the face.  $\gamma^{ij}$  is the angle between the dual edge that the primal face is mapped to and the dual edge intersecting the primal face. The factor  $3/4$  may be interpreted as the linear decrease of the field from the primal face to the barycentre of the tetrahedron towards the opposite vertex.

### 3. Magnetic scalar-potential formulation for a magnetostatic field problem for $\{\tilde{j}\} = 0$ :

$$- [\bar{D}^2][\tilde{M}_\mu^1] \left( [\tilde{D}^0]\{\tilde{\varphi}_M\} - [\tilde{J}_{Ch}^0]\{\tilde{\varphi}_{M,Ch}\} \right) - [\bar{J}^2]\{\bar{B}_{\partial\Omega}\} = 0. \quad (5.5)$$

Note that for this last equation system we discretized the Ampère-Maxwell complex on the outer oriented primal complex and the Farady complex on the inner oriented barycentric dual complex.

Neglecting cohomology contributions and the notation of inner or outer orientation, we observe a pattern in the Equations (5.3), (5.4) and (5.5):

$$[\bar{D}^{n-p-1}][M_\vartheta^{p+1}][D^p]\{\alpha\} + [\bar{J}^{n-p-1}]\{\bar{\gamma}\} = \{\bar{\eta}\}, \quad (5.6)$$

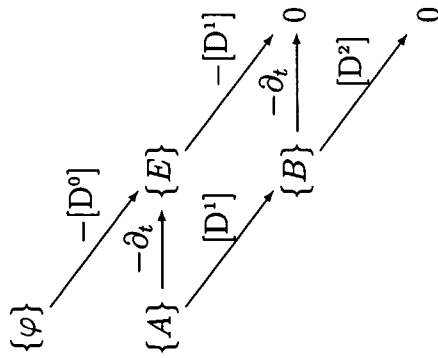
where  $\{\alpha\}$  is some potential coefficient vector,  $\{\bar{\gamma}\}$  is the Neumann data, discretized on the barycentric dual of the boundary complex and  $\{\bar{\eta}\}$  is the source coefficient vector on the dual complex. Note that the unknown potential is always



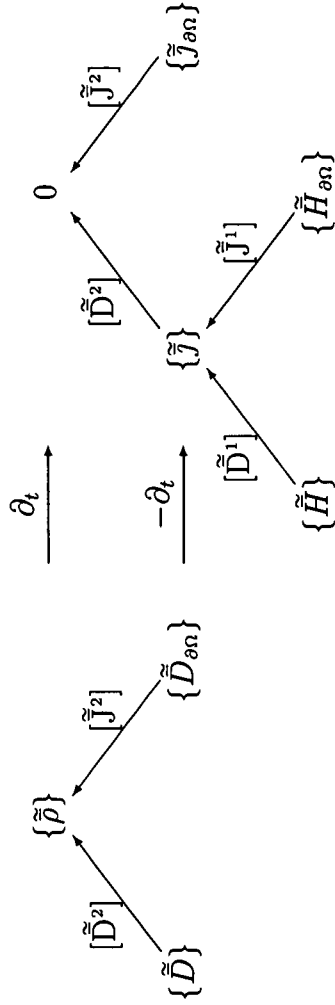
discretized on the primal complex. Consequently, for  $\{\alpha\} = \{\varphi\}$  or  $\{\alpha\} = \{A\}$ , the Faraday complex is discretized on the primal cell complex, whereas for  $\{\alpha\} = \{\tilde{\varphi}_M\}$  the Ampère-Maxwell complex is discretized on the primal cell complex.

Denoting  $\{\beta\} = [T^p]\{\alpha\}$  the Dirichlet data of the problem, we observe that, due to the topological duality, the number of Dirichlet coefficients and Neumann coefficients is identical,  $n_{p,\partial\Omega}$ . A total of  $n_{p,\partial\Omega}$  coefficients from the Dirichlet or Neumann data need to be supplied for the boundary value problem to be well posed and for the linear equation system to be solvable. Yet, the equation system will be singular due to the possibility of gauging  $\{\alpha\}$  by some element in the kernel of  $[D^p]$ .

Topological Laws,  $n = 3$



Metric Laws,  $n = 3$



$$\{\tilde{D}\} = [M_c^1]\{E\}, \quad \{\tilde{j}\} = [M_c^1]\{E\}, \quad \{\tilde{H}\} = [M_c^2]\{B\}$$

# 6

## Discrete Material Laws (3) - More Discrete Hodge Operators

The definition of a discrete Hodge operator is not unique. Different choices lead to different numerical schemes. The accuracy of a DEM formulation as well as the computational cost involved in setting it up and solving it largely depend on the choice of a discrete Hodge operator. After FIT- and geometrical Hodge, this chapter presents two more discrete Hodge operators: the Whitney Hodge operator, [32], and the Galerkin Hodge operator, [5]. Both operators rely on a local interpolation of a discrete field. A (linear) interpolation scheme, the so-called Whitney forms, is presented in Annex C. We introduce the Whitney and Galerkin Hodge operators and investigate the relations between the different definitions (geometric, Whitney, Galerkin, FIT). Note that in the following we assume the respective simplices and their sides to be oriented in the canonical way, compare page 7.

### 6.1 Whitney Hodge Operator

In Annex C the interpolation of  $p$ -cochains by Whitney  $p$ -forms  $w_i^p \in \mathcal{W}^p(\Omega)$ ,  $1 \leq i \leq n_p$ , is introduced. We will exploit this knowledge to introduce the following "natural" choice of a discrete Hodge operator, [1], [32]:

$$[M'_{\text{wh},\alpha}]^{ij} := \langle * \alpha w_j^p \mid \tilde{\varrho}_p^i \rangle. \quad (6.1)$$

Recall that the prime denotes objects related to one primal  $n$ -cell, e.g., the element matrix or the part of a dual cell that lies inside the primal  $n$ -cell. The continuous Hodge operator and the material parameter are applied to a Whitney form and its contribution is integrated over the dual  $(n-p)$ -cell. We will refer to the operator defined in Eq. (6.1) as the *Whitney Hodge operator*:

$$\begin{aligned} [M_{\text{wh},\alpha}^p] : \mathbb{R}^p &\longrightarrow \mathbb{R}^{n-p} \\ \{F\} &\longmapsto \{\tilde{G}\} = \tilde{d}_\Omega * \alpha w_\Omega \{F\}, \end{aligned}$$

where  $\tilde{d}_\Omega$  denotes the discretization on the outer oriented dual complex and  $w_\Omega$  the interpolation by Whitney forms. Furthermore it is assumed that  $\alpha$  is  $n$ -cell-wise constant.

The approximation property is fulfilled automatically by the interpolation with Whitney forms. The resulting matrix, however, is generally not symmetric as the following example demonstrates:

**Example:** We give  $\Omega$  the structure of a Euclidean vector space. A Whitney 2-form for  $n = 3$  can be written as

$$w_{j_1 j_2 j_3}^2 \cong \frac{\mathbf{x} - \mathbf{v}_{j_4}}{\|v\|},$$

where  $\mathbf{v}_{j_4}$  is the position vector of the point opposite to the face spanned by the points  $j_1, j_2$  and  $j_3$  and  $\mathbf{x}$  is the position vector of some point, compare Fig. 6.1. For  $n = 3, p = 2$ , Eq. (6.1) can be rewritten

$$[M_{\text{wh},\alpha}'^2]^{ij} = \alpha \frac{1}{3\|v\|} \int_{\bar{e}_i'} (\mathbf{x}(s) - \mathbf{v}_{j_4}) \cdot \mathbf{t}_i ds.$$

where the tangent vector  $\mathbf{t}_i$  reads

$$\mathbf{t}_i = \frac{\mathbf{c}_{i_1 i_2 i_3} - \mathbf{c}_v}{\|\mathbf{c}_{i_1 i_2 i_3} - \mathbf{c}_v\|} = \frac{\bar{\mathbf{e}}_i'}{\|\bar{\mathbf{e}}_i'\|}.$$

$i$  and  $j$  are multiindices; the first 3 entries address a primal face or a dual edge.  $\mathbf{c}_v$  denotes the barycenter of the tetrahedron  $v$  and  $\mathbf{c}_{i_1 i_2 i_3}$  the barycenter of  $f_{i_1 i_2 i_3}$ . With

$$\mathbf{c}_v - \mathbf{v}_{k_4} = 3(\mathbf{c}_{k_1 k_2 k_3} - \mathbf{c}_v)$$

the integral is solved by

$$\begin{aligned} [M_{\text{wh},\alpha}'^2]^{ij} &= \alpha \frac{\|\mathbf{c}_{i_1 i_2 i_3} - \mathbf{c}_v\|^2}{6\|v\|} + \alpha \frac{(\mathbf{c}_{i_1 i_2 i_3} - \mathbf{c}_v) \cdot (\mathbf{c}_{j_1 j_2 j_3} - \mathbf{c}_v)}{\|v\|} \\ &= \alpha \frac{\|\bar{\mathbf{e}}_i'\|^2}{6\|v\|} + \alpha \frac{\bar{\mathbf{e}}_i' \cdot \bar{\mathbf{e}}_j'}{\|v\|}. \end{aligned} \quad (6.2)$$

We can see that the first term on the right-hand side is responsible for the lack of symmetry in the Whitney Hodge operator.  $\square$

There is two main advantages of the discrete Whitney Hodge operator: its construction principle is intuitive and it is available on all polyhedral  $n$ -cells on that we can derive Whitney forms and barycentric dual cells. On the other hand it is an unsymmetric linear operator, thus, violating one of the key features that a discrete Hodge operator should have. We will come back to this issue in Sections 6.3 and D.1 and find that requiring a Hodge operator to be symmetric might in some cases be too strict.

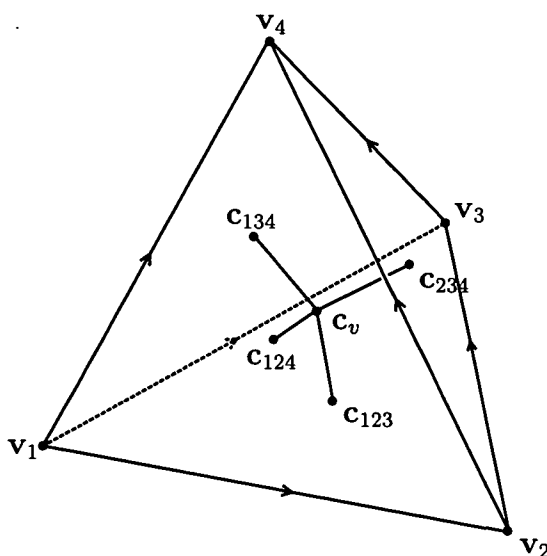


Figure 6.1: Tetrahedron with vertices and barcenters.

## 6.2 Galerkin Hodge Operator

The Galerkin Hodge operator stems from a DEM-interpretation of a Finite Element Method with Whitney forms. Following a convention, we denote  $\underline{\alpha}$  a potential, e.g.,  $\underline{A}$ ,  $\underline{\varphi}$  or  $\underline{\tilde{\varphi}}_M$  and  $\underline{\eta}$  a source field, e.g.,  $\underline{\tilde{j}}$  or  $\underline{\tilde{\rho}}$ . Consequently, we denote  $\vartheta$  the material property, elsewhere denoted by  $\alpha$ . Consider the differential equation

$$d*\vartheta d\underline{\alpha} = \underline{\eta}, \quad \underline{\alpha} \in {}^p H_d(\Omega), \quad \underline{\eta} \in {}^{n-p} H_d(\Omega). \quad (6.3)$$

For a given source  $\underline{\eta}$ , we search for a solution  $\underline{\alpha}$  in a finite-dimensional subspace  $\mathcal{W}^p(\Omega)$  of  ${}^p H_d(\Omega)$ , compare Annex C. An optimum solution is found by an orthogonalization process: we require the residual

$$R(\underline{\alpha}) = d*\vartheta d\underline{\alpha} - \underline{\eta}$$

to be orthogonal to the space of Whitney  $p$ -forms. We require that

$$\langle R(\underline{\alpha}), \underline{w}_i^p \rangle = 0, \quad \underline{w}_i^p \in \mathcal{W}^p(\Omega), \quad i = 1, \dots, n_p.$$

This approach, i.e., the orthogonalization of the residual on the solution space, is called the *Galerkin method*. We define the scalar product by

$$\langle \underline{F}, \underline{G} \rangle = \langle \underline{F} \wedge \underline{G} \mid \Omega \rangle$$

and obtain

$$\langle d*\vartheta d\underline{\alpha} \wedge \underline{w}_i^p \mid \Omega \rangle = \langle \underline{\eta} \wedge \underline{w}_i^p \mid \Omega \rangle, \quad i = 1, \dots, n_p, \quad (6.4)$$

which is called the *weighted residual* equation. By virtue of

$$\langle d(\underline{F} \wedge \underline{G}) \mid \Omega \rangle = \langle \underline{F} \wedge \underline{G} \mid \partial\Omega \rangle, \quad \underline{F} \in \mathcal{F}^p(\Omega), \underline{G} \in \mathcal{F}^{n-p}(\Omega),$$

and

$$d(\underline{F} \wedge \underline{G}) = d\underline{F} \wedge \underline{G} + (-1)^p \underline{F} \wedge d\underline{G}, \quad \underline{F} \in \mathcal{F}^p(\Omega),$$

we can rewrite Eq. (6.4)

$$(-1)^{n-p} \langle *v d\alpha \wedge dw_i^p \mid \Omega \rangle + \langle t *v d\alpha \wedge t w_i^p \mid \partial\Omega \rangle = \langle \underline{\eta} \wedge w_i^p \mid \Omega \rangle, \quad (6.5)$$

$i = 1, \dots, n_p$ , where  $t *v d\alpha = \gamma$  is the Neumann data of the field problem and  $t \alpha$  is the Dirichlet data. On a given cell complex that discretizes the domain  $\Omega$ , and with Whitney  $p$ -forms available on the complex, Eq. (6.5) is the finite element formulation of Eq. (6.3).

**Example:** For  $p = 1$ ,  $\alpha = \underline{A}$ ,  $\eta = \underline{\tilde{j}}_s$  and  $v = \nu$  we obtain

$$\langle *v d\underline{A} \wedge dw_i^1 \mid \Omega \rangle + \langle t *v d\underline{A} \wedge t w_i^1 \mid \partial\Omega \rangle = \langle \underline{\tilde{j}}_s \wedge w_i^1 \mid \Omega \rangle, \quad i = 1, \dots, n_1.$$

With  $t *v d\underline{A} = \underline{\tilde{H}}_{\partial\Omega}$  we write the finite element vector potential formulation of a magnetostatic field problem with Whitney 1-forms

$$\langle *v d\underline{A} \wedge dw_i^1 \mid \Omega \rangle + \langle \underline{\tilde{H}}_{\partial\Omega} \wedge t w_i^1 \mid \partial\Omega \rangle = \langle \underline{\tilde{j}}_s \wedge w_i^1 \mid \Omega \rangle, \quad i = 1, \dots, n_1. \quad (6.6)$$

□

Equation (6.5) is a linear equation system of  $n_p$  equations and  $n_{p,\partial\Omega} + n_p$  unknowns in the Whitney forms' coefficient vectors  $\{\alpha\}$  and  $\{\gamma\}$ .  $n_{p,\partial\Omega}$  coefficients need to be supplied for the boundary value problem to be well posed.

We can rewrite Eq. (6.5) in terms of matrix operators: We introduce the  $[K^p]$  and  $[M_{G_a,v}^p]$  matrices by

$$\begin{aligned} \langle \underline{F} \wedge \underline{G} \mid \Omega \rangle &= \{G\}^T [K^p] \{F\}, \quad \underline{F} \in \mathcal{W}^p(\Omega), \underline{G} \in \mathcal{W}^{n-p}(\Omega) \quad \text{and} \\ \langle *v \underline{F} \wedge \underline{G} \mid \Omega \rangle &= \{G\}^T [M_{G_a,v}^p] \{F\}, \quad \underline{F} \in \mathcal{W}^p(\Omega), \underline{G} \in \mathcal{W}^p(\Omega), \end{aligned}$$

with

$$\begin{aligned} [K^p]^{ij} &= \langle w_j^p \wedge w_i^{n-p} \mid \Omega \rangle \quad \text{and} \\ [M_{G_a,v}^p]^{ij} &= \langle *v w_j^p \wedge w_i^p \mid \Omega \rangle. \end{aligned} \quad (6.7)$$

Furthermore, we define the  $n_{p,\partial\Omega} \times n_{n-1-p,\partial\Omega}$  matrix

$$[K'_{\partial\Omega}]^{ij} = \langle t w_j^p \wedge t w_i^{n-1-p} \mid \partial\Omega \rangle.$$

If we now interpolate the source field  $\underline{\eta}$  by a Whitney  $(n-p)$ -form  $\underline{\eta} \in \mathcal{W}^{n-p}(\Omega)$  we can rewrite Eq. (6.5):

$$(-1)^{n-p}[\mathbf{D}^p]^T[\mathbf{M}_{\mathbf{G}_a, \vartheta}^{p+1}][\mathbf{D}^p]\{\alpha\} + [\mathbf{T}^p]^T[\mathbf{K}_{\partial\Omega}^{n-p-1}]\{\gamma\} = [\mathbf{K}^{n-p}]\{\eta\}. \quad (6.8)$$

It is, of course, not by accident that the above introduced "Galerkin-type" matrices are denoted by the symbols of a discrete Hodge operator and a transfer matrix.  $[\mathbf{M}_{\mathbf{G}_a, \vartheta}^p]$  is called the Galerkin Hodge operator and the definition of the  $[\mathbf{K}^p]$  matrix yields identical topological matrices as the definition of transfer matrices by interpolation on simplices in Section 4.3. This identity is proven by simply verifying that both definitions yield identical matrices for  $0 \leq p \leq n$  on one arbitrary simplicial cell. Now we can see that

$$[\mathbf{K}^p] = (-1)^{p(n-p)}[\mathbf{K}^{n-p}]^T,$$

compare Section 4.3. The advantage of the Galerkin-type definitions is that they can be easily applied on different types of cells, provided that there are Whitney  $p$ -forms defined on them.

With Eqs. (4.2) and (4.14) we can rewrite Eq. (6.8)

$$[\bar{\mathbf{D}}^{n-p-1}][\mathbf{M}_{\mathbf{G}_a, \vartheta}^{p+1}][\mathbf{D}^p]\{\alpha\} + [\bar{\mathbf{J}}^{n-p-1}]\{\bar{\gamma}\} = \{\bar{\eta}\}.$$

**Example:** Equation (6.6) reads

$$[\tilde{\mathbf{D}}^1][\mathbf{M}_{\mathbf{G}_a, \nu}^2][\mathbf{D}^1]\{A\} + [\tilde{\mathbf{J}}^1]\{\tilde{H}_{\partial\Omega}\} = \{\tilde{J}_s\}.$$

□

Comparison with Eq. (5.6) confirms that the Finite Element Method with Whitney forms yields a DEM equation system with a special discrete Hodge operator.

## 6.3 Relationship between Hodge Operators

### Geometrical and Whitney Hodge

We compare Eqs. (6.2) and (5.1) and find that for  $n = 3$ ,  $p = 2$ , the geometrical Hodge operator yields the symmetric part of the Whitney Hodge operator. The same holds for  $n = 2$ ,  $p = 1$  and  $n = 1$ ,  $p = 0$ . Furthermore, it is easy to verify that, for  $p = n$ ,  $[\mathbf{M}_{\mathbf{W}_h, \alpha}^n] = [\mathbf{M}_{\mathbf{ge}, \alpha}^n]$ . For  $p < (n-1)$ , however, no direct relationship between Whitney and geometrical Hodge has been found to date.

### Whitney and Galerkin Hodge

In [1] it is shown for  $n = 3$ ,  $p = 2$  and for element-wise constant isotropic material properties that

$$[\tilde{D}^1][M_{\text{Wh},\nu}^2][D^1] = [\tilde{D}^1][M_{\text{Ga},\nu}^2][D^1].$$

The Whitney and Galerkin 2-Hodge operators lie in an equivalence class that is defined for Hodge operators 'a' and 'b' by

$$[M_{a,\alpha}^p] \sim [M_{b,\alpha}^p] \iff [\bar{D}^{n-p}][M_{a,\alpha}^p][D^{p-1}] = [\bar{D}^{n-p}][M_{b,\alpha}^p][D^{p-1}]. \quad (6.9)$$

### Galerkin and geometrical Hodge

It has been shown in [1] that the discrete curlcurl-operator is the same symmetric semi-positive definite matrix whether we use the Whitney or the Galerkin Hodge operator. It can be verified by the same proof that the unsymmetric part of the Whitney Hodge operator lies in the zero-class under the equivalence relation (6.9). As a consequence, the geometrical 2-Hodge operator for  $n = 3$  lies in the same equivalence class as the respective Whitney and the Galerkin Hodges.

### FIT Hodge

The material matrices in the Finite Integration Technique, [34], are diagonal matrices. All other above introduced discrete Hodge operators are represented by sparse matrices. As a consequence, the inverse of the FIT Hodge is, again, a diagonal matrix.

We wish to apply the construction principle of the other discrete Hodge operators in order to find an inverse Hodge operator. For Whitney-form based Hodges this approach is not practicable since there are no Whitney forms on the barycentric dual complex. The geometric Hodge looks more promising in this respect.



# 7

## Boundary Element Method in DEM Notation

In this chapter we introduce a Boundary Element Method with Whitney forms in  $n = 3$  dimensions. We focus on a notation that is closely related to the DEM coefficient vector and linear operator notation. The BEM formulation we use was introduced in [23]. A more detailed survey can be found in [28].

### 7.1 Representation Formula

We introduce a representation formula of a potential  $\alpha$  in a domain  $\Omega$  in terms of source contributions in  $\Omega$  and the Dirichlet and Neumann data on some closed surface  $\Gamma$ .

Let  $\Omega^-$  denote a bounded open submanifold of a 3-dimensional affine-Euclidean space  $E_3$ . Denote  $\Gamma = \partial\Omega^-$  its boundary and  $\Omega^+$  the complement of  $\Omega^- \cup \Gamma$ .  $\Omega$  is the union  $\Omega^- \cup \Omega^+$ .  $\Gamma$  is consistently oriented with  $\Omega^-$ .<sup>1</sup> For the sake of simplicity we assume  $\Omega^-$  to be contractible.

We consider the second order equation

$$d*\vartheta d\alpha = \underline{\eta} \quad \text{in } \Omega. \quad (7.1)$$

where  $\alpha \in \mathcal{F}^p(\Omega)$  and  $\underline{\eta} \in \mathcal{F}^{n-p}(\Omega)$ ,  $p = 0, 1$ . We assume the source  $\underline{\eta}$  to be different from zero on  $\Omega^+$  only inside a sphere of finite radius  $R$ , thus accounting for the existence of the third integral in Eq. (7.2).

A necessary condition for the existence of solutions of Eq. (7.1) is that

$$d\underline{\eta} = 0.$$

---

<sup>1</sup>Eventually, the domains  $\Omega^-$  and  $\Omega^+$  will represent a DEM domain and a BEM domain, see Chapter 8.  $\Omega^-$  will contain permeable and conductive material and  $\Omega^+$  will be an air domain.

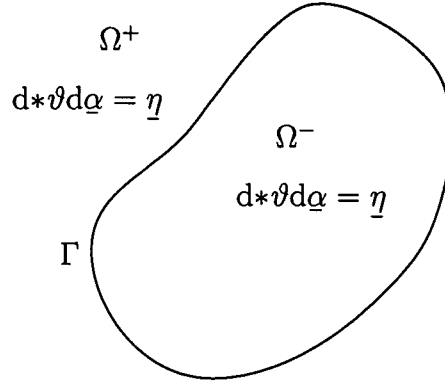


Figure 7.1: Decomposition of  $\Omega = E^3$  into the bounded domain  $\Omega^-$  and the unbounded domain  $\Omega^+$ .

The boundary data is represented by jump operators on  $\Gamma$

$$\gamma_D \alpha = \underline{j} \alpha = \underline{\beta}, \quad \gamma_N \alpha = \underline{j} * \vartheta d\alpha = \underline{\gamma},$$

where  $\gamma_D$  and  $\gamma_N$  are the Dirichlet and Neumann jumps, respectively, and  $\underline{\beta}$  and  $\underline{\gamma}$  are the Dirichlet and Neumann data. By applying the exterior derivative to  $\underline{\gamma}$  we find that

$$d\underline{\gamma} = d\underline{j} * \vartheta d\alpha = \underline{j} d* \vartheta d\alpha = \underline{j} \underline{\eta}.$$

This condition is trivially fulfilled for  $p = 0$ . For  $p = 1$  we require that  $\underline{j} \underline{\eta} = 0$ , so that the Neumann data must be a closed form,  $d\underline{\gamma} = 0$ .

### Examples:

1. For  $p = 0$  we set  $\alpha = \varphi$ ,  $\vartheta = \varepsilon_0$ ,  $\underline{\beta} = \underline{j} \varphi$  and  $\underline{\gamma} = -\underline{j} \underline{D}$ . With  $\underline{\eta} = \underline{\tilde{\rho}}$ , Eq. (7.1) yields the Poisson equation

$$d*\varepsilon_0 d\varphi = \underline{\tilde{\rho}}.$$

2. For  $p = 1$  we set  $\alpha = \underline{A}$ ,  $\vartheta = \nu_0$ ,  $\underline{\beta} = \underline{j} \underline{A}$ ,  $\underline{\gamma} = \underline{j} \underline{H}$  and  $\underline{\eta} = \underline{\tilde{j}}_s$  and find

$$d*\nu_0 d\underline{A} = \underline{\tilde{j}}_s.$$

We require that  $d\underline{\tilde{j}}_s = 0$  and  $\underline{j} \underline{\tilde{j}}_s = 0$ . □

It is shown in [23] that a solution of Eq. (7.1) can be found in terms of the Dirichlet and Neumann data and the sources in  $\Omega$ ; the *Kirchhoff representation formula* can be written as follows:

$$\begin{aligned} \alpha'(\mathbf{x}') &= \underbrace{-\langle \gamma_D \underline{G}^p \wedge \underline{\gamma} | \Gamma \rangle}_{-\Psi_{\text{SL}}^p(\underline{\gamma})(\mathbf{x}')} + \underbrace{(-1)^p \langle \gamma_N \underline{G}^p \wedge \underline{\beta} | \Gamma \rangle}_{\Psi_{\text{DL}}^p(\underline{\beta})(\mathbf{x}')} + \underbrace{\langle \underline{G}^p \wedge \underline{\eta} | \Omega \rangle}_{\Psi_{\text{Newt.}}^p(\underline{\eta})(\mathbf{x}')} \\ &\quad - \underbrace{d' \langle \gamma_D \underline{G}^{p-1} \wedge \underline{\phi} | \Gamma \rangle}_{\Psi_{\text{gauge}}^p(\underline{\phi})(\mathbf{x}')} \end{aligned} \quad (7.2)$$

where  $\underline{\phi} = \mathbf{j} * \vartheta \underline{\alpha}$  and  $\mathbf{x} \in \Omega$ ,  $\mathbf{x}' \in \Omega'$ . Primed objects lie in the so-called observation space and unprimed ones in the source space. It is assumed that  $d\underline{\eta} = 0$ .  $\underline{G}^p$  is the Green double form

$$\underline{G}^p(\mathbf{x}, \mathbf{x}') = g(\mathbf{x}, \mathbf{x}') \underline{I}^p,$$

with the fundamental solution of the scalar Laplace equation

$$g(\mathbf{x}, \mathbf{x}') = \frac{1}{4\pi\vartheta \|\mathbf{x} - \mathbf{x}'\|}$$

and the identity double form

$$\underline{I}^0 = 1,$$

$$\underline{I}^1 = dx \otimes dx' + dy \otimes dy' + dz \otimes dz',$$

$$\underline{I}^2 = (dx \wedge dy) \otimes (dx \wedge dy)' + (dy \wedge dz) \otimes (dy \wedge dz)' + (dz \wedge dx) \otimes (dz \wedge dx)',$$

$$\underline{I}^3 = (dx \wedge dy \wedge dz) \otimes (dx \wedge dy \wedge dz)'$$

Double forms are denoted with a double underbar. The addends on the right-hand side of Eq. (7.2) are denoted single-layer potential  $\Psi_{\text{SL}}^p(\underline{\gamma})(\mathbf{x}')$ , double-layer potential  $\Psi_{\text{DL}}^p(\underline{\beta})(\mathbf{x}')$ , Newton potential (or source potential)  $\Psi_{\text{Newt.}}^p(\underline{\eta})(\mathbf{x}')$  and gauge potential  $\Psi_{\text{gauge}}^p(\underline{\phi})(\mathbf{x}')$ .

### Examples:

1. For  $p = 0$ , Eq. (7.2) reads

$$\underline{\varphi}'(\mathbf{x}') = -\langle \gamma_{\text{D}} \underline{G}^0 \wedge \mathbf{j} \tilde{\underline{D}} \mid \Gamma \rangle + \langle \gamma_{\text{N}} \underline{G}^0 \wedge \mathbf{j} \underline{\varphi} \mid \Gamma \rangle + \langle \underline{G}^0 \wedge \tilde{\underline{\rho}} \mid \Omega \rangle.$$

With  $\mathbf{j} \tilde{\underline{D}} = \tilde{\underline{\sigma}}$  and  $\mathbf{j} \underline{\varphi} = *1/\varepsilon_0 \tilde{\underline{\sigma}}_{\text{DL}}$  we identify the single- and double-layer potentials as the potentials of a single-layer and a double-layer of electric charges, respectively.

2. For  $p = 1$  we obtain

$$\begin{aligned} \underline{A}'(\mathbf{x}') &= -\langle \gamma_{\text{D}} \underline{G}^1 \wedge \mathbf{j} \tilde{\underline{H}} \mid \Gamma \rangle - \langle \gamma_{\text{N}} \underline{G}^1 \wedge \mathbf{j} \underline{A} \mid \Gamma \rangle + \langle \underline{G}^1 \wedge \tilde{\underline{j}}_{\text{s}} \mid \Omega \rangle \\ &\quad - d' \langle \gamma_{\text{D}} \underline{G}^0 \wedge \mathbf{j} * \nu_0 \underline{A} \mid \Gamma \rangle. \end{aligned}$$

With  $\mathbf{j} \tilde{\underline{H}} = \tilde{\underline{K}}$  and  $\mathbf{j} \underline{A} = -*\mu_0 \tilde{\underline{K}}_{\text{DL}}$  we identify the potentials of a single-layer and a double-layer of surface currents.  $\square$

The gauge potential vanishes for  $p = 0$ . For  $p = 1$  it can be eliminated by the introduction of equivalence classes according to

$$\underline{\alpha}' \sim \underline{\alpha}' + d' \underline{\lambda}', \quad \underline{\lambda}' \in \mathcal{F}^{p-1}(\Omega'). \quad (7.3)$$

Denote with  $\mathcal{F}^p(d, \Omega)$  the space of closed  $p$ -forms.<sup>2</sup> Then the space of equivalence classes is the quotient space  $\mathcal{F}^p(\Omega)/\mathcal{F}^p(d, \Omega)$ . The double-layer potential of an equivalence class of Dirichlet data is shown to be well defined in Section F.1.

We find a representation formula for an equivalence class  $[\underline{\alpha}']$

$$[\underline{\alpha}'] = -\Psi_{\text{SL}}^{p\sim}(\underline{\gamma}) + \Psi_{\text{DL}}^{p\sim}([\underline{\beta}]) + \Psi_{\text{Newt.}}^{p\sim}(\underline{\eta}),$$

where the ' $\sim$ '-sign in the index of the potentials indicates a mapping into the quotient space of equivalence classes.

The following jump-relations are derived in [23]:

$$\begin{aligned} \mathbf{j}'\Psi_{\text{SL}}^p(\underline{\gamma}) &= 0, \\ \mathbf{j}'*\vartheta d\Psi_{\text{SL}}^p(\underline{\gamma}) &= -\underline{\gamma}, \\ \mathbf{j}'\Psi_{\text{DL}}^p(\underline{\beta}) &= \underline{\beta}, \\ \mathbf{j}'*\vartheta d\Psi_{\text{DL}}^p(\underline{\beta}) &= 0. \end{aligned}$$

### Examples:

1. We denote  $\varphi_{\text{SL}} = -\Psi_{\text{SL}}^0(\underline{\gamma})$  an electric scalar potential due to electric surface charges  $\underline{\tilde{\sigma}}$  on  $\Gamma$  and  $\varphi_{\text{DL}} = \Psi_{\text{DL}}^0(\underline{\beta})$  the potential due to a double-layer of charges  $\underline{\tilde{\sigma}}_{\text{DL}}$ . With  $\underline{\beta} = \mathbf{j}\varphi = *^2\mathbf{1}/\varepsilon_0\underline{\tilde{\sigma}}_{\text{DL}}$  and  $\underline{\gamma} = -\mathbf{j}\underline{\tilde{D}} = -\underline{\tilde{\sigma}}$ , the above relations yield

$$\begin{aligned} \mathbf{j}'\varphi_{\text{SL}} &= 0, \\ -\mathbf{j}'*\varepsilon_0 d\varphi_{\text{SL}} &= \underline{\tilde{\sigma}}, \\ \mathbf{j}'\varphi_{\text{DL}} &= *^2\mathbf{1}/\varepsilon_0\underline{\tilde{\sigma}}_{\text{DL}}, \\ \mathbf{j}'*\varepsilon_0 d\varphi_{\text{DL}} &= 0. \end{aligned}$$

2. Following an analog reasoning for  $p = 1$  we find

$$\begin{aligned} \mathbf{j}'A_{\text{SL}} &= 0, \\ \mathbf{j}'*\nu_0 dA_{\text{SL}} &= \underline{\tilde{K}}, \\ \mathbf{j}'A_{\text{DL}} &= -*^2\mu_0\underline{\tilde{K}}_{\text{DL}}, \\ \mathbf{j}'*\nu_0 dA_{\text{DL}} &= 0. \end{aligned}$$

□

At this point we have derived and studied a representation formula. The next section will show what needs to be done to formulate and solve a boundary value problem.

<sup>2</sup>On a contractible domain, for  $p \geq 1$ , closed  $p$ -forms are the coboundaries of  $(p-1)$ -forms. On a non-contractible manifold, Eq. (7.3) has to include cohomology fields as members of the zero-equivalence class.

## 7.2 Boundary Value Problem

In the previous section we have introduced a representation formula that yields the value of a potential  $\underline{\alpha}$  on a domain  $\Omega$ . The domain is divided by a closed surface  $\Gamma$  into a bounded open domain  $\Omega^-$  and an unbounded open domain  $\Omega^+$ .  $\underline{\alpha}$  can be calculated for a given distribution of single- and double-layer sources on  $\Gamma$  and sources in  $\Omega$ .

This section presents the formulation of a boundary value problem: We formulate the boundary value problem for the exterior domain  $\Omega^+$ . An analog formulation can be derived for the inner domain  $\Omega^-$ . For the boundary value problem to have a unique solution, we need to require that

$$\begin{aligned} \underline{\eta} &= 0 \quad \text{on } \Omega^-, \\ \underline{\beta} &= \mathbf{t}^+ \underline{\alpha} \quad \text{and} \quad \underline{\gamma} = \mathbf{t}^+ * \vartheta d\underline{\alpha}. \end{aligned}$$

As a consequence, we require that the potential  $\underline{\alpha}$  be zero on the entire bounded domain  $\Omega^-$ .

Under these assumptions, the Dirichlet and Neumann data cannot be chosen at will. For a given source field  $\underline{\eta}$  and given Dirichlet data (Dirichlet problem) there is one and only one  $\underline{\alpha}$  and hence  $\underline{\beta} = \mathbf{t}^+ \underline{\alpha}$  that fulfills Eq. (7.2). The Dirichlet and Neumann problems are formulated as follows:

*For given  $\underline{\beta}$  and  $\underline{\eta}$  find  $\underline{\gamma}$  such that  $\gamma_D' \underline{\alpha} = \underline{\beta}$  and  $\gamma_N' \underline{\alpha} = \underline{\gamma}$ . (Dirichlet problem)*

And similarly:

*For given  $\underline{\gamma}$  and  $\underline{\eta}$  find  $\underline{\beta}$  such that  $\gamma_D' \underline{\alpha} = \underline{\beta}$  and  $\gamma_N' \underline{\alpha} = \underline{\gamma}$ . (Neumann problem)*

Fixing Dirichlet and Neumann data at the same time yields an overdetermined system. The same reasoning holds for the Neumann problem (Neumann data and source field is given).

To solve a Dirichlet problem we apply the trace operator  $\mathbf{t}^{+'}$  on Eq. (7.4)<sup>3</sup>:

$$[\underline{\beta}'] = -\mathbf{t}^{+'} \Psi_{SL}^{p\sim}(\underline{\gamma}) + \mathbf{t}^{+'} \Psi_{DL}^{p\sim}([\underline{\beta}]) + \mathbf{t}^{+'} \Psi_{\text{Newt.}}^{p\sim}(\underline{\eta}). \quad (7.4)$$

Eq. (7.4) is called the *1st Calderón equation*.

Denote  $\Theta^-$  and  $\Theta^+$  the solid angles under which  $\Omega^-$  and  $\Omega^+$  are seen from a point  $\mathbf{x} \in \Gamma$ . With  $\Theta^- + \Theta^+ = 4\pi$  and with  $\mathbf{j} \Psi_{DL}^{p\sim} = \mathcal{I}$ , where  $\mathcal{I} : [\underline{\beta}] \mapsto [\underline{\beta}']$  is the identity operator, we find

$$\begin{aligned} \mathbf{t}^{+'} \Psi_{DL}^{p\sim} &= \frac{\Theta^+}{4\pi} \mathbf{t}^{+'} \Psi_{DL}^{p\sim} + \frac{\Theta^-}{4\pi} \mathbf{t}^{+'} \Psi_{DL}^{p\sim} \\ &= \frac{\Theta^+}{4\pi} \mathbf{t}^{+'} \Psi_{DL}^{p\sim} + \frac{\Theta^-}{4\pi} \mathbf{t}^{-'} \Psi_{DL}^{p\sim} + \frac{\Theta^-}{4\pi} \mathcal{I} \end{aligned}$$

<sup>3</sup>The trace operator on an equivalence class of potentials is defined in the obvious way,  $\mathbf{t}^+ : \mathcal{F}^p(\Omega^+)/\mathcal{F}^p(d, \Omega^+) \rightarrow \mathcal{F}^p(\Gamma)/\mathcal{F}^p(d, \Gamma)$ .

and eventually, with  $[\underline{\beta}'] = \mathcal{I}([\underline{\beta}])$ , Eq. (7.4) reads

$$\frac{\Theta^+}{4\pi} \mathcal{I}([\underline{\beta}]) - \left( \frac{\Theta^+}{4\pi} \mathbf{t}^{+'} + \frac{\Theta^-}{4\pi} \mathbf{t}^{-'} \right) \Psi_{\text{DL}}^{p\sim}([\underline{\beta}]) + \mathbf{t}^{+'} \Psi_{\text{SL}}^{p\sim}(\underline{\gamma}) = \mathbf{t}^{+'} \Psi_{\text{Newt.}}^{p\sim}(\underline{\eta}).$$

With

$$\Psi_{\text{DL}}^{*p\sim}([\underline{\beta}]) = \frac{\Theta^+}{4\pi} \mathcal{I}([\underline{\beta}]) - \left( \frac{\Theta^+}{4\pi} \mathbf{t}^{+'} + \frac{\Theta^-}{4\pi} \mathbf{t}^{-'} \right) \Psi_{\text{DL}}^{p\sim}([\underline{\beta}]),$$

we find for the equation of a Dirichlet-type boundary value problem

$$\Psi_{\text{DL}}^{*p\sim}([\underline{\beta}]) + \mathbf{t}^{+'} \Psi_{\text{SL}}^{p\sim}(\underline{\gamma}) = \mathbf{t}^{+'} \Psi_{\text{Newt.}}^{p\sim}(\underline{\eta}). \quad (7.5)$$

To solve a Dirichlet-type problem we need to invert the single-layer operator. From the resulting Neumann data  $\underline{\gamma}$  with given data  $\underline{\beta}$  and  $\underline{\eta}$  we can determine the potential in every point of  $\Omega^+$  from the Kirchhoff representation formula, Eq. (7.2).

To solve a Neumann problem, we apply the Neumann-trace  $\mathbf{t}^{+'} \ast \vartheta$  on Eq. (7.4) and obtain the second Calderón equation, which yields an equation similar to Eq. (7.5).

### 7.3 BEM Formulation

Eventually, the boundary value problem is discretized, yielding a Boundary Element Method formulation. As we have done before, we focus on the Dirichlet problem and state that a Neumann problem can be treated in a similar way.

Assume that  $\underline{\beta} \in {}^p H_d(\Gamma)$ ,  $\underline{\eta} \in {}^{3-p} H_d(d, \Omega^+)$  and  $\underline{\gamma} \in {}^{2-p} H_d(d, \Gamma)$ , compare Annex C. We approximate  $\Gamma$  by a 2-dimensional simplicial cell complex and  ${}^p H_d(\Gamma)$  by  $\mathcal{W}^p(\Gamma)$  as well as  ${}^{2-p} H_d(d, \Gamma)$  by  $\mathcal{W}^{2-p}(d, \Gamma)$ . Note that the trace of a Whitney  $p$ -form on  $\Omega^+$  lies in  $\mathcal{W}^p(\Gamma)$  and that  $\mathcal{W}^p(\Gamma)$  yields a consistent discretization of the respective traces of Sobolev spaces on  $\Gamma$ , [9].

For a discretization and for performing numerical computations we need to choose one representative  $\underline{\beta}$  from the Dirichlet data equivalence class  $[\underline{\beta}]$  and equally one representative in the image of the integral operators in Eq. (7.5). The discrete Dirichlet problem can be formulated as follows:

*For given  $\underline{\beta} \in \mathcal{W}^p(\Gamma)$  and  $\underline{\eta} \in {}^{3-p} H_d(d, \Omega^+)$  find  $\underline{\gamma} \in \mathcal{W}^{2-p}(d, \Gamma)$  such that*

$$\Psi_{\text{DL}}^{*p}(\underline{\beta}) + \mathbf{t}^{+'} \Psi_{\text{SL}}^p(\underline{\gamma}) = \mathbf{t}^{+'} \Psi_{\text{Newt.}}^p(\underline{\eta}). \quad (7.6)$$

We rewrite Eq. (7.6) by

$$\underline{\beta}_{\text{DL}}^* + \underline{\beta}_{\text{SL}} = \underline{\beta}_{\text{Newt.}}$$

where  $\underline{\beta}_{\text{DL}}^* = \Psi_{\text{DL}}^{*p}(\beta)$  and so forth. Discretization according to a DEM scheme yields

$$\{\bar{\beta}_{\text{DL}}^*\} + \{\bar{\beta}_{\text{DL}}\} = \{\bar{\beta}_{\text{Newt.}}\}, \quad (7.7)$$

where the coefficients belong to the  $\bar{n}_{p,\Gamma}$  dual  $p$ -cells on the dual boundary complex of  $\Gamma$ . We define the matrix operators

$$\begin{aligned} [\Psi_{\text{DL}}^{*p}]^{ij} &:= \langle \Psi_{\text{DL}}^{*p}(\psi_j^p) | \bar{g}_p^i \rangle, & i = 1, \dots, \bar{n}_{p,\Gamma}, \quad j = 1, \dots, n_{p,\Gamma}, \\ [\Psi_{\text{SL}}^{2-p}]^{ij} &:= \langle \mathbf{t}^{+'} \Psi_{\text{SL}}^p(\psi_j^{2-p}) | \bar{g}_p^i \rangle, & i = 1, \dots, \bar{n}_{p,\Gamma}, \quad j = 1, \dots, n_{2-p,\Gamma}, \end{aligned}$$

where  $n_{2-p,\Gamma} = \bar{n}_{p,\Gamma}$ . Both matrices are fully populated. Note that the upper index of the single-layer potential has changed from  $p$  to  $(2-p)$  in the matrix notation, now indicating that the linear operator acts upon coefficient vectors of  $(2-p)$ -cochains.

Equation (7.7) reads

$$[\Psi_{\text{DL}}^{*p}]\{\beta\} + [\Psi_{\text{SL}}^{2-p}]\{\gamma\} = \{\bar{\beta}_{\text{Newt.}}\}.$$

Finally, we require that  $\underline{\gamma}$  be a closed form. On a contractible domain this translates into

$$\{\gamma\} = [D_{\Gamma}^{1-p}]\{\lambda\}, \quad \{\lambda\} \in \mathbb{R}^{n_{1-p,\Gamma}},$$

so that

$$[\Psi_{\text{DL}}^{*p}]\{\beta\} + [\Psi_{\text{SL}}^{2-p}][D_{\Gamma}^{1-p}]\{\lambda\} = \{\bar{\beta}_{\text{Newt.}}\}.$$

To obtain  $n_{1-p,\Gamma}$  equations for the  $n_{1-p,\Gamma}$  unknowns of the Dirichlet problem, we left-multiply with  $[\bar{D}_{\Gamma}^p]$ ,

$$[\bar{D}_{\Gamma}^p][\Psi_{\text{DL}}^{*p}]\{\beta\} + [\bar{D}_{\Gamma}^p][\Psi_{\text{SL}}^{2-p}][D_{\Gamma}^{1-p}]\{\lambda\} = [\bar{D}_{\Gamma}^p]\{\bar{\beta}_{\text{Newt.}}\}. \quad (7.8)$$

Equation (7.8) is the Boundary Element Method formulation of a Dirichlet problem stemming from Eq. (7.1).

### Examples:

1. For  $p = 0$ , Eq. (7.8) reads

$$[\bar{D}_{\Gamma}^0][\Psi_{\text{DL}}^{*0}]\{\varphi_{\Gamma}\} + [\bar{D}_{\Gamma}^0][\tilde{\Psi}_{\text{SL}}^2][\bar{D}_{\Gamma}^1]\{\tilde{V}_{\Gamma}\} = -\{\bar{E}_{\text{s},\Gamma}\},$$

where  $\{\gamma\} = \{\tilde{D}_{\Gamma}\} = [\bar{D}_{\Gamma}^1]\{\tilde{V}_{\Gamma}\}$  and  $\tilde{V}_{\Gamma} \in \mathcal{W}^1(\Gamma)$  denotes an electric vector potential.

2.  $p = 1$  yields

$$[\bar{D}_{\Gamma}^1][\Psi_{\text{DL}}^{*1}]\{A_{\Gamma}\} - [\bar{D}_{\Gamma}^1][\tilde{\Psi}_{\text{SL}}^1][\bar{D}_{\Gamma}^0]\{\tilde{\varphi}_{\text{M},\Gamma}\} = \{\bar{B}_{\text{s},\Gamma}\},$$

where  $\{\gamma\} = \{\tilde{H}_{\Gamma}\} = -[\bar{D}_{\Gamma}^0]\{\tilde{\varphi}_{\text{M},\Gamma}\}$ . □

On non-contractible domains, cohomology contributions are taken into account by

$$\{\gamma\} = [D_\Gamma^{1-p}]\{\lambda\} + [\text{Ch}_\Gamma^0]\{\lambda_{\text{Ch}}\}.$$

To the  $\bar{n}_{p+1,\Gamma}$  linear equations of the lines of  $[\bar{D}_\Gamma^p]$  in Eq. (7.8), we add  $n_{H^p}$  lines that contain the transposed coefficient vectors  $\{h^1\}^T, \dots, \{h^{n_{H^p}}\}^T$  of representatives of the  $n_{H^p}$  different homology classes,  $[h^1], \dots, [h^{n_{H^p}}] \in H_p(\Gamma)$ .

Note that Eq. (7.8) is a discretization of an ungauged formulation of the Dirichlet problem. We neglected the gauge-potential in the Kirchhoff representation formula. The resulting potential is only defined up to a coboundary of a  $(p-1)$ -cochain.



# 8

## Coupling of DEM with BEM

We have outlined a discrete theory of (quasistatic) electromagnetism on a bounded domain in Chapters 2-6. Chapter 7 introduced the Boundary Element Method as a method to calculate the electromagnetic field on an unbounded domain. We also stated that a BEM formulation could be found for bounded domains. The advantages of DEM over BEM are

- Provided a Mesh-Generator package exists, DEM is relatively easy to implement.
- The DEM matrices are sparse; they use little memory and take less time for setup.
- Non-linear media can be considered in the discrete Hodge operators.
- From a solution vector, the field at any point of the DEM domain is obtained by the interpolation with Whitney forms at little computational cost.
- Conductive media can be considered in the quasistatic regime.
- The method is relatively easy to understand and thus easier to use and more flexible for development.

On the other side BEM has significant advantages over DEM:

- Only the boundary needs to be meshed and not the entire domain of interest.
- Source fields are easy to consider at a very high accuracy.
- Moving inelastic bodies do not pose a problem since the entire boundary mesh can be moved (no remeshing).

Some problem types make a combination of both methods' advantages desirable. This chapter discusses the coupling of BEM and DEM as well as the linear properties of the resulting system of linear equations.

### 8.1 DEM-BEM Coupling

In both methods, DEM and BEM, we made the assumption that all electromagnetic fields jump to zero on the boundary of the respective domain. This assumption led to the introduction of a boundary term in the DEM formulation of a field

problem. In BEM we required the fields to jump to zero in order to derive a unique boundary value problem.

Assume that we solve a problem

$$d*\vartheta d\alpha = \eta, \quad \alpha \in \mathcal{F}^p(\Omega) \quad (8.1)$$

on a closed subdomain  $\Omega^-$ , bounded by  $\Gamma = \partial\Omega^-$ , with a DEM formulation and on the unbounded complement  $\Omega^+$  of  $\Omega^-$ ,  $\Omega^- \cup \Omega^+ = \Omega$ , with a BEM formulation. We use the boundary complex of the DEM primal complex as a boundary 2-complex for BEM. Both methods discretize the Dirichlet data on the primal boundary complex. The Neumann data is discretized on the primal boundary complex in BEM and on the dual boundary complex in DEM. Both methods assume the fields to jump to zero on their boundary. By equivalencing these jumps, i.e., equivalencing Dirichlet and Neumann data on  $\Gamma$ , we obtain two coupled equation systems that, when solved simultaneously, yield an approximate solution for Eq. (8.1) on the entire domain  $\Omega$ .

We recall the general DEM equation system, given in Eq. (5.6), for  $n = 3$ ,  $p = 0, 1$ :

$$[\bar{D}^{2-p}][M_\vartheta^{p+1}][D^p]\{\alpha\} + [\bar{J}^{2-p}]\{\bar{\gamma}\} = \{\bar{\eta}\},$$

where the Neumann data can be rewritten as

$$\{\bar{\gamma}\} = [K_\Gamma^{2-p}]\{\gamma\} = [K_\Gamma^{2-p}][D_\Gamma^{1-p}]\{\lambda\},$$

where  $\{\lambda\}$  is the coefficient vector of some  $(1-p)$ -cochain  $\underline{\lambda}$ . The BEM equation system, Eq. (7.8), was derived in the previous section:

$$[\bar{D}_\Gamma^p][\Psi_{DL}^{*p}]\{\beta\} + [\bar{D}_\Gamma^p][\Psi_{SL}^{2-p}][D_\Gamma^{1-p}]\{\lambda\} = [\bar{D}_\Gamma^p]\{\bar{\beta}_s\},$$

where we write  $\{\bar{\beta}_s\}$  for  $\{\bar{\beta}_{\text{Nemt.}}\}$ , calling it the source potential. With  $\{\beta\} = [T^p]\{\alpha\}$  we can combine both systems,

$$\begin{pmatrix} [\bar{D}^{2-p}][M_\vartheta^{p+1}][D^p] & [\bar{J}^{2-p}][K_\Gamma^{2-p}][D_\Gamma^{1-p}] \\ [\bar{D}_\Gamma^p][\Psi_{DL}^{*p}][T^p] & [\bar{D}_\Gamma^p][\Psi_{SL}^{2-p}][D_\Gamma^{1-p}] \end{pmatrix} \begin{pmatrix} \{\alpha\} \\ \{\lambda\} \end{pmatrix} = \begin{pmatrix} \{\bar{\eta}\} \\ [\bar{D}_\Gamma^p]\{\bar{\beta}_s\} \end{pmatrix}. \quad (8.2)$$

### Examples:

1. The electrostatic DEM-BEM equation system,  $p = 0$ , reads

$$\begin{pmatrix} -[\tilde{D}^2][M_\varepsilon^1][D^0] & [\tilde{J}^2][\tilde{K}_\Gamma^2][\tilde{D}_\Gamma^1] \\ [\tilde{D}_\Gamma^0][\Psi_{DL}^{*0}][T^0] & [\tilde{D}_\Gamma^0][\tilde{\Psi}_{SL}^2][\tilde{D}_\Gamma^1] \end{pmatrix} \begin{pmatrix} \{\varphi\} \\ \{\tilde{V}_\Gamma\} \end{pmatrix} = \begin{pmatrix} \{\tilde{\rho}_s\} \\ -\{\tilde{E}_{s,r}\} \end{pmatrix}.$$

2. For  $p = 1$ , we find the magnetostatic DEM-BEM equation system

$$\begin{pmatrix} [\tilde{D}^1][M_\mu^2][D^1] & -[\tilde{J}^1][\tilde{K}_\Gamma^1][\tilde{D}_\Gamma^0] \\ [\tilde{D}_\Gamma^1][\Psi_{DL}^{*1}][T^1] & -[\tilde{D}_\Gamma^1][\tilde{\Psi}_{SL}^1][\tilde{D}_\Gamma^0] \end{pmatrix} \begin{pmatrix} \{A\} \\ \{\tilde{\varphi}_{M,r}\} \end{pmatrix} = \begin{pmatrix} \{\tilde{j}_s\} \\ \{\tilde{B}_{s,r}\} \end{pmatrix}.$$

3. An alternative electrostatic formulation for  $p = 1$  and  $\underline{\tilde{\rho}} = 0$  in  $\Omega^-$  is given by

$$\begin{pmatrix} [\bar{D}^1][\tilde{M}_{1/\epsilon}^2][\tilde{D}^1] & -[\bar{J}^1][K_R^1][D_R^0] \\ [\tilde{D}_R^1][\tilde{\Psi}_{DL}^1][\tilde{T}^1] & -[\tilde{D}_R^1][\Psi_{SL}^1][D_R^0] \end{pmatrix} \begin{pmatrix} \{\tilde{V}\} \\ \{\varphi_R\} \end{pmatrix} = \begin{pmatrix} \{0\} \\ \{\tilde{D}_{s,r}\} \end{pmatrix}.$$

4. Finally, we consider a magnetostatic scalar-potential formulation for  $\underline{\tilde{j}} = 0$  in  $\Omega^-$ ,

$$\begin{pmatrix} -[\bar{D}^2][\tilde{M}_\mu^1][\tilde{D}^0] & [\bar{J}^2][K_R^2][D_R^1] \\ [\tilde{D}_R^0][\tilde{\Psi}_{DL}^{*0}][\tilde{T}^0] & [\tilde{D}_R^0][\Psi_{SL}^2][D_R^1] \end{pmatrix} \begin{pmatrix} \{\tilde{\varphi}_M\} \\ \{A_R\} \end{pmatrix} = \begin{pmatrix} 0 \\ -\{\tilde{H}_{s,r}\} \end{pmatrix}.$$

The BEM right-hand side  $\{\tilde{H}_{s,r}\}$  can be calculated in two ways: From a current-distribution in  $\Omega^+$  or from double-layers of magnetic charges, representing line-current loops. For line-current loops, both approaches are equivalent, see Section F.2.  $\square$

## 8.2 The Kernel of the DEM-BEM System Matrix

We shall investigate the kernel of the DEM-BEM matrix as well as the kernel of its transpose. We show that the kernel of the DEM-BEM matrix is the same as the kernel of its transpose. As we will see in Chapter 9, this property is crucial for the application of a number of powerful solution techniques.

Referring to Eq. (8.2) we will have to proof that

$$\ker([\bar{D}^{2-p}][M_\sigma^{p+1}][D^p]) = \ker([\bar{D}^{2-p}][M_\sigma^{p+1}][D^p])^T, \quad (8.3 a)$$

$$\ker([\bar{D}_R^p][\Psi_{DL}^{*p}][T^p]) \supset \ker([\bar{D}^{2-p}][M_\sigma^{p+1}][D^p]), \quad (8.3 b)$$

$$\ker([\bar{J}^{2-p}][K_R^{2-p}][D_R^{1-p}])^T = \ker([\bar{D}_R^p][\Psi_{DL}^{*p}][T^p]), \quad (8.3 c)$$

as well as

$$\ker([\bar{J}^{2-p}][K_R^{2-p}][D_R^{1-p}]) = \ker([\bar{D}_R^p][\Psi_{SL}^{2-p}][D_R^{1-p}]) \quad (8.4 a)$$

$$= \ker([\bar{D}_R^p][\Psi_{SL}^{2-p}][D_R^{1-p}])^T \quad (8.4 b)$$

$$= \ker([\bar{D}_R^p][\Psi_{DL}^{*p}])^T. \quad (8.4 c)$$

By Poincaré's 1st lemma we find that  $[D^{p-1}]$  lies in the kernel of the DEM domain-matrix. We denote  $[D^{-1}]$  a constant  $n_0$ -coefficient vector lying in the kernel of  $[D^0]$ . Furthermore,

$$\begin{aligned} ([\bar{D}^{2-p}][M_\sigma^{p+1}][D^p])^T &= [D^p]^T [M_\sigma^{p+1}]^T [\bar{D}^{2-p}]^T \\ &= [\bar{D}^{2-p}][M_\sigma^{p+1}]^T [D^p], \end{aligned}$$

which proofs Eq. (8.3 a). It is proven in Annex F that the double layer potential of coboundaries of  $(p-1)$ -forms yield closed  $p$ -forms. As a consequence,

$$[\bar{D}_r^p][\Psi_{\text{DL}}^{*p}][D_r^{p-1}]\{\omega\} = [\bar{D}_r^p][\bar{D}_r^{p-1}]\{\bar{\zeta}\} = 0, \quad \{\omega\} \in \mathbb{R}^{n_{p-1}}, \{\bar{\zeta}\} \in \mathbb{R}^{\bar{n}_{p-1}},$$

which proofs Eq. (8.3 b). Moreover, we find

$$\begin{aligned} ([\bar{J}^{2-p}][K_r^{2-p}][D_r^{1-p}])^T &= [D_r^{1-p}]^T[K_r^{2-p}]^T[\bar{J}^{2-p}]^T \\ &= (-1)^{p+1}(-1)^{p(2-p)}[\bar{D}_r^p][K_r^p][T^p] \\ &= -[K_r^p][D_r^p][T^p], \end{aligned}$$

which proofs Eq. (8.3 c). For the second column of the DEM-BEM matrix, we see that  $[D_r^{-p}]$  is the kernel on both sides of Eq. (8.4 a). Equations (8.4 b) and (8.4 c) are proven by virtue of  $[\bar{D}_r^p]^T = (-1)^{p+1}[D_r^{1-p}]$ .

Denote with  $[B^p]$  the DEM-BEM system matrix. We have found that

$$\ker [B^p] = \ker [B^p]^T. \quad (8.5)$$

Denote by  $[U]$  the kernel matrix of the DEM-BEM system

$$[U] := \begin{pmatrix} [D_r^{p-1}] \\ [D_r^{-p}] \end{pmatrix}. \quad (8.6)$$

Equation (8.5) is equivalent to

$$[B^p][U] = [B^p]^T[U] = 0,$$

which implies that

$$[U]^T[B^p] = 0.$$

The image of the DEM-BEM system matrix is orthogonal to its kernel.

# 9

## Solver Strategies for the DEM-BEM Coupled System

In the previous chapter we discussed the coupling of a DEM formulation with a Boundary Element Method. Solving the resulting system of linear equations is what will preoccupy us in this chapter. We discuss the relevant properties of the system matrix and propose two approaches to deal with the singularity of the system. For the sake of simplicity we change our notation from DEM notation to the standard notation of linear algebra literature. We therefore denote  $\mathbf{A}$  the DEM-BEM system matrix,  $\mathbf{b}$  the right-hand side,  $\mathbf{x}$  the solution vector and so forth.

### 9.1 General Properties and Solver Strategies

We are dealing with the ill-posed equation system

$$\mathbf{Ax} = \mathbf{b}. \tag{9.1}$$

The matrix  $\mathbf{A}$  is singular. Its kernel is known. The matrix  $\mathbf{U}$  holds the basis vectors of the kernel in its columns, compare Eq. (8.6). We know that

$$\mathbf{AU} = \mathbf{U}^T \mathbf{A} = 0,$$

the image of the matrix  $\mathbf{A}$  is orthogonal to its kernel. There are infinitely many solutions to our system if  $\mathbf{b}$  lies in the image of  $\mathbf{A}$ ,  $\mathbf{U}^T \mathbf{b} = 0$ ; there is no solution if  $\mathbf{b}$  has a component in the kernel of  $\mathbf{A}$ . In the latter case we say the right-hand

side is inconsistent with the DEM-BEM matrix. Using DEM notation we find

$$\begin{aligned} \mathbf{U}^T \mathbf{b} &= \left( [\mathbf{D}^{p-1}]^T, [\mathbf{D}_r^{-p}]^T \right) \begin{pmatrix} \{\bar{\eta}\} \\ [\bar{\mathbf{D}}_r] \{\bar{\beta}_s\} \end{pmatrix} \\ &= - \left( [\bar{\mathbf{D}}^{3-p}], [\bar{\mathbf{D}}_r^{p+1}] \right) \begin{pmatrix} \{\bar{\eta}\} \\ [\bar{\mathbf{D}}_r^p] \{\bar{\beta}_s\} \end{pmatrix}. \end{aligned} \quad (9.2)$$

We see that the BEM-part of the right-hand side does not pose a problem. It is orthogonal to the kernel of  $\mathbf{A}$ . For the DEM-part to lie in the image of the system matrix we have to require that the dual coboundary of the right-hand side vanishes. For  $p = 0$ , the condition is trivially fulfilled. For  $p = 1$ , however, it might pose a problem, as the following example illustrates.

**Example:** For  $p = 1$ , magnetostatics, Eq. (9.2) implies that the discrete source current density on the dual complex must be free of divergence. We found in Section 4.5 that in order to match this condition, the discrete current density must be free of divergence on the primal grid and the jump of the current density on the domain boundary must be zero, i.e., no entering or exiting currents on the boundary.

It is a frequent problem in magnetostatic DEM that this last condition is violated. The problem occurs when we determine the coefficients of the discrete current density by integration of an ideal vector field, e.g., a (circular) cylindrical vector field, over primal faces. The boundary of the DEM coil domain can generally not perfectly approximate a cylindrical coil. As a consequence, the vector-field is not perfectly tangential to the coil-boundary. Small amounts of positive and negative currents on the boundary-faces are the result. Under the assumption that all currents outside the primal coil domain are zero, these currents must jump to zero on the domain boundary, thus, violating the zero-dual-divergence condition.  $\square$

We define an optimum solution  $\mathbf{x}^*$  of Eq. (9.1) that fulfills

$$\mathbf{A} \mathbf{x}^* = \mathbf{b}^*$$

where  $\mathbf{b}^*$  is the orthogonal projection of  $\mathbf{b}$  into the image of  $\mathbf{A}$ .

The following properties of the equation system are relevant for a choice of a solution technique: The system matrix is asymmetric and singular with a possibly inconsistent right-hand side. The matrix' image is orthogonal to its kernel. The matrix is built of four blocks, two of which are sparse while the other two are dense. The dense BEM matrices are usually compressed in order to save on computation time and storage space. Different methods (ACA, Fast Multipole Method) are known for this purpose. The individual elements of the compressed matrices are

generally not accessible. The compression algorithms, however, provide routines for matrix-vector multiplication.

An asymmetric system can be solved iteratively, e.g., with a GMRES algorithm, [29]. To have good convergence, the conditioning of the equation system needs to be improved. We define the condition number of a singular system as the quotient of the largest and the smallest non-zero singular value. We have found that the conditioning of the DEM-BEM system can be considerably improved by only the use of a preconditioner for the upper left block, the DEM domain-matrix. The BEM matrices are generally sufficiently well-behaved to allow for satisfactory convergence of the solver if only the DEM domain-block is well-conditioned.

In the following, we make two propositions that will allow us to deal with a singular system in presence of an inconsistent right-hand side. The first approach is a regularization of the DEM-BEM system, resulting in a regular matrix  $\mathbf{A}$ . The second approach introduces an adapted GMRES algorithm that yields an optimum solution even in the presence of an inconsistent right-hand side. Both approaches require that the system matrix image is orthogonal to its kernel.

## 9.2 Regularization

Suppose that  $\mathbf{b}$  lies in the image of  $\mathbf{A}$ . Hence, it is orthogonal to  $\mathbf{U}$ . We can require that  $\mathbf{x}$  be orthogonal to  $\mathbf{U}$  and find that

$$(\mathbf{A} + \alpha \mathbf{U}\mathbf{U}^T) \mathbf{x} = \mathbf{b}$$

has an identical solution vector as the original system. Since  $\text{im } \mathbf{U}\mathbf{U}^T = \ker \mathbf{A}$  and  $\ker \mathbf{U}\mathbf{U}^T = \text{im } \mathbf{A}$ , the entire equation system is now regular. The factor  $\alpha$  can be used to improve the conditioning of the regularized matrix. It can be shown that, if  $\mathbf{b}$  does not lie in the image of the system matrix, the solution is an optimum solution,  $\mathbf{x} = \mathbf{x}^*$ ,  $\mathbf{A}\mathbf{x}^* = \mathbf{b}^*$ .

Since on a contractible domain for the DEM-system alone  $\mathbf{U} = [\mathbf{D}^0]$  and  $[\mathbf{D}^0]^T = -[\bar{\mathbf{D}}^2]$ , the above regularization method is sometimes called a discrete grad div-regularization.

The regularization generally increases the condition-number. There is, however, a large number of high-performing preconditioners available for regular matrices.

## 9.3 Adapted GMRES

The GMRES solver [29] is an iterative Krylov-subspace solver well suited for asymmetric regular or singular matrices with a consistent right-hand side. It searches for a solution of the equation  $\mathbf{A}\mathbf{x} = \mathbf{b}$  in the subspace  $K_m$  of  $\mathbb{R}^n$ ,

$$K_m = \text{span} \{ \mathbf{r}, \mathbf{A}\mathbf{r} \dots \mathbf{A}^{m-1}\mathbf{r} \}, \quad \mathbf{r} \in \mathbb{R}^n.$$

An orthonormal basis  $\{\mathbf{v}_1, \dots, \mathbf{v}_m\}$  of  $K_m$  is found by the recursive Arnoldi algorithm, compare steps 4-13 in Algorithm 9.3.1,

$$h_{j+1,j}\mathbf{v}_{j+1} = \mathbf{A}\mathbf{v}_j - \sum_{i=1}^j h_{ij}\mathbf{v}_i.$$

The GMRES algorithm uses the initial residual  $\mathbf{r}_0 = \mathbf{A}\mathbf{x}_0 - \mathbf{b}$  as start vector  $\mathbf{r}$  to build a Krylov subspace. With  $\mathbf{V}_m$  being the matrix of the basis vectors, a basic GMRES algorithm is given in Algorithm 9.3.1.

#### Algorithm 9.3.1 (GMRES)

1. Compute  $\mathbf{r}_0 = \mathbf{b} - \mathbf{A}\mathbf{x}_0$ ,  $\beta = \|\mathbf{r}_0\|_2$
2. Define the  $(m+1) \times m$  matrix  $\mathbf{H}_m$ ,  
set  $\mathbf{H}_m = \mathbf{0}$
3. Define the  $n \times (m+1)$  matrix  $\mathbf{V}_{m+1}$  and  
set  $\mathbf{v}_1 = \mathbf{r}_0/\beta$
4. For  $j = 1, 2, \dots, m$  Do:
5.     Compute  $\mathbf{w}_j = \mathbf{A}\mathbf{v}_j$
6.     For  $i = 1, \dots, j$  Do:
7.          $h_{ij} = (\mathbf{w}_j, \mathbf{v}_i)$
8.          $\mathbf{w}_j = \mathbf{w}_j - h_{ij}\mathbf{v}_i$
9.     EndDo
10.      $h_{j+1,j} = \|\mathbf{w}_j\|_2$ .
11.     If  $h_{j+1,j} < \varepsilon$  set  $m = j$  and go to 14
12.      $\mathbf{v}_{j+1} = \mathbf{w}_j/h_{j+1,j}$
13. EndDo
14. Compute  $\mathbf{y}_m$  the minimizer of  
 $\|\mathbf{A}\mathbf{V}_m\mathbf{y}_m - \mathbf{b}\|_2$  and  $\mathbf{x}_m = \mathbf{x}_0 + \mathbf{V}_m\mathbf{y}_m$ .

[29] gives an inexpensive method for the determination of the minimum of  $\|\mathbf{A}\mathbf{V}_m\mathbf{y}_m - \mathbf{b}\|_2$ .

If the right-hand side  $\mathbf{b}$  does not lie in the image of the matrix  $\mathbf{A}$ , the GMRES algorithm gives the optimum solution  $\mathbf{x}^*$ ; the algorithm will, however, not be suited to detect convergence.

We propose to overcome this problem by solving the related problem

$$\mathbf{A}\mathbf{x} = \mathbf{A}\mathbf{b}.$$

We generate two Krylov bases  $\mathbf{V}_m$  and  $\mathbf{V}'_m$  that are related via  $\mathbf{V}_m = \mathbf{A}\mathbf{V}'_m$ . After solving the above equation by  $\mathbf{x} = \mathbf{V}_m\mathbf{y}_m$ , we exchange the bases, using the same coefficients, thus obtaining  $\mathbf{x}' = \mathbf{V}'_m\mathbf{y}_m$ , which is a solution of  $\mathbf{A}\mathbf{x} = \mathbf{b}$ .

The two Krylov bases are built from appropriate start vectors  $\mathbf{v}'_1$  and  $\mathbf{v}_1 = \mathbf{A}\mathbf{v}'_1$  according to

$$h_{j+1,j}\mathbf{v}_{j+1} = \mathbf{A}\mathbf{v}_j - \sum_{i=1}^j h_{ij}\mathbf{v}_i,$$

$$h_{j+1,j}\mathbf{v}'_{j+1} = \mathbf{v}_j - \sum_{i=1}^j h_{ij}\mathbf{v}'_i.$$



The adapted algorithm is given in Algorithm 9.3.2.

**Algorithm 9.3.2 (Adapted GMRES - AGMRES)**

1. Provide  $\mathbf{x}'_0$  and  $\mathbf{x}_0 = \mathbf{A}\mathbf{x}'_0$
2. Compute  $\mathbf{r}_0 = \mathbf{A}\mathbf{b} - \mathbf{A}\mathbf{x}_0$ ,  $\mathbf{r}'_0 = \mathbf{b} - \mathbf{x}_0$   
and  $\beta = \|\mathbf{r}_0\|_2$
3. Define the  $(m+1) \times m$  matrix  $\mathbf{H}_m$ ,  
set  $\mathbf{H}_m = \mathbf{0}$
4. Define the  $n \times (m+1)$  matrices  $\mathbf{V}_{m+1}$ ,  $\mathbf{V}'_{m+1}$  and set  $\mathbf{v}_1 = \mathbf{r}_0/\beta$ ,  $\mathbf{v}'_1 = \mathbf{r}'_0/\beta$
5. For  $j = 1, 2, \dots, m$  Do:
6.     Compute  $\mathbf{w}_j = \mathbf{A}\mathbf{v}_j$
7.      $\mathbf{w}'_j = \mathbf{v}_j$
8.     For  $i = 1, \dots, j$  Do:
9.          $h_{ij} = (\mathbf{w}_j, \mathbf{v}_i)$
10.          $\mathbf{w}_j = \mathbf{w}_j - h_{ij}\mathbf{v}_i$
11.          $\mathbf{w}'_j = \mathbf{w}'_j - h_{ij}\mathbf{v}'_i$
12.     EndDo
13.      $h_{j+1,j} = \|\mathbf{w}_j\|_2$ .
14.     If  $h_{j+1,j} = 0$  set  $m = j$  and go to 18
15.      $\mathbf{v}_{j+1} = \mathbf{w}_j/h_{j+1,j}$
16.      $\mathbf{v}'_{j+1} = \mathbf{w}'_j/h_{j+1,j}$
17. EndDo
18. Compute  $\mathbf{y}_m$  the minimizer of  
 $\|\mathbf{A}\mathbf{V}_m\mathbf{y}_m - \mathbf{b}\|_2$  and  $\mathbf{x}_m = \mathbf{x}_0 + \mathbf{V}_m\mathbf{y}_m$ .
19. Compute  $\mathbf{x}'_m = \mathbf{x}'_0 + \mathbf{V}'_m\mathbf{y}_m$ .

The algorithm is suited for restarts. It is numerically as stable as the Algorithm 9.3.1. Note that a vanishing residual  $\mathbf{r}_m = \mathbf{A}\mathbf{b} - \mathbf{A}\mathbf{x}_m = \mathbf{A}(\mathbf{b} - \mathbf{A}\mathbf{x}'_m) = \mathbf{A}\mathbf{r}'_m$  implies that the residual  $\mathbf{r}'_m$  lies completely in the kernel of  $\mathbf{A}$ .  $\mathbf{x}'_m$  is the optimum solution for  $\mathbf{A}\mathbf{x} = \mathbf{b}$ . This reasoning only holds if  $\ker \mathbf{A} = \ker \mathbf{A}^\top$ , as is the case for the DEM-BEM system matrix.

The AGMRES-approach overcomes the problem of an inconsistent right-hand side without altering the condition number of the system matrix. Since most advanced algorithms for preconditioning are, however, only available for regular matrices, we are left with the problem of finding a good preconditioner.

# 10

## Numerical Results

The main motivation for this thesis was the development of a more accurate tool for the electromagnetic simulation of accelerator magnets in 3 dimensions. In this chapter we first illustrate the problems encountered with a coupled FE-BE method using Lagrangian node-based shape functions in 3 dimensions. We then describe the new approach, mainly focussing on the solver strategies that were adopted. We present numerical results that validate the new algorithm.

### 10.1 The Existing FEM-BEM Code

CERN and the Robert Bosch GmbH have been collaborating over the past years to develop tools for the simulation of electromagnetic fields. The coupling of a Boundary Element Method and a Finite Element Method yielded advantages for both sides of the collaboration. At Bosch it was the problem of moving parts (valves, motors) that made FEM-BEM coupling desirable; at CERN it was the need for a most accurate modelling of the superconducting coils.

A FEM-BEM code in 2 dimensions, using 2nd order Lagrangian shape functions (equivalent to 2nd order Whitney 0-forms) and a vector-potential formulation, had proven excellent properties in terms of computational efficiency and accuracy. Inspired by the success of the 2-dimensional code, a 3-dimensional code was developed, based on the principle that, for magnetostatics, the Maxwell gauge ( $\text{div } A = 0$ ) causes the vectorial Laplace equation to be identical with the curlcurl equation. Moreover, the Laplace equation in cartesian coordinates decouples into three scalar Laplace equations of the kind that was solved successfully in 2 dimensions. The results looked promising, but not quite accurate, compare Fig. 10.1. The matrix of the gauged system being regular, the iterative solvers converged within the limits of machine precision. The results, however, showed that, in presence of sharp corners and jumps in the material properties (e.g., change of magnetic permeability between iron and air), the node-based FEM-BEM algorithm yielded wrong results. The field was expunged from the object's corners. The effect got

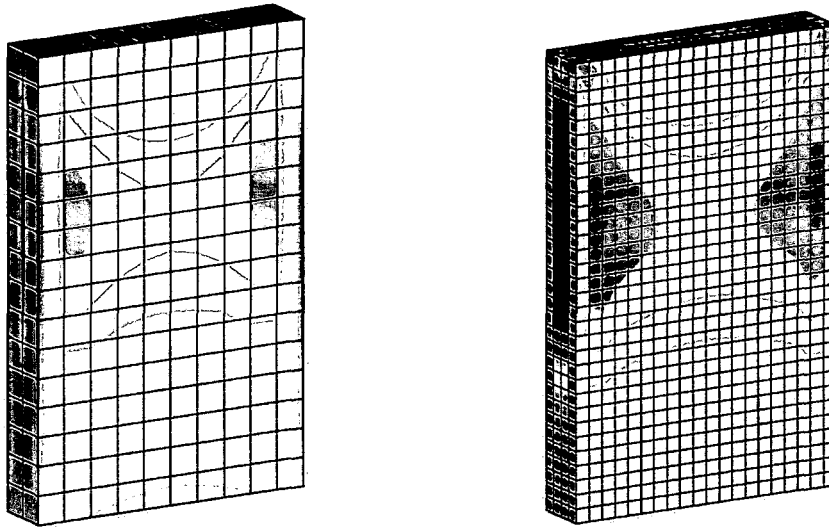


Figure 10.1: Plate of constant relative magnetic permeability  $\mu_r = 100$  in the field of a ring-shaped coil. The ring is centered on the long axis of the plate and the coil sits in the upper part of the plate. The contour plot indicates the modulus of the magnetic induction on the surface of the plate as a result of a node-based FEM-BEM calculation. The calculation was performed for different discretization densities.

even worse after an increase of discretization density. Moreover, the convergence of the iterative solvers deteriorated in the above-mentioned cases.

The above effects were encountered by many members of the computational electromagnetism community. The mathematical explanation is known, [5]: The node-based Lagrangian shape functions do not span the functional space that the magnetic vector-potential "lives" in. For a gauged formulation that space is  $\mathbf{H}_{\text{curl}}(\Omega) \cap \mathbf{H}_{\text{div}}(\Omega)$ , compare Annex C. Node-based shape functions, however, approximate  $H_{\text{grad}}(\Omega)$ . The problem lies in the continuity of fields in the different spaces: a field in  $(H_{\text{grad}})^3(\Omega)$  is continuous in its tangent and normal component, whereas  $\mathbf{H}_{\text{curl}}(\Omega)$  accounts for tangential continuity and allows for jumps of the normal component on element boundaries. Problem types that require the normal component of a magnetic vector potential to jump, cannot be treated in the functional space  $(H_{\text{grad}})^3(\Omega)$ .<sup>1</sup> A jump of the normal component of the magnetic vector-potential allows for a jump of the tangent component of the magnetic induction, e.g., on the boundary of two domains with different magnetic permeability.

A consistent discretization of  $\mathbf{H}_{\text{curl}}(\Omega) \cap \mathbf{H}_{\text{div}}(\Omega)$  has not been found to date. As a consequence, we have to use an ungauged formulation with solutions living

<sup>1</sup>The  $z$ -component of a magnetic vector-potential in a 2-dimensional calculation is continuous on the 2-dimensional plane. This is the reason why a 2-dimensional FEM-BEM coupling was successful with node-based shape functions.

in  $\mathbf{H}_{\text{curl}}(\Omega)$ . A discretization of  $\mathbf{H}_{\text{curl}}(\Omega)$  is given by edge-based Whitney 1-forms,  $\mathcal{W}^1(\Omega)$ . Therefore, a Finite Element Method with Whitney 1-forms as shape functions avoids the above described problems.

Among the variety of DEM formulations presented in the preceding chapters, we chose the Galerkin-method, i.e., the Finite Element Method with Whitney 1-forms as shape functions, for the implementation. The reason for this lies in the existing FEM program infrastructure that we could reuse for the new algorithm. Moreover, Whitney 1-forms are available on tetrahedra, prisms and hexahedra, which makes the method more flexible than, e.g., FIT or the geometrical-Hodge based DEM formulation.

## 10.2 Whitney-Form Based FEM

In a first step, a stand-alone FEM program was implemented for tetrahedra, hexahedra and prisms. We use the adapted GMRES algorithm, compare Algorithm 9.3.2, to deal with the problem of an inconsistent right-hand side described on page 78. As a preconditioner we opted for an incomplete LU-factorization (ILU). Given the symmetry of the FEM system matrix, incomplete Cholesky-factorization would have been an option, but it is numerically instable when performed on a singular matrix with a large kernel. ILU is more stable in that respect. Several other preconditioning (PC) techniques have been investigated (diagonal PC, band-diagonal PC, block PC, approximate inverse PC) but they all proved ineffective. Finally, the ILUT $p$  algorithm was chosen (Incomplete LU-factorization with Threshold and tuning parameter  $p$ ), [29].

The FEM implementation includes eddy-current calculations as well as non-linear material properties that are treated with a Newton algorithm, compare Sections E.2 and E.3.

## 10.3 Whitney Form Based Coupling of FEM and BEM

The Whitney form BEM program was first developed as a stand-alone program in the course of a PhD-thesis, [28]. Its coupling with FEM required new solver strategies. It has been said before that an excellent preconditioning of the FEM domain block alone could yield a FEM-BEM system matrix that is sufficiently well conditioned to yield reasonably fast convergence. The ILUT $p$  algorithm, that had performed well for the stand-alone FEM program, could not serve this purpose. Better preconditioners, however, require a regular matrix. The first step in implementing a solver therefore was the implementation of a regularization, compare Section 9.2. For a preconditioner we found, after a lengthy trial phase, the RIC2S algorithm (Robust Incomplete Cholesky 2nd order Stabilized factorization) that

is based on a  $\mathbf{U}^T\mathbf{U} + \mathbf{U}^T\mathbf{R} + \mathbf{R}^T\mathbf{U}$  factorization of a general symmetric, positive definite matrix, [22]. The high effectiveness of this algorithm, however, is accompanied by considerable computational cost in both, setup time and storage space requirements.

The computational cost of the preconditioning can be reduced by the AMD algorithm, [12]. AMD is an Approximate Minimum Degree ordering algorithm to permute sparse matrices prior to numerical factorization. The permutation minimizes the non-zero entries in a factorization (typically LU or Cholesky), thus, saving on time and storage space.

The coupled FE-BE method was implemented for eddy-current calculations as well as non-linear materials, compare Sections E.2 and E.3. As for the plate problem in Fig. 10.1 we can state that the problem is resolved by the new, Whitney-form based, FEM-BEM coupling. Figure 10.2 shows the results of the same calculation using the new algorithm. To demonstrate the capability to calculate real-world problems, we choose a short model of the LHC main dipole magnet, see Figs. 10.3 and 10.4.

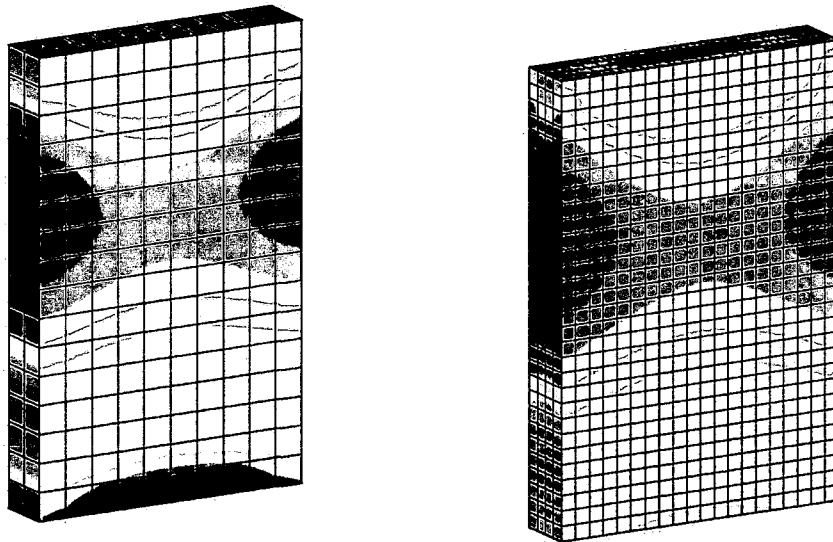


Figure 10.2: Plate of constant relative magnetic permeability  $\mu_r = 100$  in the field of a ring-shaped coil. The ring is centered on the long axis of the plate and the coil sits in the upper part of the plate. The contour plot indicates the modulus of the magnetic induction on the surface of the plate as a result of an edge-based FEM-BEM calculation. The calculation was performed for different discretization densities.



Figure 10.3: Short model of the LHC main dipole magnet. Left: Cell complex (finite element mesh) discretizing the iron yoke of the magnet. Note the holes in the yoke that indicate the existence of non-empty homology and cohomology spaces on the complex. Right: Modulus of the magnetic induction. The calculation was performed with the Whitney-form based FEM-BEM algorithm. The non-linear magnetic permeability of the yoke iron was considered in the calculation.

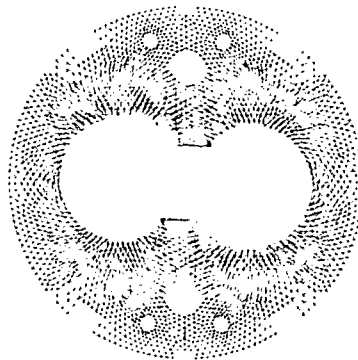


Figure 10.4: Cross-section of the LHC main dipole magnet. The field icons of the magnetic induction are displayed. The calculation was performed with the Whitney-form based FEM-BEM algorithm. The non-linear magnetic permeability of the yoke iron was considered in the calculation.

## Conclusions and Outlook

In the introduction we mentioned two driving forces for the advancement of this thesis: the need for a more accurate 3-dimensional modelling of accelerator magnets, and the wish to come to a full understanding of the Finite Element Method as a variant of the theory of discrete electromagnetism.

As for the new FEM-BEM code, we have pointed out in the last chapter that a coupling of FEM and BEM with Whitney 1-forms as shape functions solves the vector-potential formulation of a quasi-magnetostatic field problem accurately and efficiently. FEM with Whitney 1-forms is a state-of-the-art technique, applied in a growing number of codes in the computational electromagnetism community. A successful Whitney-form based coupling of FEM with BEM, however, is not as well documented in literature.

On the way to a successful implementation of a FEM-BEM code, the problem of an inconsistent right-hand side in the FEM equation system, see page 78 and Section 4.5, fostered further theoretical considerations, owing to which we can now give answers to the three introductory questions:

1. Is it possible to introduce a comprehensive and solely discrete theory of electromagnetism based on a simplicial cell complex (tetrahedral mesh)?

We had said that this question is essentially equivalent to the question whether or not we can find a solely geometrically defined Hodge operator on a simplicial complex. We introduced a geometrical Hodge operator in Chapter 5.

2. Can we interpret and rewrite the Finite Element Method (with Whitney-forms as shape functions) in terms of the operators of discrete electromagnetism?

The answer to this question lies in a DEM-interpretation of the FEM boundary term and of the Galerkin-type  $[K^p]$ -matrices. We have introduced a boundary term to the DEM formulation as a consequence of the jump of all discrete electromagnetic fields to zero on the boundary of the primal cell complex in Section 4.4. Furthermore, we defined the transfer matrices, mapping coefficient vectors on the primal complex into coefficient vectors on the dual complex in Section 4.3. In Section 6.2 we showed that a DEM formulation with jump term, transfer matrices and the Galerkin-Hodge operator is identical to the Finite Element Method with Whitney-forms.

# Appendix A

## Selected Topics of Vector Analysis

The following paragraphs are not intended to be an introduction to vector analysis, neither do they present a comprehensive survey of the vector analysis tools that are used in this thesis. For an introductory course we recommend [2] and [3]. As a reference book for mathematical definitions we refer to [21] and [11]. We want to give a mere collection of definitions, useful formulas and theorems that are used throughout the thesis.

### Differential $p$ -Forms

Let  $\Omega$  be a  $C^\infty$  differentiable manifold. Let  $(x^1, \dots, x^n)$  denote the local coordinates in the image of a coordinate chart.  $(\partial_{x^1}, \dots, \partial_{x^n})$  is a basis of the tangent space  $T_P\Omega$  in point  $P \in \Omega$ .  $(dx^1, \dots, dx^n)$  is the dual basis of cotangent vectors.  $\mathcal{F}^p(\Omega)$  denotes the space of differential  $p$ -forms on  $\Omega$ . The dimension of the space of  $p$ -forms is  $\binom{n}{p}$ .

Let  $(dx, dy, dz)$  denote the orthonormalized basis covectors of  $\mathbb{R}^3$ .  $p$ -forms for  $p = 0, 1, 2, 3$  are expressed in terms of basis  $p$ -forms:

$$\begin{aligned} \text{0-form } \underline{F} &= f, \\ \text{1-form } \underline{F} &= f_x dx + f_y dy + f_z dz, \\ \text{2-form } \underline{F} &= f_x dy \wedge dz + f_y dz \wedge dx + f_z dx \wedge dy, \\ \text{3-form } \underline{F} &= f dx \wedge dy \wedge dz. \end{aligned}$$

For  $n = 2$  we find

$$\begin{aligned} \text{0-form } \underline{F} &= f, \\ \text{1-form } \underline{F} &= f_x dx + f_y dy, \\ \text{2-form } \underline{F} &= f dx \wedge dy. \end{aligned}$$

For any two forms, their wedge product commutes according to

$$\underline{F} \wedge \underline{G} = (-1)^{pq} \underline{G} \wedge \underline{F}, \quad \underline{F} \in \mathcal{F}^p(\Omega), \quad \underline{G} \in \mathcal{F}^q(\Omega).$$



### 3. Can a DEM formulation on a closed domain be coupled to a Boundary Element Method?

Different DEM formulations vary only in the choice of a discrete Hodge operator. Having shown that DEM-BEM coupling works for the Galerkin-Hodge operator, there is no conceivable reason why DEM-BEM coupling should encounter any substantial obstacles with Hodge operators other than the Galerkin-Hodge.

Having resolved a number of problems in the collaborative effort so far, there are still open questions and tasks to be completed. The program development is a work in progress.

- Currently in the works is the implementation of the Kirchhoff representation formula that allows to evaluate the electromagnetic fields due to single-layer, double-layer and Newton sources in the BEM domain.
- Another topic in process is the implementation of symmetries that will save considerably on computational resources.
- An algorithm for the identification of instances of each homology class on a cell complex has been proposed in [16]. Its implementation in the FEM-BEM code is the next topic waiting in the queue.
- The electromagnetic problem being solved, it can be coupled to a mechanical problem, e.g., to simulate a motor or a valve, [25]. This electro-mechanical coupling had been implemented in the preceding node-based FEM-BEM algorithm. That coupling now needs to be adapted to the new algorithm (e.g., evaluation of the Maxwell-stress tensor).
- Finally, it seems that there should be room for improvement in the applied solver strategy. An alternative to the preconditioned iterative solver approach based on the inversion of  $\mathcal{H}$ -matrices, [4], is currently under investigation.

With regard to theoretical issues treated in this thesis, our attention is drawn to a more in depth investigation of the geometrical Hodge operator. First of all, its accuracy needs to be validated in a DEM code. Second, we have mentioned before that a geometrical definition of an inverse Hodge operator, mapping  $(n - p)$ -cochains on the dual complex into  $p$ -cochains on the primal complex, is conceivable.<sup>1</sup> Such an inverse Hodge could serve in the introduction of a discrete coderivative operator or as a step towards a geometrical preconditioning technique for DEM equation systems. Third, we should be interested in higher-order spatial approximations. We could define geometrical Hodge operators on higher-order cell complexes and compare their properties with higher-order Whitney form based Hodge operators.

---

<sup>1</sup>Under "inverse discrete Hodge" we do not necessarily understand the algebraic inverse of the geometrical Hodge operator. In the same way the discrete Hodge approximates the properties of the continuous Hodge operator, the inverse discrete Hodge should approximate the continuous inverse Hodge operator.

### Odd $p$ -Form

An odd  $p$ -form differs from an even  $p$ -form in that it "senses" a change of inner orientation and reacts with a sign change. Denote  $[o]$  an equivalence class of even permutations of basis tangent vectors that represents the positive orientation of  $\Omega$ . An odd form can be defined from even forms with the equivalence

$$(\underline{F}, [o]) \sim (-\underline{F}, -[o]).$$

Odd forms are denoted by an overtilde sign,  $\tilde{F}$ .

### Double Forms

Double forms are differential forms in one space,  $\mathcal{F}^p(\Omega)$ , with coefficients that are differential forms in a different space,  $\mathcal{F}^q(\Pi)$ . Double forms are used for integral transformations of differential forms on  $\Omega$  into differential forms on  $\Pi$ . Let

$$\underline{\underline{G}} = \underline{\pi} \otimes \underline{\omega}, \quad \underline{\omega} \in \mathcal{F}^p(\Omega), \quad \underline{\pi} \in \mathcal{F}^q(\Pi).$$

Then

$$\begin{aligned} \mathcal{G} : \mathcal{F}^{n-p}(\Omega) &\longrightarrow \mathcal{F}^q(\Pi) \\ \underline{\eta} &\longmapsto \langle \underline{\underline{G}} \wedge \underline{\eta} \mid \Omega \rangle, \end{aligned}$$

defines an integral transformation. We denote double forms with a double underbar.

### Pull-back, Trace Operator

A mapping  $\varphi : \Omega \rightarrow \Pi$  maps points in the  $n$ -dimensional manifold  $\Omega$  into points in the  $m$ -dimensional manifold  $\Pi$ . It induces a mapping  $\phi : \mathbb{R}^n \rightarrow \mathbb{R}^m$  of coordinates  $\phi : (x^1, \dots, x^n) \rightarrow (u^1, \dots, u^m)$ .

We derive a mapping  $\varphi^* : \mathcal{F}^p(\Omega) \rightarrow \mathcal{F}^p(\Pi)$ ; differential  $p$ -forms transform according to

$$\varphi^* \underline{F} = \sum_{I \in \mathcal{I}_p^n} \sum_{K \in \mathcal{I}_p^m} \varphi^* f_I(u^1, \dots, u^m) \frac{\partial x^I}{\partial u^K} du^K.$$

$I$  and  $K$  are multiindices with

$$i_\mu \in \{1, \dots, n\}, \quad k_\nu \in \{1, \dots, m\}, \quad \mu, \nu = 1, \dots, p.$$

Denote by  $[J]$  the Jacobian,  $[J] \in \mathbb{R}^{m \times n}$  with

$$[J]^{ik} = \frac{\partial x^i}{\partial u^k}.$$

Denote  $[J'_K] \in \mathbb{R}^{p \times p}$  a matrix extracted from the Jacobian; the  $p$  lines are chosen by the multiindex  $I$ , the  $p$  columns by the multiindex  $K$ . We define

$$\frac{\partial x^I}{\partial u^K} = \det[J'_K].$$

A special pull-back transformation is the trace operator  $\mathfrak{t} : \mathcal{F}^p(\Omega) \mapsto \mathcal{F}^p(\partial\Omega)$ . It maps a  $p$ -form on  $\Omega$  into a  $p$ -form on the boundary  $\partial\Omega$ . For two adjacent domains,  $\Omega^-, \Omega^+$  with  $\partial\Omega^- = \partial\Omega^+$ , we define the jump operator  $\mathfrak{j}$  as the difference of the traces in the respective domains:

$$\mathfrak{j} = \mathfrak{t}^+ - \mathfrak{t}^-.$$

## Exterior Derivative

The exterior derivative operator  $d : \mathcal{F}^p(\Omega) \mapsto \mathcal{F}^{p+1}(\Omega)$  is defined as

$$d := \sum_{i=1}^n dx^i \wedge \partial_{x^i}.$$

We find that for  $n = 3$  it acts as a gradient operator on 0-forms, a curl-operator on 1-forms and a divergence-operator on 2-forms. It is zero when acting on 3-forms.

We give some properties of the exterior derivative:

$$\begin{aligned} d(\underline{F} + \underline{G}) &= d\underline{F} + d\underline{G}, \\ d(\underline{F} \wedge \underline{G}) &= d\underline{F} \wedge \underline{G} + (-1)^p \underline{F} \wedge d\underline{G}, \quad \underline{F} \in \mathcal{F}^p(\Omega), \\ d d &= 0, \\ d \mathfrak{t} \underline{F} &= \mathfrak{t} d\underline{F}. \end{aligned}$$

The third property sums up the first lemma of Poincaré (curl grad = 0 and div curl = 0).

A differential  $p$ -form in the kernel of the exterior derivative is called a *closed* form. The space of closed forms on a domain  $\Omega$  is denoted  $\mathcal{F}^p(d, \Omega)$ . A differential  $p$ -form in the image of the exterior derivative is called an *exact* form. The space of exact forms is a subset of the space of closed forms.

## Hodge operator

The Hodge operator in a Euclidean basis  $(dx, dy, dz)$  of the cotangent vector space of  $\mathbb{R}^3$  is defined by

$$* : \begin{cases} 1 & \mapsto dx \wedge dy \wedge dz & \mapsto 1 \\ dx & \mapsto dy \wedge dz & \mapsto dx. \end{cases}$$

The mappings of  $dy$  and  $dz$  are obtained by cyclic permutation.

For a curvilinear orthogonal coordinate chart the metric coefficients are defined as

$$[G]^{ij} = \langle \partial_{u^i}, \partial_{u^j} \rangle = \begin{cases} 0 & \text{for } i \neq j, \\ \partial_{u^i x} \partial_{u^j x} + \partial_{u^i y} \partial_{u^j y} + \partial_{u^i z} \partial_{u^j z} & \text{for } i = j. \end{cases}$$

With  $[G] = \text{diag}((\alpha_1)^2, (\alpha_2)^2, (\alpha_3)^2)$  we find for the Hodge operator in a curvilinear coordinate system

$$*_\alpha : \begin{cases} 1 & \mapsto \alpha_1 \alpha_2 \alpha_3 du^1 \wedge du^2 \wedge du^3 & \mapsto 1 \\ du^i & \mapsto \frac{\alpha_j \alpha_k}{\alpha_i} du^j \wedge du^k & \mapsto du^i, \end{cases} \quad (\text{A.1})$$

$ijk \in \{123, 231, 312\}$ .

On a plane, the 2-Hodge operator for orthogonal coordinates  $(u, v)$ ,  $[G^2] = \text{diag}(\alpha_1, \alpha_2)$ , is given by

$$*_\alpha^2 : \begin{cases} 1 & \mapsto \alpha_1 \alpha_2 du \wedge dv & \mapsto 1 \\ du & \mapsto \frac{\alpha_2}{\alpha_1 \alpha_2} dv & \mapsto -dv \\ dv & \mapsto -\frac{\alpha_1}{\alpha_1 \alpha_2} du & \mapsto du. \end{cases}$$

For a positive definite metric we find

$$**\underline{F} = (-1)^{p(n-p)} \underline{F}, \quad \underline{F} \in \mathcal{F}^p(\Omega);$$

Especially, for  $n = 3$ ,  $** = 1$ .

### Coderivative

The coderivative  $\delta : \mathcal{F}^p(\Omega) \rightarrow \mathcal{F}^{p-1}(\Omega)$  is defined (for a positive definite metric) by

$$\delta \underline{F} = (-1)^{n(p+1)+1} * d * \underline{F}, \quad \underline{F} \in \mathcal{F}^p(\Omega).$$

As a consequence of the first Poincaré lemma

$$\delta \delta = 0.$$

The Laplace-Beltrami Operator  $\Delta : \mathcal{F}^p(\Omega) \rightarrow \mathcal{F}^p(\Omega)$  is defined as

$$\Delta = d \delta + \delta d.$$

It is, up to a sign-change, the equivalent of the scalar and vector Laplace operator in classical vector analysis.

A differential  $p$ -form in the kernel of the coderivative is called *coclosed*. A differential  $p$ -form in the image of the coderivative is called *coexact*.

### Stokes Theorem

Without proof, compare, e.g., [21], we formulate the Stokes theorem

$$\langle \underline{F} | \partial m \rangle = \langle d \underline{F} | m \rangle, \quad \underline{F} \in \mathcal{F}^p(\Omega),$$

where  $m$  is a  $(p+1)$ -submanifold of  $\Omega$ . For  $p = 1$  it yields the classical Stokes theorem; for  $p = 2$  the Gauss theorem.

# Appendix B

## Maxwell Equations in Differential Form Notation

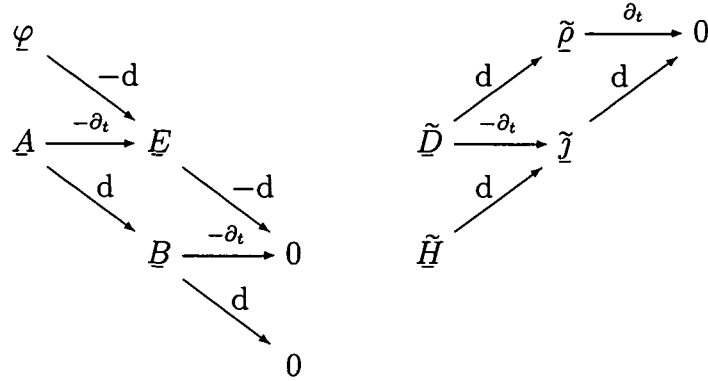
We introduce the governing equations of electromagnetism, the Maxwell equations, in differential form (DF) notation.

The electromagnetic fields and their physical dimensions (PD) are given in the following table:

DF	Physical Quantity	PD	
$\varphi$	even 0-form	electric scalar potential	U
$A$	even 1-form	magnetic vector potential	UT
$\tilde{\varphi}_M$	odd 0-form	magnetic scalar potential	I
$\tilde{V}$	odd 1-form	electric vector potential	IT
$\underline{E}$	even 1-form	electric field	U
$\underline{B}$	even 2-form	magnetic induction	UT
$\tilde{H}$	odd 1-form	magnetic field	I
$\tilde{D}$	odd 2-form	electric displacement	IT
$\tilde{j}$	odd 2-form	electric current density	I
$\tilde{\rho}$	odd 3-form	electric charge density	IT
$\tilde{\sigma}$	odd 2-form	electric surface charge	IT
$j_M$	even 2-form	magnetic current density	U
$\rho_M$	even 3-form	magnetic charge density	UT
$\sigma_M$	even 2-form	magnetic surface charge	UT
$\underline{M}$	odd 1-form	magnetization	I
$\underline{P}$	odd 2-form	electric polarization	IT

The topological equations of the electromagnetic theory are summarized in a topo-

logical diagram:



Each position in the diagram is given by the sum over the incoming arrows. We see that the topological equations split into two complexes: the Faraday complex with the fields  $\underline{\varphi}$ ,  $\underline{A}$ ,  $\underline{E}$ ,  $\underline{B}$  and the Ampère-Maxwell complex, where we find  $\underline{\tilde{H}}$ ,  $\underline{\tilde{D}}$ ,  $\underline{\tilde{j}}$ ,  $\underline{\tilde{\rho}}$ . On the Faraday side the potentials  $\underline{\varphi}$  and  $\underline{A}$  are defined by

$$\begin{aligned} -d\underline{\varphi} - \partial_t \underline{A} &= \underline{E} \\ d\underline{A} &= \underline{B}, \end{aligned}$$

up to a gauging transformation

$$\begin{aligned} \underline{\varphi}' &= \underline{\varphi} - \partial_t \lambda, \\ \underline{A}' &= \underline{A} + d\lambda. \end{aligned}$$

The Faraday law reads

$$d\underline{E} = -\partial_t \underline{B}.$$

Furthermore we find that the magnetic induction is free of sources,

$$d\underline{B} = 0.$$

On the Ampère-Maxwell side we find the local Ampère law as modified by Maxwell

$$d\underline{\tilde{H}} - \partial_t \underline{\tilde{D}} = \underline{\tilde{j}},$$

the Gauss law

$$d\underline{\tilde{D}} = \underline{\tilde{\rho}}$$

and the law of charge-conservation

$$d\underline{\tilde{j}} = -\partial_t \underline{\tilde{\rho}}.$$

The material laws are expressed by Hodge operators and material parameters,

$$\begin{aligned} \underline{\tilde{j}} &= *\kappa \underline{E}, \\ \underline{\tilde{D}} &= *\varepsilon \underline{E}, \\ \underline{\tilde{H}} &= *\nu \underline{B}, \end{aligned} \tag{B.1}$$

with the conductivity  $\kappa$ ,  $pd(\kappa) = I U^{-1}$ , the electric permeability  $\varepsilon$ ,  $pd(\varepsilon) = I T U^{-1}$  and the magnetic reluctivity  $\nu = 1/\mu$ ,  $pd(\nu) = I(UT)^{-1}$ , where  $\mu$  is the magnetic permeability.

For  $n = 3$ , the material laws may be expressed in terms of so-called metric-adapted Hodge operators. Let  $\alpha$  in Eq. (A.1) denote a possibly anisotropic, non-linear, inhomogeneous material property tensor.  $[G_\alpha]$  denotes the  $\alpha$ -adapted metric on  $\Omega$ , e.g,  $\text{diag}((\alpha_1)^2, (\alpha_2)^2, (\alpha_3)^2)$ . For isotropic material properties,  $\alpha_1 = \alpha_2 = \alpha_3$ , we find

$$*_\alpha : \begin{cases} 1 & \mapsto & \alpha^3 dx \wedge dy \wedge dz & \mapsto & 1 \\ dx & \mapsto & \alpha dy \wedge dz & \mapsto & dx. \end{cases}$$

We introduce  $*_\kappa$ ,  $*_\varepsilon$  and  $*_\mu$ , the conductivity- as well as electric and magnetic permeability adapted Hodge operators. We find  $*_\mu \underline{B} = *_\mu^{-1} \underline{B} = *\nu \underline{B}$ ,  $*_\kappa \underline{E} = *\kappa \underline{E}$  and  $*_\varepsilon \underline{E} = *\varepsilon \underline{E}$ .

We mention that in the London-theory of superconductivity the local Ohm's law, Eq. (B.1), is replaced by

$$\underline{\tilde{j}}^* = -*\frac{1}{\Lambda} \underline{A},$$

where  $\underline{\tilde{j}}^*$  is the current density of super-electrons (Cooper pairs) and  $\Lambda$  is the London constant, [8]. The 1st and the 2nd London equation follows from the topological diagram:

$$\begin{aligned} \underline{E} &= \partial_t(*\Lambda \underline{\tilde{j}}^*), & (1\text{st London equation}) \\ d*\Lambda \underline{\tilde{j}}^* &= -\underline{B}. & (2\text{nd London equation}) \end{aligned}$$

# Appendix C

## Local Interpolation of Coefficient Vectors

### C.1 Whitney Forms

In this section we want to reconstruct a continuous  $p$ -form  $\underline{F} \in \mathcal{F}^p(\Omega)$  from the coefficients of a  $p$ -cochain  $\underline{F} \in \mathcal{C}^p(\Omega)$ . The reconstructed field  $\underline{F}$  is an element of the finite dimensional space of Whitney  $p$ -forms  $\mathcal{W}^p(\Omega)$ . This subsection is based on [14] and [7].

Whitney forms have to fulfill the following requirements:

1. The *trace* of a Whitney form and of its exterior derivative on an interelement boundary has to be *unique* - it has to be fixed by the cochain coefficients associated with the respective boundary cell. Consequently, Whitney 0-forms yield  $C^0$ -continuity, Whitney 1-forms tangential continuity and Whitney 2-forms normal continuity. No continuity requirements need to be met by Whitney 3-forms.
2. The *exact sequence property* must hold for the spaces of Whitney forms; the exterior derivative of a Whitney  $p$ -form must yield a valid  $(p + 1)$ -form. As a consequence, the 1<sup>st</sup> Poincaré lemma holds.
3. Whitney-forms that yield 1st order approximations must be suited to *represent constant forms* without approximation errors.

Whitney basis forms will be denoted  $w^p$  and the interpolation of a  $p$ -cochain  $\underline{F}$  by Whitney forms will be denoted  $\underline{F}$  with an untertilde sign. On one element the interpolation reads

$$\underline{F} = \{F\}^1 w_1^p + \dots + \{F\}^{n_p} w_{n_p}^p.$$

The space of Whitney  $p$ -forms is denoted  $\mathcal{W}^p(\Omega)$ ,  $w_i^p \in \mathcal{W}^p(\Omega)$ .

To find Whitney  $p$ -forms we rely on a finding of Section 4.3: Any simplicial  $p$ -manifold  $s_p$ ,  $s_p \cap \varrho_n = s_p$ , can be represented as a linear combination of  $p$ -cells  $\varrho_p^i$ ,  $i = 1, \dots, n_p$  in the boundary of  $\varrho_n$ . As we will see, contracting  $s_p$  into a point yields the basis elements of Whitney  $p$ -forms.



### Whitney 0-Forms

Whitney 0-forms are given by the barycentric coordinates of a point in an  $n$ -cell,  $w_i^0 = \lambda_i(\mathfrak{x})$ .  $\mathcal{W}^0(\Omega)$  is the  $n_0$ -dimensional space of Whitney 0-forms. We know from the definition of barycentric coordinates that

$$\langle w_i^0 | \mathfrak{e}_0^j \rangle = \delta_i^j,$$

with  $\delta_i^j$  the Kronecker delta. Recall that  $\langle w_i^0 | \mathfrak{e}_0^j \rangle$  denotes the integral of the Whitney 0-form  $i$  over the 0-cell  $j$ , i.e., the point-evaluation of the 0-form  $i$  in node  $j$ . Whitney 0-forms are continuous across  $n$ -cell boundaries.

### Whitney 1-Forms

We use the interpolation of a line segment  $\mathfrak{s}_1$  between the points  $\mathfrak{x}^1$  and  $\mathfrak{x}^2$  to derive Whitney 1-forms. Equation (4.8) reads

$$\mathfrak{s}_1 = \sum_{i < j} (\lambda_i(\mathfrak{x}^1)\lambda_j(\mathfrak{x}^2) - \lambda_i(\mathfrak{x}^2)\lambda_j(\mathfrak{x}^1)) \mathfrak{e}_1^{ij}.$$

Therefore

$$\langle \underline{F} | \mathfrak{s}_1 \rangle = \sum_{i < j} (\lambda_i(\mathfrak{x}^1)\lambda_j(\mathfrak{x}^2) - \lambda_i(\mathfrak{x}^2)\lambda_j(\mathfrak{x}^1)) \langle \underline{F} | \mathfrak{e}_1^{ij} \rangle.$$

Consider the related line segment  $\mathfrak{s}'_1(t)$  between  $\mathfrak{x}^1$  and  $\mathfrak{x}^1 + t\mathfrak{v}$  with some coefficient  $t$ ,  $0 \leq t \leq 1$ , and  $\mathfrak{v} = \mathfrak{x}^2 - \mathfrak{x}^1$ . A differential 1-form is defined by

$$\underline{F}(\mathfrak{x}^1)(\mathfrak{v}) := \lim_{t \rightarrow 0} \frac{1}{t} \langle \underline{F} | \mathfrak{s}'_1(t) \rangle,$$

where  $\mathfrak{v}$  is the tangent vector in  $\mathfrak{x}^1$  pointing to  $\mathfrak{x}^2$ . We evaluate

$$\begin{aligned} \lim_{t \rightarrow 0} \frac{1}{t} \sum_{i < j} (\lambda_i(\mathfrak{x}^1)\lambda_j(\mathfrak{x}^2) - \lambda_i(\mathfrak{x}^2)\lambda_j(\mathfrak{x}^1)) &= \\ &= \sum_{i < j} (\lambda_i(\mathfrak{x})d\lambda_j(\mathfrak{x}) - \lambda_j(\mathfrak{x})d\lambda_i(\mathfrak{x})). \end{aligned}$$

Consequently we find that

$$\begin{aligned} \underline{F}(\mathfrak{x})(\mathfrak{v}) &:= \lim_{t \rightarrow 0} \frac{1}{t} \langle \underline{F} | \mathfrak{s}'_1(t) \rangle \\ &= \sum_{i < j} (\lambda_i(\mathfrak{x})d\lambda_j(\mathfrak{x}) - \lambda_j(\mathfrak{x})d\lambda_i(\mathfrak{x})) \langle \underline{F} | \mathfrak{e}_1^{ij} \rangle \\ &= \sum_{i < j} (\lambda_i(\mathfrak{x})d\lambda_j(\mathfrak{x}) - \lambda_j(\mathfrak{x})d\lambda_i(\mathfrak{x})) \{F\}^k, \end{aligned}$$

where  $k$  is a multiindex with  $k_1 = i$  and  $k_2 = j$ . The individual summands are the weighted Whitney 1-forms  $w_{ij}^1 \in \mathcal{W}^1(\Omega)$ ,

$$w_{ij}^1 = \lambda_i(\mathfrak{x})d\lambda_j(\mathfrak{x}) - \lambda_j(\mathfrak{x})d\lambda_i(\mathfrak{x}),$$

compare [14]. We use Whitney 1-forms to locally interpolate 1-cochains on a simplicial cell.  $\mathcal{W}^1(\Omega)$  denotes the space of Whitney 1-forms. The integrals of Whitney-forms along primal edges read

$$\langle w_{ij}^1 | \varrho_1^{kl} \rangle = \delta_{ij}^{kl},$$

with  $\delta_{kl}^{ij}$  the Kronecker delta. This corresponds to the required tangential continuity of Whitney 1-forms. Note that the normal component of Whitney 1-forms may jump on the  $n$ -cell boundary between two adjacent  $n$ -cells.

### Whitney $p$ -Forms

For general  $n$  and  $p$ , Whitney forms on simplicial cells are given by, compare, e.g., [7],

$$w_{k_1 \dots k_{p+1}}^p(\mathfrak{x}) := p! \sum_{i=1}^{p+1} (-1)^{i+1} \lambda_{k_i}(\mathfrak{x}) d\lambda_{k_1}(\mathfrak{x}) \wedge \dots \wedge d\lambda_{k_{i-1}}(\mathfrak{x}) \wedge d\lambda_{k_{i+1}}(\mathfrak{x}) \wedge \dots \wedge d\lambda_{k_{p+1}}(\mathfrak{x}),$$

with  $k$  a  $(p+1)$ -tuple denoting the  $(p+1)$  vertices of the respective  $p$ -cell. For the integrals of Whitney  $p$ -forms on  $p$ -cells we find

$$\langle w_{k_1 \dots k_{p+1}}^p | \varrho_p^{l_1 \dots l_{p+1}} \rangle = \delta_{k_1 \dots k_{p+1}}^{l_1 \dots l_{p+1}},$$

with the Kronecker delta  $\delta_{k_1 \dots k_{p+1}}^{l_1 \dots l_{p+1}}$ .

## C.2 Sobolev Spaces

In this section we define special functional spaces, the so-called Sobolev spaces. We identify those Sobolev spaces that allow for an adequate modelling of physical fields in electromagnetism. We state that the above introduced Whitney forms yield consistent discretizations of the respective Sobolev spaces. Information on the topic is found, e.g., in [10] and [15]. In this section we denote with the letter  $H$  special Hilbert spaces. Elsewhere the letter  $H$  is reserved for homology and cohomology spaces and for the magnetic field.

Denote by  $C_0(\Omega)$  the space of real or complex continuous functions with finite support on  $\Omega$ , i.e., the functions in  $C_0$  are different from zero only on a finite

subspace of  $\Omega$ . Furthermore, denote by  $C_0^m(\Omega)$ , ( $m \in \mathbb{N}_0$ ) all  $f \in C_0(\Omega)$  of that all derivatives  $\partial_{x_1}^{p_1} \dots \partial_{x_n}^{p_n} f$  of order  $p_1 + p_2 + \dots + p_n \leq m$  in  $\Omega$  exist. We write

$$D^p := \partial_{x_1}^{p_1} \dots \partial_{x_n}^{p_n},$$

where  $p$  is the multiindex  $(p_1, \dots, p_n)$ ,  $p_i \in \mathbb{N}_0$  and  $|p| = p_1 + \dots + p_n$ .  $C_0^\infty(\Omega)$  is the space of functions in  $C_0(\Omega)$  that can be differentiated an arbitrary number of times. The space of square-integrable functions is defined as

$$L_2(\Omega) := \{f \in C_0^\infty \mid \int_{\Omega} \|f(x)\|_2^2 d\Omega < \infty\}.$$

The Sobolev space  $H_m(\Omega)$  is the space of those functions  $f \in L_2(\Omega)$  with the property that all derivatives  $D^p f$  of order  $|p| \leq m$  are in  $L_2(\Omega)$ :

$$H_m(\Omega) := \{f \in L_2(\Omega) \mid D^p f \in L_2(\Omega), |p| \leq m\}.$$

A bilinear product (scalar product) is declared on  $H_m(\Omega)$  by

$$\langle f, g \rangle_m := \sum_{0 \leq |p| \leq m} \langle D^p f, D^p g \rangle, \quad \text{for } f, g \in H_m(\Omega).$$

$\langle f, g \rangle$  is defined as

$$\langle f, g \rangle := \int_{\Omega} f(x)g(x)^* d\Omega.$$

The star denotes the conjugate complex function. For vector valued functions with all components in  $L_2(\Omega)$  we define

$$\mathbf{L}_2(\Omega) := (L_2(\Omega))^n.$$

The scalar product for vector valued functions reads

$$\langle \mathbf{u}, \mathbf{v} \rangle := \int_{\Omega} \mathbf{u}(x) \cdot \mathbf{v}(x)^* d\Omega.$$

For vector fields with all components in  $H_m(\Omega)$  we define

$$\mathbf{H}_m(\Omega) := (H_m(\Omega))^n.$$

## C.3 Special Sobolev Spaces

For  $n = 3$  we define the following Sobolev spaces (similar spaces can be defined for  $n < 3$ ):

$$\begin{aligned} H_{\text{grad}}(\Omega) &:= \{f \in L_2(\Omega) \mid \text{grad } f \in \mathbf{L}_2(\Omega)\}, \\ \mathbf{H}_{\text{curl}}(\Omega) &:= \{\mathbf{u} \in \mathbf{L}_2(\Omega) \mid \text{curl } \mathbf{u} \in \mathbf{L}_2(\Omega)\}, \\ \mathbf{H}_{\text{div}}(\Omega) &:= \{\mathbf{u} \in \mathbf{L}_2(\Omega) \mid \text{div } \mathbf{u} \in L_2(\Omega)\}. \end{aligned}$$

The respective scalar products are defined by

$$\begin{aligned}\langle f, g \rangle_{\text{grad}} &:= \langle f, g \rangle + \langle \text{grad } f, \text{grad } g \rangle, \\ \langle \mathbf{u}, \mathbf{v} \rangle_{\text{curl}} &:= \langle \mathbf{u}, \mathbf{v} \rangle + \langle \text{curl } \mathbf{u}, \text{curl } \mathbf{v} \rangle, \\ \langle \mathbf{u}, \mathbf{v} \rangle_{\text{div}} &:= \langle \mathbf{u}, \mathbf{v} \rangle + \langle \text{div } \mathbf{u}, \text{div } \mathbf{v} \rangle.\end{aligned}$$

It can easily be verified that  $H_{\text{grad}}(\Omega) = H_1(\Omega)$ .

Finally, we denote by  ${}^0H_{\text{grad}}(\Omega)$ ,  ${}^1\mathbf{H}_{\text{curl}}(\Omega)$ ,  ${}^2\mathbf{H}_{\text{div}}(\Omega)$ ,  ${}^3L_2(\Omega)$  the spaces of differential 0-, 1- and 2-forms that are isomorphic to the respective scalar and vector valued functions for a given metric on  $\Omega$ . The isomorphism between vectors and differential forms is discussed, e.g., in [21]. We can denote the different spaces more generally by  ${}^pH_d(\Omega)$ .

As we require the  $p$ -forms representing the electromagnetic fields as well as their time-derivatives to be in  ${}^pH_d(\Omega)$  we require that the electromagnetic energy of the fields in  $\Omega$  is finite. Note that, occasionally, it might be favourable to release this constraint. Generally, however,  ${}^pH_d(\Omega)$  is a good choice to model the electromagnetic fields.

The space of Whitney forms  $\mathcal{W}^p(\Omega) \subset {}^pH_d(\Omega)$  strives to the entire of  ${}^pH_d(\Omega)$  as the complex' discretization density increases and the following diagram commutes:

$$\begin{array}{ccccccc} \mathcal{F}^0(\Omega) & \xrightarrow{d} & \mathcal{F}^1(\Omega) & \xrightarrow{d} & \dots & \xrightarrow{d} & \mathcal{F}^n(\Omega) \\ \downarrow d_\Omega & & \downarrow & & \downarrow & & \downarrow \\ \mathbb{R}^{n_0} & \xrightarrow{[D^0]} & \mathbb{R}^{n_1} & \xrightarrow{[D^1]} & \dots & \xrightarrow{[D^{n-1}]} & \mathbb{R}^{n_n} \\ \downarrow w_\Omega & & \downarrow & & \downarrow & & \downarrow \\ \mathcal{W}^0(\Omega) & \xrightarrow{d} & \mathcal{W}^1(\Omega) & \xrightarrow{d} & \dots & \xrightarrow{d} & \mathcal{W}^n(\Omega), \end{array}$$

where  $d_\Omega$  denotes discretization and  $w_\Omega$  the interpolation by Whitney forms.

In [14] and [13] procedures are introduced that allow to derive Whitney forms on polyhedral cells other than simplicial ones, e.g., on prisms or pyramids.

# Appendix D

## Discretization of the Poynting Theorem

In this chapter we take a closer look at the energy stored in an electromagnetic field. We derive a discretization of the Poynting theorem and find a discrete form of the energy balance equation for a bounded domain. We then proceed with the investigation of a voltage-driven coil in the quasistatic regime. The time-derivative of the linked magnetic flux induces a voltage that opposes the terminal source voltage. Throughout this chapter we only consider  $n = 3$  dimensions.

### D.1 The Poynting Theorem

The exterior derivative of the Poynting vector  $S = \underline{E} \wedge \tilde{H}$  yields

$$\begin{aligned} dS &= d(\underline{E} \wedge \tilde{H}) = d\underline{E} \wedge \tilde{H} - \underline{E} \wedge d\tilde{H} \\ &= -\partial_t \underline{B} \wedge \tilde{H} - \underline{E} \wedge \partial_t \tilde{D} - \underline{E} \wedge \tilde{j}. \end{aligned}$$

This is the local formulation of the Poynting theorem. Integrating over  $\Omega$  yields the integral formulation:

$$\langle \underline{E} \wedge \tilde{H} \mid \partial\Omega \rangle + \langle \partial_t \underline{B} \wedge \tilde{H} + \underline{E} \wedge \partial_t \tilde{D} \mid \Omega \rangle = -\langle \underline{E} \wedge \tilde{j} \mid \Omega \rangle. \quad (\text{D.1})$$

We identify  $\partial_t w = \partial_t \underline{B} \wedge \tilde{H} + \underline{E} \wedge \partial_t \tilde{D}$ , the time derivative of the electromagnetic energy density,  $r = -\underline{E} \wedge \tilde{j}$  the power density and  $q = \underline{E} \wedge \tilde{H}$  the energy flux density. The Poynting theorem gives an energy balance equation

$$\begin{aligned} \langle \partial_t w \mid \Omega \rangle + \langle q \mid \partial\Omega \rangle &= \langle r \mid \Omega \rangle \\ \dot{W}(\Omega) + Q(\partial\Omega) &= R(\Omega), \end{aligned}$$

with  $\dot{W}(\Omega)$  the time derivative of the electromagnetic energy inside  $\Omega$ ,  $Q(\partial\Omega)$  the total energy flux through the boundary of  $\Omega$  and  $R(\Omega)$  the total rate of energy

production in  $\Omega$ . The total energy in  $\Omega$  is obtained by a time-integration

$$\begin{aligned}\underline{w} &= \int (\partial_t \underline{B} \wedge \tilde{\underline{H}} + \underline{E} \wedge \partial_t \tilde{\underline{D}}) dt, \\ W(\Omega) &= \langle \underline{w} | \Omega \rangle.\end{aligned}$$

For linear material we find that

$$\underline{w} = \frac{1}{2} \underline{B} \wedge \tilde{\underline{H}} + \frac{1}{2} \underline{E} \wedge \tilde{\underline{D}}.$$

Discretization of the domain  $\Omega$  and approximation of the involved fields by Whitney forms yields

$$\langle \mathbf{t} \underline{E} \wedge \mathbf{t} \tilde{\underline{H}} | \partial\Omega \rangle + \langle \partial_t \underline{B} \wedge \tilde{\underline{H}} + \underline{E} \wedge \partial_t \tilde{\underline{D}} | \Omega \rangle = -\langle \underline{E} \wedge \tilde{\underline{j}} | \Omega \rangle$$

and thus

$$\{\tilde{\underline{H}}_{\partial\Omega}\}^T [K_{\partial\Omega}^1] \{E_{\partial\Omega}\} + \{\tilde{\underline{H}}\}^T [K^2] \{\partial_t B\} + \{\partial_t \tilde{\underline{D}}\}^T [K^1] \{E\} = -\{\tilde{\underline{j}}\}^T [K^2] \{E\}.$$

In the magneto(quasi)static approximation of Maxwell's equations Eq. (D.1) reads

$$\langle \underline{E} \wedge \tilde{\underline{H}} | \partial\Omega \rangle + \langle \partial_t \underline{B} \wedge \tilde{\underline{H}} | \Omega \rangle = -\langle \underline{E} \wedge \tilde{\underline{j}} | \Omega \rangle$$

and

$$\begin{aligned}\dot{W}(\Omega) &= \langle \partial_t \underline{B} \wedge \tilde{\underline{H}} | \Omega \rangle \\ &\approx \langle \partial_t \underline{B} \wedge \tilde{\underline{H}} | \Omega \rangle \\ &\approx \{\tilde{\underline{H}}\}^T [K^2] \{\partial_t B\}.\end{aligned}\tag{D.2}$$

We may also write

$$\begin{aligned}\dot{W}(\Omega) &= \langle * \nu \underline{B} \wedge \partial_t \underline{B} | \Omega \rangle \\ &= \langle * \nu d\underline{A} \wedge d\partial_t \underline{A} | \Omega \rangle \\ &\approx \{\partial_t A\}^T [D^1]^T [M_{G_{a,\nu}}^2] [D^1] \{A\}.\end{aligned}$$

This is an interesting result: In the discrete expression of the magnetostatic energy, the discrete Hodge operator appears in the same constellation with discrete derivative operators,  $[\bar{D}^1][M_{G_{a,\nu}}^2][D^1]$ , as in the discrete curlcurl-equation. We see that the Whitney and the geometric 2-Hodge operators will yield the same approximation for the energy in  $\Omega$ , recall Section 6.3. We stated before that a Hodge operator needs to be symmetric. For the energy product to be symmetric in its discrete form we now find that, if we use the electric scalar potential or the magnetic vector potential, the unsymmetric part of the discrete Hodge operator only needs to lie in the zero-equivalence class defined by Eq. (6.9).

## D.2 Flux Linkage and Voltage Driven Coils

From Eq. (D.2) we obtain with

$$d(\partial_t \underline{A} \wedge \underline{\tilde{H}}) = d\partial_t \underline{A} \wedge \underline{\tilde{H}} - \partial_t \underline{A} \wedge d\underline{\tilde{H}}$$

another expression for the time derivative of the magnetic energy

$$\dot{W}(\Omega) = \langle \partial_t \underline{A} \wedge \underline{\tilde{j}} \mid \Omega \rangle + \langle \partial_t \underline{A} \wedge \underline{\tilde{H}} \mid \partial\Omega \rangle.$$

The discrete approximation yields

$$\dot{W}(\Omega) \approx \{\tilde{j}\}^T [K^1] \{\partial_t A\} + \{\tilde{H}_{\partial\Omega}\}^T [K_{\partial\Omega}^1] \{\partial_t A_{\partial\Omega}\}.$$

Let now  $\Omega$  be a domain containing a coil wound from a line-current like conductor. Let the domain be sufficiently large, i.e., the distance  $R$  from the domain boundary to the coil is large with respect to the coil size. In this case the boundary term  $\partial_t \underline{A} \wedge \underline{\tilde{H}}$  is proportional to  $R^{-3}$ , [26]. It contributes only marginally and can be neglected,

$$\dot{W}(\Omega) = \langle \partial_t \underline{A} \wedge \underline{\tilde{j}} \mid \Omega \rangle.$$

For so-called thin-wire coils, the current density can be written

$$\underline{\tilde{j}} = \underline{\tilde{I}} \underline{\tau},$$

with the constant odd 0-form  $\underline{\tilde{I}}$  representing the current in the conductor and the even 2-form  $\tau$  denoting the winding density. A discretization reads

$$\{\tilde{j}_c\} = \underline{\tilde{I}} [K_c^2] \{\tau\},$$

with  $[K_c^2]$  the transfer matrix restricted to the DEM coil.

Neglecting currents outside the coil, we find for the magnetic energy

$$\dot{W}(\Omega_c) = \underline{\tilde{I}} \langle \partial_t \underline{A} \wedge \underline{\tau} \mid \Omega_c \rangle.$$

At the same time we know that

$$\dot{W}(\Omega_c) = \underline{\tilde{I}} \dot{\Psi}_L,$$

where  $\Psi_L$  denotes the "linked" magnetic flux,  $\Psi_L = N\Psi$  with  $N$  the number of windings in the coil. We therefore find that

$$\dot{\Psi}_L = \langle \partial_t \underline{A} \wedge \underline{\tau} \mid \Omega_c \rangle$$

or

$$\dot{\Psi}_L \approx \{\tau\}^T [K_c^1] \{\partial_t A\}.$$

The coil current of a voltage driven coil (as opposed to a current driven coil) is determined from

$$U = \dot{\Psi}_L + R\tilde{I},$$

where  $U$  is the coil's terminal voltage and  $R$  is the coil resistance. The magneto-quasistatic equation system in presence of a voltage driven coil reads

$$[\tilde{D}^1][M_c^2][D^1]\{A\} + [M_c^1]\{\partial_t A\} - [K_c^2]\{\tau\}\tilde{I} = \{\tilde{j}_s\},$$

$$\{\tau\}^T [K_c^1]\{\partial_t A\} + R\tilde{I} = U.$$

$\{\tilde{j}_s\}$  holds coefficients of current-driven coils. The current in the voltage-driven coil is determined by the second equation.



# Appendix E

## Discrete Material Laws (4) - Anisotropy, Eddy Currents, Non-linearity

We present three more topics in the theory of discrete electromagnetism all of which are related to the discrete material laws: anisotropy, eddy-currents and non-linearity. The sections on eddy-currents and non-linearities are mainly intended as a reference for the implementation in the Edyson program code, compare Chapter 10.

### E.1 Anisotropy

Anisotropic material laws enter the DEM in the discrete Hodge operators. The Equations (5.1), (6.1) and (6.7) give three definitions of discrete Hodge operators:

$$\begin{aligned} [M'_{ge,\alpha}]^{ij} &= \frac{\| \bar{\varrho}'^i_{n-p} \wedge * \alpha \tilde{\varrho}'^j_{n-p} \|}{\| \varrho_n \|}, \\ [M'_{wh,\alpha}]^{ij} &= \langle * \alpha \varpi_j^p \mid \tilde{\varrho}'^i_p \rangle, \\ [M'_{Ga,\alpha}]^{ij} &= \langle * \alpha \varpi_j^p \wedge \varpi_i^p \mid \Omega \rangle. \end{aligned}$$

Introducing anisotropy is simple. We only need to replace the isotropic material parameter  $\alpha$  by a tensorial anisotropic parameter  $\alpha$ .

For an alternative approach, recall the idea of metric-adapted Hodge operators, introduced in Annex B. To obtain an anisotropic Hodge we introduce the  $\alpha$ -adapted metric thus affecting the Hodge operator:

$$[M'_{ge,\alpha}] = \frac{\| \bar{\varrho}'^i_{n-p} \wedge *_{\alpha} \tilde{\varrho}'^j_{n-p} \|}{\| \varrho_n \|}.$$

Recall that a 1-dimensional Newton algorithm solves

$$f(x) = 0.$$

From a start-value  $x_0$  we use

$$f(x_0) + \partial_x f(x) \delta x = 0$$

and solve for  $\delta x$ . The update of the solution is done by  $x_1 = x_0 + \delta x$ .

For the time-transient equation system in Section E.2 we identify  $x_0$  with  $(\{A^t + \Delta A^i\}^T, \tilde{I}^{t+\Delta t, i}, \{\varphi_{M,\Gamma}^t + \Delta \varphi_{M,\Gamma}\}^T)^T$ , where  $i$  denotes the  $i$ th Newton iteration, and  $f(x_0)$  with  $(\{N_\Omega\}^T, N_I, \{N_\Gamma\}^T)^T$ ,

$$\begin{aligned} \{N_\Omega\} &= [\tilde{D}^1][M_\nu^2(A^t + \Delta A^i)][D^1]\{A^t + \Delta A^i\} - [\tilde{J}^1][\tilde{K}_\Gamma^1][\tilde{D}_\Gamma^0]\{\varphi_{M,\Gamma}^t + \Delta \varphi_{M,\Gamma}^i\} \\ &\quad + [M_\kappa^1]\{\Delta A^i/\Delta t\} - [K_C^2]\{\tau\}\tilde{I}^{t+\Delta t, i} - \{\tilde{j}_s^{t+\Delta t}\}, \\ N_I &= \{\tau\}^T [K_C^1][T_C^1]\{\Delta A^i/\Delta t\} - U^{t+\Delta t}, \\ \{N_\Gamma\} &= [\bar{D}_\Gamma^1][\Psi_{DL}^{*1}][T^1]\{A^t + \Delta A^i\} - [\bar{D}_\Gamma^1][\tilde{\Psi}_{SL}^1][\tilde{D}_\Gamma^0]\{\varphi_{M,\Gamma}^t + \Delta \varphi_{M,\Gamma}^i\} - \{\bar{B}_{S,\Gamma}^{t+\Delta t}\}. \end{aligned}$$

We define

$$[N^1] = \frac{\partial([\tilde{D}^1][M_\nu^2(A^t + \Delta A^i)][D^1])}{\partial\{A\}}\{A^t + \Delta A^i\}.$$

Now we have to solve

$$\begin{aligned} [N^1]\{\delta A\} + [\tilde{D}^1][M_\nu^2(A^t + \Delta A^i)][D^1]\{\delta A\} - [\tilde{J}^1][\tilde{K}_\Gamma^1][\tilde{D}_\Gamma^0]\{\delta \varphi_{M,\Gamma}\} &+ \\ [M_\kappa^1]\{\delta A/\Delta t\} - [K_C^2]\{\tau\}\delta \tilde{I} &= -\{N\}, \\ \{\tau\}^T [K_C^1][T_C^1]\{\delta A/\Delta t\} + R\delta \tilde{I} &= -N_I, \\ [\bar{D}_\Gamma^1][\Psi_{DL}^{*1}][T^1]\{\delta A\} - [\bar{D}_\Gamma^1][\tilde{\Psi}_{SL}^1][\tilde{D}_\Gamma^0]\{\delta \varphi_{M,\Gamma}\} &= -\{N_\Gamma\}. \end{aligned}$$

The update is done by

$$\begin{aligned} \{\Delta A^{i+1}\} &= \{\Delta A^i\} + \{\delta A\}, \\ \tilde{I}^{t+\Delta t, i+1} &= \tilde{I}^{t+\Delta t, i} + \delta \tilde{I}, \\ \{\Delta \varphi_{M,\Gamma}^{i+1}\} &= \Delta \varphi_{M,\Gamma}^i + \delta \varphi_{M,\Gamma}. \end{aligned}$$

Note that the metric-adapted Hodge operator acting on  $p$ -vectors is defined by

$$*_\alpha : \begin{cases} 1 & \mapsto \frac{1}{\alpha_1\alpha_2\alpha_3} \mathbf{u}^1 \wedge \mathbf{u}^2 \wedge \mathbf{u}^3 & \mapsto 1 \\ \mathbf{u}^i & \mapsto \frac{\alpha_i}{\alpha_j\alpha_k} \mathbf{u}^j \wedge \mathbf{u}^k & \mapsto \mathbf{u}^i, \end{cases}$$

whereas the metric-adapted Hodge operator acting on  $p$ -covectors ( $p$ -forms) is given by

$$*_\alpha : \begin{cases} 1 & \mapsto \alpha_1\alpha_2\alpha_3 du^1 \wedge du^2 \wedge du^3 & \mapsto 1 \\ du^i & \mapsto \frac{\alpha_j\alpha_k}{\alpha_i} du^j \wedge du^k & \mapsto du^i, \end{cases}$$

$ijk \in \{123, 231, 312\}$ .

## E.2 Eddy Currents

We solve the time-transient vector-potential formulation in presence of voltage driven coils, compare Section D.2. The boundary conditions are given by the coupling to a BEM formulation:

$$\begin{aligned} [\tilde{\mathbf{D}}^1][\mathbf{M}_\nu^2][\mathbf{D}^1]\{A\} - [\tilde{\mathbf{J}}^1][\tilde{\mathbf{K}}_\Gamma^1][\tilde{\mathbf{D}}_\Gamma^0]\{\varphi_{\mathbf{M},\Gamma}\} + [\mathbf{M}_\kappa^1]\{\partial_t A\} - [\mathbf{K}_\mathbf{C}^2]\{\tau\}\tilde{I} &= \{\tilde{j}_s\}, \\ \{\tau\}^\top[\mathbf{K}_\mathbf{C}^1][\mathbf{T}_\mathbf{C}^1]\{\partial_t A\} + R\tilde{I} &= U, \\ [\bar{\mathbf{D}}_\Gamma^1][\Psi_{\text{DL}}^{*1}][\mathbf{T}^1]\{A\} - [\bar{\mathbf{D}}_\Gamma^1][\tilde{\Psi}_{\text{SL}}^1][\tilde{\mathbf{D}}_\Gamma^0]\{\varphi_{\mathbf{M},\Gamma}\} &= \{\bar{B}_{\text{S},\Gamma}\}. \end{aligned}$$

We use an implicit Euler scheme, i.e., we replace  $\{\partial_t A^{t+\Delta t}\}$  by  $\{\Delta A/\Delta t\}$ . We calculate the field after one time-step  $\Delta t$ :

$$\begin{aligned} [\tilde{\mathbf{D}}^1][\mathbf{M}_\nu^2][\mathbf{D}^1]\{A^t + \Delta A\} - [\tilde{\mathbf{J}}^1][\tilde{\mathbf{K}}_\Gamma^1][\tilde{\mathbf{D}}_\Gamma^0]\{\varphi_{\mathbf{M},\Gamma}^t + \Delta\varphi_{\mathbf{M},\Gamma}\} + \\ [\mathbf{M}_\kappa^1]\{\Delta A/\Delta t\} - [\mathbf{K}_\mathbf{C}^2]\{\tau\}\tilde{I}^{t+\Delta t} &= \{\tilde{j}_s^{t+\Delta t}\}, \\ \{\tau\}^\top[\mathbf{K}_\mathbf{C}^1][\mathbf{T}_\mathbf{C}^1]\{\Delta A/\Delta t\} + R\tilde{I}^{t+\Delta t} &= U^{t+\Delta t}, \\ [\bar{\mathbf{D}}_\Gamma^1][\Psi_{\text{DL}}^{*1}][\mathbf{T}^1]\{A^t + \Delta A\} - [\bar{\mathbf{D}}_\Gamma^1][\tilde{\Psi}_{\text{SL}}^1][\tilde{\mathbf{D}}_\Gamma^0]\{\varphi_{\mathbf{M},\Gamma}^t + \Delta\varphi_{\mathbf{M},\Gamma}\} &= \{\bar{B}_{\text{S},\Gamma}^{t+\Delta t}\}. \end{aligned}$$

For given  $\Delta t$ ,  $\{A^t\}$ ,  $\{\varphi_{\mathbf{M},\Gamma}^t\}$ ,  $\{\tilde{j}_s^{t+\Delta t}\}$ ,  $U^{t+\Delta t}$  and  $\{\bar{B}_{\text{S},\Gamma}^{t+\Delta t}\}$  we can solve for  $\{\Delta A\}$ ,  $\{\Delta\varphi_{\mathbf{M},\Gamma}^t\}$  and  $\tilde{I}^{t+\Delta t}$ .

## E.3 Non-linearity

For non-linear material properties, e.g., a  $B(\underline{H})$  curve, a solution to a field problem cannot be found in one step; it needs to be found iteratively. The Newton algorithm is a powerful iterative solver.

## F.1 Double-Layer Potential of an Equivalence Class

The double-layer potential of an equivalence class according to Eq. (7.3) is well defined since

$$\begin{aligned}
(-1)^p \Psi_{\text{DL}}^p(d\lambda) &= \langle \mathbf{j} * d\underline{G}^p \wedge d\lambda \mid \Gamma \rangle \\
&= (-1)^p \langle \mathbf{j} d * d\underline{G}^p \wedge \lambda \mid \Gamma \rangle \\
&= -\langle \mathbf{j} * \delta d\underline{G}^p \wedge \lambda \mid \Gamma \rangle = \langle \mathbf{j} * d\delta \underline{G}^p \wedge \lambda \mid \Gamma \rangle \\
&= (d\delta)' \langle \mathbf{j} * \underline{G}^p \wedge \lambda \mid \Gamma \rangle.
\end{aligned} \tag{F.1}$$

The double-layer potential of a coboundary is itself a coboundary. The zero-equivalence class is mapped into the zero-equivalence class and the double-layer potential of equivalence classes is well defined.

## F.2 Equivalence of Current Loops and Magnetic Double Layers

We show two ways to calculate the BEM right-hand side of a magnetic scalar potential formulation due to a current loop, compare Section 8.1. The Newton (or source-) potential for  $p = 1$  yields

$$\tilde{H}'_s = *'d' \langle \underline{G}^1 \wedge \tilde{\mathbf{j}} \mid \Omega^2 \rangle.$$

For a closed current loop we find

$$\tilde{H}'_s = *'d' \langle \underline{G}^1 \wedge \tilde{\mathbf{I}} \mid \partial\Lambda \rangle, \tag{F.2}$$

where  $\tilde{\mathbf{I}}$  is the line-current zero-form and  $\Lambda$  is any surface that is bounded by the current loop.

Alternatively we may calculate the BEM right-hand side from  $\tilde{H}'_{s,\Gamma} = -d\tilde{\varphi}'_{M,\Gamma}$  with

$$\tilde{\varphi}'_{M,\Gamma} = \langle \underline{G}^0 \wedge \underline{\rho}_M \mid \Omega^+ \rangle.$$

Although magnetic charges have not been discovered, we will show that a double layer of magnetic surface charges,  $\underline{\sigma}_{M,\text{DL}}$ , yields the same magnetic field as Eq. (F.2). We find, e.g., in [18] that the magnetic scalar potential due to a magnetic double-layer is given by

$$\tilde{\varphi}'_{M,\Gamma} = \nu_0 \langle \mathbf{t} * d\underline{G}^0 \wedge *^2 \underline{\sigma}_{M,\text{DL}} \mid \Lambda \rangle.$$

# Appendix F

## BEM Potentials

In the following we use the Euclidean metric. Thus the Hodge-operators are not defined under a material-adapted metric and neither is the Green function  $g(\mathbf{x}, \mathbf{x}')$  of the Laplace-Beltrami operator. From  $dg(\mathbf{x}, \mathbf{x}') = -d'g(\mathbf{x}, \mathbf{x}')$  we derive the following useful properties for  $\mathbf{x} \neq \mathbf{x}'$ ,  $p = 0, 1, 2$ .

$$\begin{aligned}d' \underline{\underline{G}}^p &= \delta \underline{\underline{G}}^{p+1}, \\d \underline{\underline{G}}^p &= \delta' \underline{\underline{G}}^{p+1}.\end{aligned}$$

It follows directly that

$$\begin{aligned}\delta d' \underline{\underline{G}}^p &= 0, \\ \delta' d \underline{\underline{G}}^p &= 0, \\ \delta d \underline{\underline{G}}^p &= (\delta d)' \underline{\underline{G}}^p, \\ d \delta \underline{\underline{G}}^{p+1} &= (d \delta)' \underline{\underline{G}}^{p+1}.\end{aligned}$$

Furthermore, from  $(d\delta + \delta d)\underline{\underline{G}}^p = 0$  for  $\mathbf{x} \neq \mathbf{x}'$  we find

$$\begin{aligned}d \delta \underline{\underline{G}}^p &= -\delta d \underline{\underline{G}}^p, \\ (d \delta)' \underline{\underline{G}}^p &= -(\delta d)' \underline{\underline{G}}^p.\end{aligned}$$

Setting for  $\tilde{q}$

$$*^1 \underline{K}_{M,T} = \frac{\tilde{q}}{\varepsilon_0},$$

we get for the vector potential due to a thin tube of magnetic surface currents

$$\tilde{V}'_s = \langle \mathbf{t} * d\underline{G}^1 \wedge \varepsilon_0 *^1 \underline{K}_{M,T} \mid \Pi \rangle.$$

We understand that both formulations, magnetic scalar potential and electric vector-potential, are directly related to the problem cohomology contributions. In both cases, the source-free space where  $d\underline{H} = 0$  or  $d\underline{D} = 0$  is not contractible. For  $\tilde{H}$ , because we need to cut out the torus of a line current loop and for  $\tilde{D}$ , because we need to eliminate the two cavities containing the point charges. However, a potential formulation for  $\tilde{H}$  and  $\tilde{D}$  is possible, if we account for the cohomology contributions and thus for the non-zero periods of the forms, by means of concentrated fields on suitable sub-domains. The magnetic double layer represents a concentrated magnetic field that is added to any closed loop integral that contains a non-zero current. The tube of magnetic surface-currents represents a "fibre" of electric flux that contributes to the integral of  $\tilde{D}'_s$  over any closed surface that contains one of the point charges.<sup>1</sup>

---

<sup>1</sup>Macroscopic magnetic dipoles, by the way, would yield a magnetic flux density that could be represented by a thin electric coil. The coil is equivalent to a magnetic flux fibre.

$*^2$  denotes the 2-dimensional Hodge operator on  $\Lambda$ . We recognize the double-layer potential of Eq. (7.2). We derive for the magnetic source field of a double layer

$$\begin{aligned}
\tilde{H}'_s &= -d'\nu_0 \langle \mathbf{t} * d\underline{G}^0 \wedge *^2 \underline{\sigma}_{M,DL} \mid \Lambda \rangle \\
&= -d'\delta'\nu_0 \langle \mathbf{t} * \underline{G}^1 \wedge *^2 \underline{\sigma}_{M,DL} \mid \Lambda \rangle \\
&= -d'\delta'*\nu_0 \langle \mathbf{t} \underline{G}^2 \wedge *^2 \underline{\sigma}_{M,DL} \mid \Lambda \rangle \\
&= d'*'\nu_0 \langle \mathbf{t} \underline{G}^2 \wedge *^2 \underline{\sigma}_{M,DL} \mid \Lambda \rangle \\
&= -*\delta'd'\nu_0 \langle \mathbf{t} \underline{G}^2 \wedge *^2 \underline{\sigma}_{M,DL} \mid \Lambda \rangle \\
&= *\delta'd'\nu_0 \langle \mathbf{t} \underline{G}^2 \wedge *^2 \underline{\sigma}_{M,DL} \mid \Lambda \rangle \\
&= *\delta'd'\nu_0 \langle \mathbf{t} d\underline{G}^1 \wedge *^2 \underline{\sigma}_{M,DL} \mid \Lambda \rangle.
\end{aligned} \tag{F.3}$$

We assume the magnetic dipole-moment density  $\underline{\sigma}_{M,DL}$  to be constant on  $\Lambda$  and find that

$$\begin{aligned}
d(\mathbf{t} \underline{G}^1 \wedge *^2 \underline{\sigma}_{M,DL}) &= \mathbf{t} d\underline{G}^1 \wedge *^2 \underline{\sigma}_{M,DL} - \mathbf{t} \underline{G}^1 \wedge d*^2 \underline{\sigma}_{M,DL} \\
&= \mathbf{t} d\underline{G}^1 \wedge *^2 \underline{\sigma}_{M,DL}.
\end{aligned}$$

Thus, we can apply Stokes' theorem on the last line of Eq. (F.3) and find

$$\tilde{H}'_s = *\delta'd'\nu_0 \langle \mathbf{t} \underline{G}^1 \wedge *^2 \underline{\sigma}_{M,DL} \mid \partial\Lambda \rangle. \tag{F.4}$$

By setting

$$*^2 \underline{\sigma}_{M,DL} = \mu_0 \tilde{I}$$

we have proven that the magnetic field due to a current loop, Eq. (F.2), and due to a magnetic double-layer, Eq. (F.4), are equivalent.

By an analog reasoning we can show that the electric flux density  $\tilde{D}'_s$  due to a pair of positive and negative electric point charges can be calculated from an electric scalar potential,  $\tilde{D}'_s = -\varepsilon_0 * d\varphi'_s$ , or from an electric vector potential,  $\tilde{D}'_s = d\tilde{V}'_s$ . The Newton potential of point charges reads

$$\tilde{D}'_s = -*'\delta' \langle \underline{G}^0 \wedge \tilde{q} \mid \partial\Pi \rangle, \tag{F.5}$$

where  $\Pi$  is an arbitrary line between the locations of the two charges, oriented from the negative charge to the positive charge.  $\tilde{q}$  is the constant and positive point-charge 0-form. By analogy to the above reasoning we find that the electric flux density due to pairs of point charges can not only be determined from the electric scalar potential; it may alternatively be determined from an electric vector potential due to a thin tube of magnetic surface currents along the line  $\Pi$ . Applying the same manipulations that led from Eq. (F.3)<sub>1</sub> to Eq. (F.4), we can rewrite Eq. (F.5) as

$$\tilde{D}'_s = d' \langle \mathbf{t} * d\underline{G}^1 \wedge \tilde{q} \mid \Pi \rangle.$$

- [12] T.A. Davis, An Approximate Minimum Degree Ordering Algorithm, *SIAM J. Matrix Anal. Applic.*, 17(4), 886-905, 1996
- [13] P. Dular et al., Mixed Finite Elements Associated with a Collection of Tetrahedra, Hexahedra and Prisms, *IEEE Transactions on Magnetism*, Vol. 30, No. 4, p. 2980-2983, 1994
- [14] V. Gradinaru and R. Hiptmair, Whitney Forms on Pyramids, *Technical Report 113*, SFB 382, Universität Tübingen, <http://www.uni-tuebingen.de/uni/opx/reports.html>, as of September 2004, 1999
- [15] R. Hiptmair, Finite Elements in Computational Electromagnetism, *Acta Numerica*, 11:237-339, 2002
- [16] R. Hiptmair and J. Ostrowski, Generators of  $H_1(\Gamma_h, \mathbb{Z})$  for Triangulated Surfaces: Construction and Classification, *Technical Report 160*, SFB 382, Universität Tübingen, <http://www.uni-tuebingen.de/uni/opx/reports.html>, as of September 2004, 2001
- [17] R. Hiptmair, Discrete Hodge Operators, *Technical Report 166*, SFB 382, Universität Tübingen, <http://www.uni-tuebingen.de/uni/opx/reports.html>, as of September 2004, 2001
- [18] J.D. Jackson, *Classical Electrodynamics*, John Wiley & Sons, 3rd Edition, 2001
- [19] K. Jänich, *Lineare Algebra*, Springer Lehrbuch, 8. Auflage, Berlin, 1999
- [20] K. Jänich, *Topologie*, Springer Lehrbuch, 7. Auflage, Berlin, 2000
- [21] K. Jänich, *Vektoranalysis*, Springer Lehrbuch, 3. Auflage, Berlin, 2000
- [22] I.E. Kaporin, High Quality Preconditioning of a General Symmetric Positive Definite Matrix Based on its  $\mathbf{U}^T\mathbf{U} + \mathbf{U}^T\mathbf{R} + \mathbf{R}^T\mathbf{U}$ -Decomposition, *Numer. Linear Algebra Appl.*, 5, 483-509, 1998
- [23] S. Kurz, Ö. Rain, V. Rischmüller, S. Rjasanow, Discretization of Boundary Integral Equations by Differential Forms on Dual Grids, *IEEE Transactions on Magnetism*, Vol. 40, No. 2, March 2004, p.826-829
- [24] S. Kurz and S. Russenschuck, The Application of the BEM-FEM Coupling Method for the Accurate Calculation of Fields in Superconducting Magnets, *Electrical Engineering*, 1999
- [25] S. Kurz, Die numerische Behandlung elektromechanischer Systeme mit Hilfe der Kopplung der Methode der finiten Elemente und der Randelementmethode, *Fortschritt-Berichte VDI*, Reihe 21 Elektrotechnik, Nr. 252, 1998



# Bibliography

- [1] P. Alotto and I. Perugia, Matrix Properties of a Vector Potential Cell Method for Magnetostatics, *IEEE Transactions on Magnetics*, Vol. 40, No. 2, p.1045-1048, 2004
- [2] P. Bamberg and S. Sternberg, *A Course in Mathematics for Students of Physics 1*, Cambridge University Press, 1988
- [3] P. Bamberg and S. Sternberg, *A Course in Mathematics for Students of Physics 2*, Cambridge University Press, 1990
- [4] M. Bebendorf, *Effiziente numerische Lösung von Randintegralgleichungen unter Verwendung von Niedrigrang-Matrizen*, Dissertation an der Universität des Saarlandes, 2000
- [5] A. Bossavit, *Computational Electromagnetism*, Academic Press, San Diego, 1998
- [6] A. Bossavit, Computational Electromagnetism and Geometry: Building a Finite-Dimensional "Maxwell's House". (2): Network Constitutive Laws., *J. Japan Soc. Appl. Electromagn. & Mech.*, 7(3):294-301, 1999
- [7] A. Bossavit, Computational Electromagnetism and Geometry: Building a Finite-Dimensional "Maxwell's House". (4): From Degrees of Freedom to Fields., *J. Japan Soc. Appl. Electromagn. & Mech.*, 8:102-109, 2000
- [8] W. Buckel, *Supraleitung*, VCH Verlagsgesellschaft, Basel, 1990
- [9] A. Buffa and P. Ciarlet, On Traces for Functional Spaces Related to Maxwell's Equations, *Mathematical Methods in the Applied Sciences*, 24:9-48, 2001
- [10] K. Burg et al., *Höhere Mathematik für Ingenieure*, Band V, 179ff., 1993
- [11] Y. Choquet-Bruhat et al., *Analysis, Manifolds and Physics, Part I: Basics*, 2nd edition, Elsevier Science B.V, Amsterdam, 1996

- [26] G. Lehner, *Elektromagnetische Feldtheorie für Ingenieure und Physiker*, 3. Auflage, Springer Lehrbuch, 1990
- [27] A. Prechtl, *Physikalische Dimensionen mathematischer Objekte*, <http://www.gte.tuwien.ac.at/forschung/1publika1/data/998562789.pdf>, as of July 2004
- [28] O. Rain, *Kantenelementbasis BEM mit DeRham-Kollokation für Elektromagnetismus*, Dissertation an der Universität des Saarlandes, 2004
- [29] Y. Saad, *Iterative Methods for Sparse Linear Systems*, PWS Publishing Company, Boston, 1996
- [30] R. Schürhuber, *Electromagnetic Theories from an Algebraic Topological Perspective*, Dissertation am Institut für Grundlagen und Theorie der Elektrotechnik, Technische Universität Wien, 2003
- [31] K. Straube, *Berechnung elektromagnetischer Feldprobleme mit Hilfe der Methode der finiten Elemente unter Anwendung der diskreten 1-Formen*, Diplomarbeit an der Hochschule Mittweida (FH), 2002
- [32] Tarhasaari and L. Kettunen, Some realizations of a Discrete Hodge Operator: a Reinterpretation of Finite Element Techniques, *IEEE Transactions on Magnetics*, Vol. 35, No. 3, p. 1494-1497, 1999
- [33] E. Tonti, On the Mathematical Structure of a Large Class of Physical Theories, *Rend. Acc. Lincei*, Vol. LII, pp. 48-56, [www.dic.units.it/perspage/tonti](http://www.dic.units.it/perspage/tonti), as of September 2004, 1972
- [34] T. Weiland, Time domain electromagnetic field computations with finite difference methods, *Int. J. Num. Model.* 9, 295-319, 1996
- [35] T. Weiland, On the numerical solutions of Maxwell's equations and applications in the field of accelerator physics, *Part. Accel.* 15, 245-292, 1984